Full Counting Statistics of Transport through Quantum Dot Aharonov-Bohm Interferometers

Dissertation

zur Erlangung des Grades
„Doktor der Naturwissenschaften“

am Fachbereich Physik
der Universität Duisburg-Essen

von
Dipl.-Phys. Daniel Urban

Referent: Prof. Dr. J. König
Koreferent: Prof. Dr. R. Fazio
Tag der mündlichen Prüfung: 20. April 2009

Zusammenfassung

Diese Arbeit beschäftigt sich mit der Statistik des elektronischen Transports durch mesoskopische Interferometer mit eingebetteten Quantenpunkten. Die Möglichkeit der Ladungsträger, das System auf verschiedenen Pfaden zu passieren, führt zu Interferenz. Aufgrund des Aharonov-Bohm Effekts kann mittels eines externen Magnetfeldes zwischen konstruktiver und destruktiver Interferenz umgeschaltet werden. Interferenz und starke Wechselwirkung auf dem Quantenpunkt induzieren Korrelationen im Elektronenstrom. Die Methode der vollen Zählstatistik studiert solche Korrelationen durch Bestimmen der kumulantenerzeugenden Funktion des zugrundeliegenden stochastischen Prozesses. Die hierfür erforderliche Information über die zeitliche Entwicklung des Systems ist in einer verallgemeinerten Mastergleichung kodiert. Diese berücksichtigt Wechselwirkung, Spin und räumliche Ausdehnung der Wellenfunktion in Systemen mit mehr als einem Quantenpunkt. Die Übergangsraten werden mit Hilfe eines diagrammatischen Realzeit-Zugangs auf der Keldysh-Kontur systematisch in der Tunnelkopplung entwickelt, wobei Wechselwirkungseffekte exakt behandelt werden.

Als minimale Modelle, die die beschriebenen Effekte zeigen, werden ein Interferometer mit Quantenpunkten in einem oder beiden Armen behandelt. In beiden Fällen tritt sowohl sub- als auch super-Poissonsches Verhalten auf.

Ohne Wechselwirkung sind alle Transportgrößen des Einzelpunkt-Interferometers aufgrund der Onsager-Relationen eine gerade Funktion des magnetischen Flusses und die Transportstatistik ist Poissonsch. Wechselwirkung ändert dies in zweierlei Hinsicht: Zum einen induziert sie Korrelationen, die die Statistik der bestehenden Prozesse sub-Poissonsch werden lassen. Zum anderen verursacht sie neue Prozesse mit einer ungeraden Flussabhängigkeit. Diese zeigen stark super-Poissonsches Verhalten in einem Parameterbereich, in dem alle anderen Prozesse Poissonsch werden. Die Messung der Zählstatistik erfolgt typischerweise über Echtzeit-Detektion einzelner Elektronen während sie den Quantenpunkt passieren. Es wird gezeigt, dass ein solches Messverfahren eine andere Statistik ergibt, da Prozesse, die den Ladungszustand des Quantenpunktes erhalten, nicht detektiert werden.

Die Statistik des zweiten untersuchten Systems, eines Interferometers mit einem Quantenpunkt in jedem Arm, hängt wesentlich davon ab, dass bei der Beschreibung des Systems der Spin-Freiheitsgrad berücksichtigt wird: Für einen speziellen Parametersatz (verschwindender Fluss, entartete Ein-Elektronenzustände) zerfällt der Hilbertraum des Systems in zwei entkoppelte Unterräume. In beiden ist Transport möglich, allerdings mit unterschiedlichen Statistiken. In einer solchen Situation ist es nicht möglich, die Zählstatistik im stationären Grenzfall zu definieren, da sie von den Anfangswerten abhängen würde. In realistischen Systemen führt allerdings jede kleine Störung, z.B. durch Spin-Relaxation, zu einer Kopplung der Unteräume. Im Falle einer schwachen Kopplung zeigt das System stark super-Poissonsches Verhalten, ähnlich dem Telegraphenrauschen, mit Kumulanten die für vollständige Entkopplung divergieren.

Summary

This thesis is concerned with the study of transport through multiply connected geometries including quantum dots. The fact that electrons can pass the system along distinct paths gives rise to interference effects. These can be tuned through the Aharonov-Bohm effect by means of a magnetic field. The quantum dots introduce Coulomb interaction, such that at most a single electron can occupy each dot at any given time. Both Coulomb interaction and interference introduce time correlations in the electronic current. These correlations are studied in full counting statistics, which aims at the calculation of the cumulant generating function of the underlying stochastic process. The time evolution of the system is described by a generalized master equation that takes into account the full density matrix, describing spin, interaction and the delocalized nature of the electron wave function in systems with several dots. The kernel of the master equation is calculated within a real-time diagrammatic approach on the Keldysh contour. This techique allows a systematic expansion in the tunnel coupling while treating Coulomb interaction exactly.

Two minimal models are discussed: a two-path interferometer with a quantum dot in one arm and an interferometer with one quantum dot in each arm. In both systems, depending on the parameter set, both sub- and super-Poissonian statistics are found.

For the single dot interferometer it is known that in absence of Coulomb interaction Onsager relations require the statistics to be an even function of the magnetic flux and the statistics are found to be Poissonian. The effect of charge interaction is twofold: Firstly it introduces correlations that suppress the statistics below the Poissonian value. Secondly, Onsager relations do not hold and new transport processes with an odd flux dependence appear. They exhibit strongly super-Poissonian statistics in a regime in which all other transport processes are uncorrelated. To date there is only one truly successful technique for the measurement of counting statistics: real-time detection of electrons as they pass the quantum dot. It is shown that such a detection scheme gives different statistics, since it is insensitive to processes conserving the dot state.

As a second system an interferometer with quantum dots in both arms is studied. Its statistics depend crucially on the inclusion of spin in the system description: For a very specific parameter set (vanishing flux, degenerate electronic levels) the system's Hilbert space decomposes into two uncoupled subspaces. Transport is possible within either of the subspaces, albeit with different statistics. In such a situation it is impossible to define the counting statistics in the stationary limit, since they would depend on the initial condition. However, this situation is unrealistic since any small deviation of the system parameters (e.g., by experimental imperfections such as spin relaxation) results in coupling of the subspaces. If this coupling is weak the system exhibits strongly super-Poissonian statistics, similar to a random telegraph signal, with the cumulants diverging in the limit of complete decoupling.

Contents

1 Introduction

The systems examined in this thesis are interferometers with one and two quantum dots embedded in the arms. They are good examples for mesoscopic systems. While the term "mesoscopic" is applied to a broad class of systems and phenomena, it generally describes systems in which classical and quantum mechanical phenomena are combined. It turns out that the systems are typically smaller than (macroscopic) objects in everyday life, yet larger than microscopic objects like atoms–hence the term *meso*scopic was coined. Typically they are constructed from hundreds of thousands of atoms and typical length scales are in the nanometer range.

The classical phenomena relevant to the present work are related to the granularity of charge: On one hand, the granularity of these charge carriers is exploited in several ways: via charge interaction effects and through its allowing to count individual charges. The occurrence of charging effects in nanoscale structures is a well known phenomenon. Two electrons always experience Coulomb repulsion. If they are separated only by small distances, e.g., by confining them to a nanoscopic region in space, this charging energy can assume significant values. This is in particular the case in ***quantum dots***. Typical mesoscopic, metallic structures are of the order of 100 nm, which results in charging energies corresponding to temperatures of 1 K. Smaller structures, such as quantum dots made of molecules etc., can result in charging energies which become relevant even at room temperature. The charging energy is a purely classical effect. Its existence is not related to the granularity of charge. However, the charge quantization causes the charging energy to always assume a finite value.

Since electric charge is quantized it is intuitively clear that the individual charge carriers can in principle be counted as they traverse the structure. Conceptually this enables current measurement with perfect precision. More interestingly fluctuations of the current are accessible in this way. In the systems at hand, current is transported in tunnel processes. It is in the nature of tunnel junctions that knowledge about whether a particle is transmitted or reflected exists only in the form of probabilities. This give rise to current fluctuations. Counting the charges then gives access to these fluctuations, allowing to obtain the probability that a given number of charges has traversed the system after a given time. This is called ***full counting statistics***, since it describes the full probability distribution function of charge transfer–in contrast to conventional noise studies which access only the second moment the distribution. The granularity of charge allows an intuitive interpretation of this distribution function.

Since the mechanisms causing fluctuations are in general of quantum mechanical origin, for the calculation of the counting statistics a quantum mechanical theory is needed. In the specific case relevant to this thesis transport of electrons occurs due to ***tunneling***, an entirely quantum mechanical process. It introduces a probabilistic element in transport that gives rise to current fluctuations. Additional fluctuations

are introduced through the internal dynamics of the quantum dot systems.

A second quantum mechanical element is due to the very nature of the systems: the structures under consideration are ***interferometers*** in which electrons can take two different paths to progress from a common source to a common drain. In order for quantum effects to occur coherence along these paths is crucial, i.e., the phase coherence length has to be larger than the size of the structure. For this reason experimental realizations are fabricated with small spatial extensions of several micrometers and operated at low temperatures (liquid helium), so that the main source of decoherence, phonon-coupling, is reduced. In order to tune the interference between constructive and destructive, a parameter is needed that controls the phase of the electrons. While many mechanisms are known that affect the phase, here one is chosen, whose theoretical description and experimental realization are rather elementary: the ***Aharonov-Bohm*** effect. It arises when exposing the system to a magnetic field that penetrates the area between the two interfering paths. The magnetic field causes a relative phase difference proportional to the magnetic flux. Since the area of the paths is usually fixed, the phase difference is controllable in a simple and precise manner by tuning the magnetic field.

A third quantum mechanical aspect in this work arises in the second system studied, an interferometer with one quantum dot embedded in each arm. Under the influence of strong charge interaction, each dot can be occupied by at most one electron. Thus both dots together form a realization of a prototypical quantum mechanical system, the ***two-level system***. A single electron occupying the double dot is not required to occupy only one dot, but may enter any linear combination of the levels. An appropriate description is then provided by an isospin, analogous to a particle with a spin of 1/2.

The aim of this thesis is to analyze the counting statistics of Aharonov-Bohm interferometers with embedded quantum dots. The statistics depend on the internal dynamics of the system. This is motivates a study of the counting statistics, since information about the noise and even more so about the entire statistics helps in understanding the underlying transport processes.

This thesis is structured as follows. First, the fundamental concepts relevant for the systems under study are introduced in *Chapter 2*. This includes charging effects and a short characterization of various tunneling regimes. The largest part of the chapter is devoted to the two types of Aharonov-Bohm interferometers examined in this thesis. A numbers effects are discussed which are experimentally and/or theoretically relevant.

Then, the concept of full counting statistics (FCS) is introduced in *Chapter 3*. As a background, properties of current noise are discussed and an overview over mechanisms resulting in enhanced noise is given. This overview is motivated by the fact that enhanced noise plays a major role also in the present thesis. After showing that the knowledge of higher cumulants of the current distribution function is feasible, the theory of full counting statistics is introduced in general terms and two examples, a single and a double barrier are discussed, already demonstrating how the FCS can be obtained. As an important example one additional method for the calculation of FCS is shown, before an overview over the concepts for the measurement of counting statistics is given.

The theoretical approach for the calculation of the counting statistics of quantum-dot interferometers is presented in *Chapter 4*. It relies on a real-time diagrammatic technique for the description of the time evolution of a system weakly coupled to several reservoirs. The system itself is described by a reduced density matrix with the reservoir degrees of freedom traced out. The time evolution of this reduced density matrix is governed by a generalized master equation, the kernel of which can be obtained with a diagrammatic approach on the Keldysh contour. In this way it is possible to treat interaction effects in the intermediate system exactly. It is demonstrated how this kernel is related to the generating function for the system's counting statistics.

Finally the results are discussed in the last two chapters. The single dot Aharonov-Bohm interferometer is discussed in *Chapter 5*. The counting statistics are first analyzed for the case of detection at source or drain interface. The generating function contains two distinct processes with different dependence on flux and different statistics. The processes with odd flux dependence are shown possess strongly super-Poissonian statistics in a parameter regime, that is commonly associated with Poissonian transport. The second part of the chapter discusses the counting statistics that would be measured by a detector for the charge state of the quantum dot. The processes with even flux dependence are invisible to this kind of detector, but also the processes with odd flux dependence follow different statistics.

The statistics of the double dot interferometer are discussed in Chapter 6. The system's Liouville space is found to decompose into two separate subspaces. The coupling between these subspaces is mediated by tunneling, but depends on the Aharonov-Bohm phase. When the phase assumes multiples of π, the coupling vanishes. Since these subspaces have different transport statistics, a kind of generalized random telegraph noise arises: the system continually switches between the subspaces. For phase values near π this switching becomes very slow and the statistics become super-Poissonian. The thesis ends with a conclusion in *Chapter 7*.

2 Charge transport in dot-ring geometries

The transport properties of mesoscopic systems stand out since in the mesoscopic regime unique combinations of effects occur. On the one hand the systems are small enough for single charge effects to appear, and on the other hand interference effects are possible. This chapter briefly introduces the concepts relevant for charge transport in dot-ring geometries.

The first section deals with single charge effects. Due to the limited size, the structure is sensitive to the addition or removal of individual electrons for two reasons. Firstly the classical electromagnetic repulsion between charges brought to close proximity results in an additional charging energy being necessary to add an electron to the dot. Secondly, since the electrons are restricted to an area whose length scales are comparable to the electron's Fermi wavelength, the quantum mechanical level splitting becomes important.

The second section briefly discusses sequential and co-tunneling processes through quantum dots. Finally the Aharonov-Bohm effect is introduced and the properties of interferometers containing single and double quantum dots are discussed.

2.1 Single charge effects

Quantum dots are mesoscopic structures in which the charge carriers are confined to such small lengths d that the associated energy scale $h^2/(m^*d)^2$ becomes comparable to the Fermi energy [1]. This results in a discrete density of states on the dot. In addition, due to their small size quantum dots have a very limited capacitance of several pF or even aF (in case of quantum dots consisting of single molecules). This gives rise to strong Coulomb interaction, leading to correlated transport through the dot. Throughout this thesis quantum dots are considered which are sufficiently small that only a single quantum mechanical level participates in transport.

For the realization of quantum dots a number of possibilities exist. The strongest confinement is achieved when single molecules are contacted, often by placing the molecule in a metallic break junction. Similarly carbon nanotubes can be contacted. Quantum dots can also be realized in semiconductor structures in several ways. Overgrowing a substrate with a material whose lattice constance differs from that of a substrate results in strain, which gives rise to self-organized growth of quantum dots. The probably most versatile method however consists in defining the dots in a two-dimensional electrons gas (2DEG). For this purpose top gates are grown on top of the 2DEG. Upon applying negative voltages to them, the area under the gates is depleted from electrons. By proper design of the shape of the depletion gates quantum dots can be defined in such a way that both the size and shape of the dot is tunable and furthermore the coupling to leads or other dots can be tuned, since the barriers are

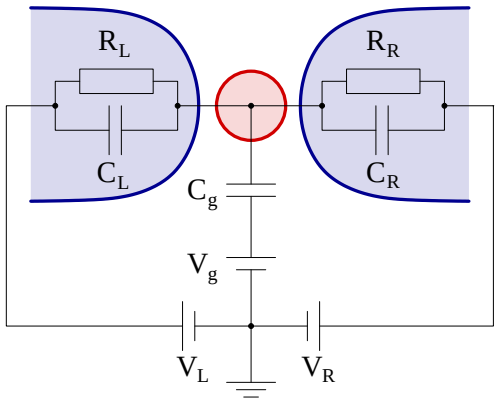

Figure 2.1: The equivalent circuit of a quantum dot (red). The tunnel contacts to the leads (blue) can be described by resistances R and capacitances C, the gate is also coupled capacitively.

also defined by gates. This allows the construction of complicated structures, including the interferometers studied here. An example of such an advanced structure is shown in Fig. 2.6.

2.1.1 Charging energy

As has been said, quantum dots are structure in which electrons are confined to a small region of space. This gives rise to charging effects: an initially electrically neutral dot can be charged with one electron without the cost of charging energy. The net charge becomes $(-e)$ and the resulting electric field repells other electrons, so that a stronger force is needed to charge the dot doubly. This corresponds to a charging energy

$$E_{ch} = \int dQ\, V = \frac{Q^2}{2C}\,, \tag{2.1}$$

where C denotes the total capacitance of the quantum dot (Fig. 2.1)

$$C = C_L + C_R + C_g. \tag{2.2}$$

For typical dots it ranges $10^{-15}\,\mathrm{F}$ down to $10^{-18}\,\mathrm{F}$.

The potential of the dot can be tuned via the potentials of the leads and the gate voltage. This can be described as an external charge en_x

$$en_x = (C_L V_L + C_R V_R + C_g V_g)\,. \tag{2.3}$$

The total potential energy of the dot is then

$$E_{ch} = \frac{e^2}{2C}\,(N - n_x)^2\,, \tag{2.4}$$

where N denotes the number of excess charges on the dot. The physical realization of the excess charges N found on the dot minimizes E_{ch}. Figure 2.2(a) shows E_{ch} as a

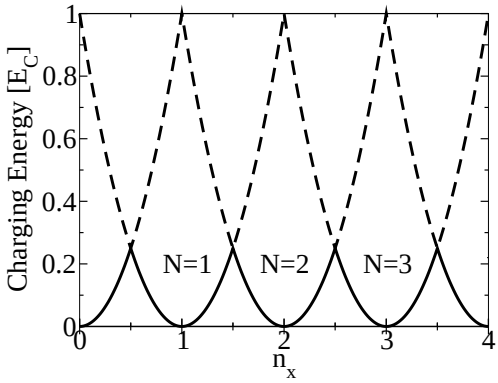

(a) The charging energy varies quadratically as a function of the gate tuned external charge n_x for a given dot occupation N. At half integer values of the external charge n_x two charge states are possible.

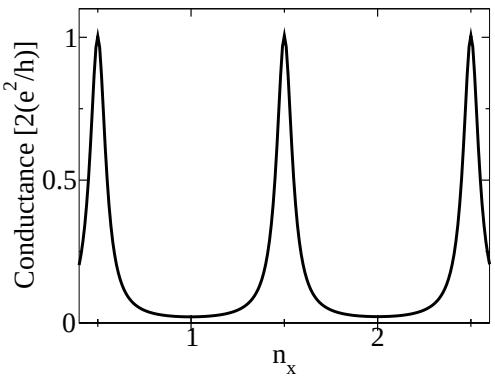

(b) At the points of fixed dot charge transport through the dot is suppressed by Coulomb blockade. At half-integer values of the external charge n_x transport is possible, giving rise to Coulomb oscillations. At zero temperature the shape of these resonances is given by a Breit-Wigner function as shown.

Figure 2.2: The number of charges on the dot depends on the gate voltage. The discreteness of charge leads to an oscillatory behavior of the conductance.

function of n_x. For integer values of n_x the charging energy is minimized and the dot charge state is sharply defined. Whenever the number of charges is fixed, transport is suppressed by *Coulomb blockade*. For half-integer values of n_x two adjacent charge states have equal charging energies. Therefore the excess charge of the dot can fluctuate between N and $N+1$ electrons without changing the potential energy of the dot, so that transport is allowed. Since the number of charges on the dot is not fixed, transport through the dot is possible, so that periodic peaks appear in the conductance, the *Coulomb oscillations*. The system is referred to as a "single electron transistor" as it can be switched between a conducting and an isolating state by changing the gate voltage and in the conducting state only a single electron can pass at a time (see Fig. 2.2(b)).

The conductance peaks are broadened for two reasons. Finite temperature leads to broadening of the Fermi-distribution by k_BT, so that some source electrons have energies higher than the Fermi energy, while some drain states below the Fermi energy are empty, so that transport occurs in an energy interval of the order k_BT around the levels. At the same time the dot levels are broadened due to the coupling to the leads. This results in a Breit-Wigner lineshape for resonant transport, with the width given by the tunneling rate $\Gamma/\hbar$ between dot and lead.

2.1.2 Level separation due to confinement

Besides the strong Coulomb interaction, quantum dots show energy level separation due to geometrical confinement. In a confining potential, the momentum of the electrons gets quantized so that their de Broglie wavelength matches the dimensions of

the structure. If the energy difference ΔE between two levels exceeds the thermal broadening, the quantum dot is characterized by a discrete density of states. For this reason they are also often referred to as artificial atoms. A substantial difference to natural atoms is however that the atomic properties can be tuned. The level spacing for instance is determined by the size of the dot, while its shape determines the symmetries of the wave function. In lateral quantum dots in two-dimensional electron gases both properties are accessible by tuning the gate voltages.

The level spacing ΔE depends only on the geometric size of the dot, while the charging energy E_{ch} additionally depends on the capacitances. Thus it is possible to increase ΔE so far that effectively only one level remains in the relevant energy range. The dot can then be treated as consisting only of a single level. For reasons of simplicity this work focusses on this type of quantum dot.

2.2 Higher orders of tunneling

In a weakly tunnel coupled quantum dot only sequential tunneling processes have to be taken into account. This means that transport occurs due to electrons tunneling onto and off the dot in an uncorrelated way, i.e., one at a time (Fig. 2.3(a)). This is described by first order perturbation theory in the tunnel coupling [2]. In lowest order the dot levels appear as delta-peaks and the width of the conduction peak is determined entirely by temperature: away from the Coulomb peaks tunneling is exponentially suppressed at low temperatures.

Processes of the next higher order are called co-tunneling processes. They are accessible in second order perturbation theory, two electrons tunnel coherently (Fig. 2.3(b)) [3]. As can be seen from the figure, this implies that the structure need not be tuned to resonance. This leads to lifting of the Coulomb blockade, so that transport is suppressed only algebraically and not exponentially. In addition, it causes an intrinsic broadening of the dot levels—the system behaves as if it was closer to resonance: the conductance in the Coulomb blockade regime, but also on the resonances, is increased.

The extreme case for strong coupling is the Kondo regime, in which electrons are found in a delocalized, coherent state in dot and leads: If the dot is occupied by an odd number of electrons it is spin polarized and the local dot spin gets screened by the lead electrons for temperatures lower than the Kondo-temperature which gives rise to an increased conductance for gate voltages, for which sequential transport is maximally suppressed. A narrow conductance peak appears at $n_x = m + 12/2$ in Fig. 2.2(b).

In this work only lowest order transport is studied. Still, co-tunneling processes play a role in the single dot interferometer (Sec. 5), where amplitudes of co-tunneling processes interfere with amplitudes of sequential tunneling processes.

2.3 Aharonov-Bohm interferometry

Interference effects appear in two-path interferometers where an incoming beam is split up into two parts, traversing along different trajectories, and finally brought to interference (Fig. 2.4). If the only influence of the separate trajectories is that the

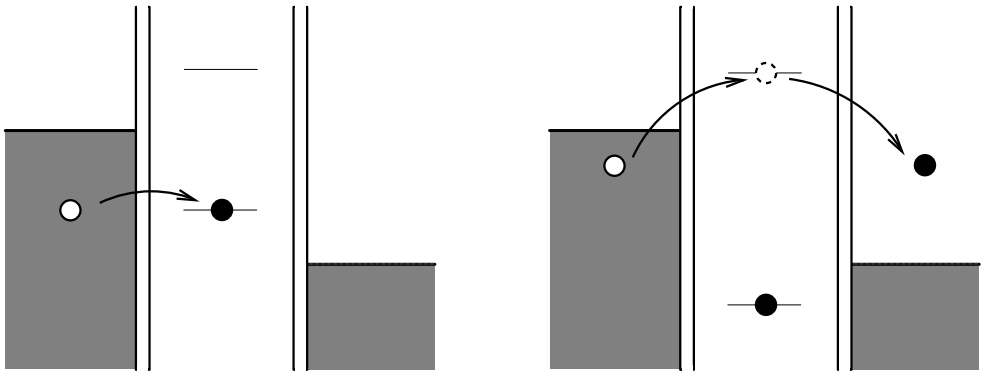

(a) In *sequential tunneling* electrons tunnel through the dot in two uncorrelated processes.

(b) In *co-tunneling* electrons pass through the dot via a virtual state. This allows transport even in the Coulomb blockade regime.

Figure 2.3: First and second order tunnel processes.

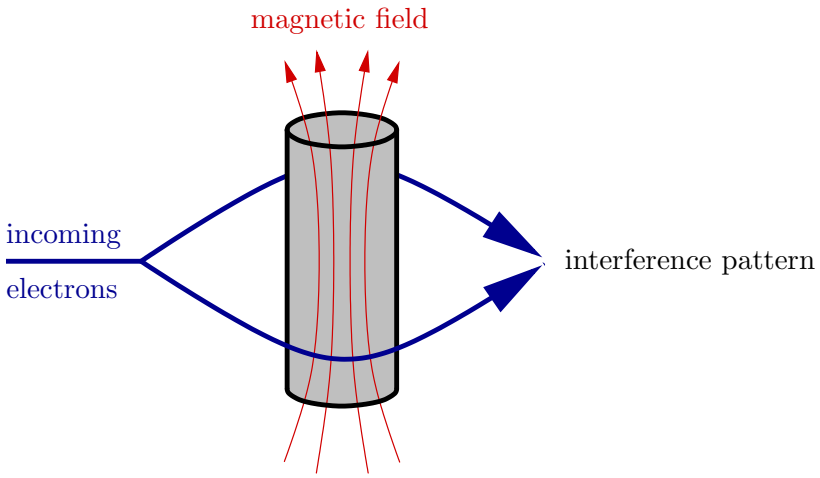

Figure 2.4: The Aharonov-Bohm effect. An incoming electron beam is split up into two parts, which propagate along different spatial paths. These paths enclose a magnetic flux, so that the electrons acquire different phases and show flux-dependent interference effects, when brought back together. This happens also if the electrons do not experience the magnetic field itself.

particles pick up a relative phase ϕ, the outgoing wave function is

$$\Psi_{\text{out}} \quad = \quad \Psi_1 + e^{i\phi}\Psi_2, \tag{2.5}$$

where Ψ_i $(i = 1, 2)$ are the wave functions for transmission through arm i. The probability of observing the particle behind the interferometer is thus given as

$$|\Psi_{\text{out}}|^2 \quad = \quad |\Psi_1|^2 + |\Psi_2|^2 + 2|\Psi_1||\Psi_2|\cos\phi. \tag{2.6}$$

If the transparencies of both arms are equal, $|\Psi_1| = |\Psi_2|$, full destructive interference is possible for $\phi = \pi$.

While the possible origins of such phase differences are plentiful, in this thesis it is thought of as arising from the Aharonov-Bohm (AB) effect, since it is conceptionally simple and experimentally well accessible. It was first described theoretically by Aharonov and Bohm [4] that electrons following a closed loop acquire an additional phase $\phi = \Phi\, 2\pi e/h$ if the loop is penetrated by a magnetic flux Φ. Historically the insight gained from the AB-effect was related to the physical relevance of the vector potential. It had originally been thought of as being merely a mathematical construction without direct physical relevance. The magnetic flux can be written as both a surface integral ofr the magnetic field $\mathbf{B}$ over the surface enclosed by the loop or as the line integral of the vector potential $\mathbf{A}$ along the loop

$$\Phi = \int_S \mathbf{B}\cdot \mathrm{d}\mathbf{S} = \oint_{\partial S} \mathbf{A}\cdot \mathrm{d}\mathbf{r}. \tag{2.7}$$

The interference effect appears also if the magnetic field is concentrated to a region inside the loop. This means that interference is possible also if the electrons have not encountered a magnetic field along their path-it is only the flux that matters.

The appearance of interference can be hindered in realistic systems in several ways. Obviously the structure has to be phase coherent, i.e., isolated from external baths and smaller than the phase coherence length of the charge carriers. However, in addition to this there are other, more subtle requirements. For instance, it is very likely that several transport channels are open in both paths. For interference to occur these channels must match in energy. Electrons whose energy matches only a channel in one arm, propagate only along this path and actually do not pass an interferometer. It is, however, not necessary that all channels are matched: the mismatching ones just result in a background transmission so that the visibility of the Aharonov-Bohm signal is reduced but can still be large enough to be observed. Such a background current can also exist if only a single, fully coherent channel contributes. In this case the transmission probabilities through upper and lower arm might differ and, as is apparent from Eq. (2.6), this also causes a flux independent contribution.

Two theoretical approaches for the description of interferometers suggest themselves: the scattering approach and the tunneling approach (Fig. 2.5). The models differ in the way in which the interferometer is connected to the leads. In the scattering picture electrons first enter a “fork”, which splits up into the lower and the upper path. In contrast the dots are directly connected to the leads in the tunneling model. The

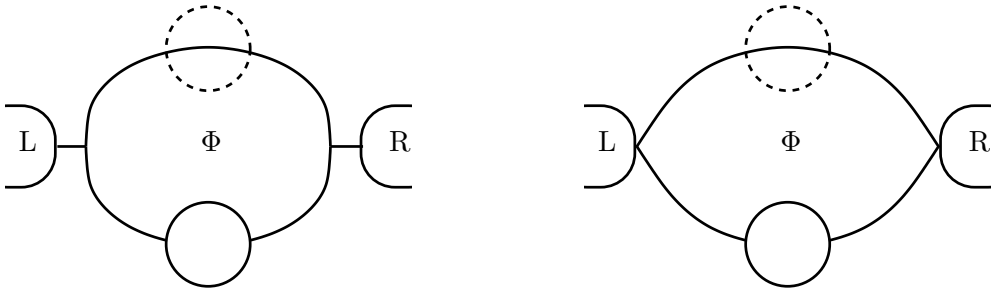

(a) Scattering model of an ABI: electrons enter first a beamsplitter and then the quantum dot.

(b) Tunneling model of an ABI: electrons enter the dots directly from the leads.

Figure 2.5: For non-interacting electrons the tunneling model and the scattering model of an ABI with one or two embedded quantum dots are equivalent.

tunneling model thus excludes multiple reflections at the interfaces. Under the assumption of noninteracting electrons and interferometers small enough that no orbital phases play a role it has been shown that the two models coincide if a specific symmetry of the forks is assumed [5]. Different parameters of the fork can be absorbed in a renormalization of the coupling parameters for the arms. In this thesis, the tunneling approach is followed.

2.3.1 Interferometry with single dots

Embedding a single quantum dot in one of the arms of an interferometer conserves coherence. Still, the introduction of a dot has influence on the transport properties. First, the symmetry of the system has changed. This has impact on phase dependence. Second, simply due to the fact that the electron has to pass an intermediate, localized level, its phase changes. This effect should also be visible in the phase dependence of the interferomter. Finally, if the electron is localized on the dot, there are additional source of decoherence. Spin-flip processes constitute such a source that is immanent in the system itself. Another arises if a charge detector is coupled to the dot. Since it determines the electrons position, the question naturally arises whether coherence is conserved. These questions will be adressed in the following sections.

Phase locking

In general two types of interferometers have to be distinguished: open and closed interferometers. Photonic double slit interferometers are always of the first kind. They are open in the sense that some of the injected photons can leave the interferometer and neither arrive at the drain nor are they reflected to the source. They are instead lost to the environment. In electronic interferometers open setups can be realized, however it can also be arranged that all injected electrons reach the drain, which is referred to as a closed interferometer. This is the kind studied in this thesis.

In general, for all two terminal systems the following relation holds

$$\frac{\partial I(V,\phi)}{\partial V} = \frac{\partial I(-V,-\phi)}{\partial V}. \tag{2.8}$$

It immediately yields the Onsager relation

$$\left.\frac{\partial I(\phi)}{\partial V}\right|_{V=0} = \left.\frac{\partial I(-\phi)}{\partial V}\right|_{V=0}, \tag{2.9}$$

which states that the linear conductance is an even function of magnetic flux. This phenomenon is referred to as *phase locking*.

While the relation Eq. (2.9) holds in general, it has been shown that specific symmetries of the interferometer can be exploited to obtain more general relations [6]. In the case of the single dot interferometer there are no such symmetries which would lead to stronger statements.

Transmission phase of quantum dots

It is known from elementary scattering theory that a particle's wave function receives an additional phase upon scattering. This phase changes by π as the energy of the impinging particle is tuned through a resonant level [7]. Regrettably this phase is not accessible by studying the transmitted current, since it depends solely on the absolute value of the wave function. What is more, a conductance measurement is not even able to decide whether the transmission process was coherent or whether the phase information was lost upon passing the level (as might happen upon scattering of the electron inside the potential well). The transmission phase can be accessed only if the stream going through the level is brought to interference with a stream that has not passed the level.

Such an experiment was carried out by Yacoby *et al.* [8]. The device consisted of a reference arm and a quantum dot in parallel (Fig. 2.6). The barriers of the quantum dot were controlled by two quantum point contacts, while its electrostatic potential was controlled by a third (plunger) gate. As a novelty, a metallic air bridge was fabricated in a special lithographic process, that allowed to contact the area enclosed by the two paths. The structure was tuned such that only a small number of modes contributed in both arms. Conductance measurements showed clear Aharonov-Bohm oscillations–the first demonstration that transport through a quantum dot has coherent contributions. Upon tuning the electrostatic potential of the dot level, consecutive Coulomb peaks could be probed. It could be therefore be expected that the change of the transmission phase caused by tuning the level through resonance, as discussed above, can be observed. Indeed, a change of the transmission phase by π at an energy inside the resonance peak was found. However, the width over which the phase changes is much ($\sim$ 10 times) smaller than would be compatible with the simple scattering picture, which predicts the width to be given by temperature (Fig. 2.6).

As has been discussed above in the context of phase locking, the conductance oscillations of a single dot ABI are bound to be an even function of the magnetic flux. This implies that the phase measured in the two-terminal setup of Ref. [8] can only be zero

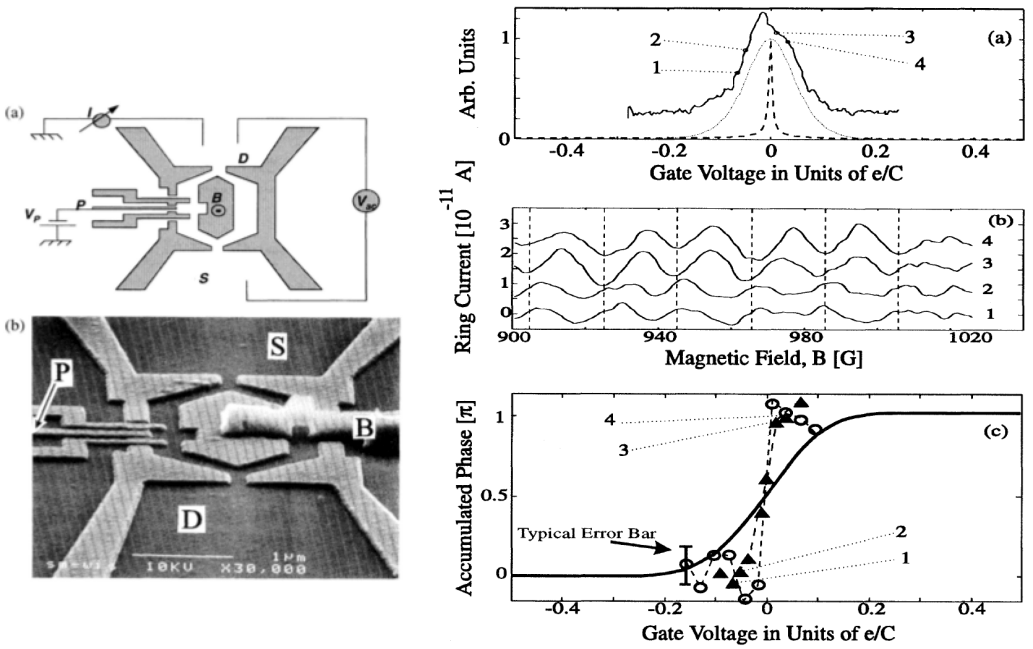

(a) Experimental setup for the measurement of the transmission phase of a quantum dot. Metallic gates appear as light grey. One of them the plunger gate (P) is used to defined the quantum dot, while other gates are needed to define the interferometer paths.

(b) (top) Level broadening at $T = 0$ (dashed), at $k_B T > \Gamma$ (dotted) and the experimental result (shifted up, solid). (middle) AB-oscillations at the points marked in the conductance peak. The phase jumps between 2 and 3. (bottom) Phase behavior as the dot is tuned through two resonances (triangles and circles). The solid lines show the behavior expected from the scattering picture.

Figure 2.6: Setup and results of the first experimental study of the phase lapse phenomenon [8].

or π and no width can be attributed to the change, precisely as observed (the observed width can be attributed to inaccuracies, such as fluctuations of the dot potential).

In order to be able to observe the transmission phase it is thus necessary to devise a different measurement scheme. For this purpose Schuster *et al.* employed a device which resembled more an open double slit setup, in which phase locking does not occur [9]. The conductance of the quantum dot was tuned to a value larger than in Yacobi's experiment. This made possible the measurement of AB-oscillations also in the Coulomb valleys, a regime not accessible in the earlier experiment. Since phase locking does not occur, the transmission phase of the dot is indeed accessible. The phase shift of π upon tuning through resonance still appears.

Deep in the Coulomb blockade valleys no AB-oscillations are visible, but the phase exhibits a peculiar behavior: it jumps back down by π to the value it had left of the resonance. This phenomenon is referred to as "phase lapse". It can be explained [10] within the scattering picture, assuming all resonances to be of the same Breit-Wigner form. However, since the experiment [9] was not carried out in the weak coupling regime, it cannot be explained by this argument.

Studies of the phase lapse phenomenon are far too numerous to be discussed here [11]. For instance, it has been described that the phase behavior is not the same for all Coulomb peaks; the universal behavior discussed above holds only for large numbers of electrons in the dot. For lower numbers mesoscopic features appear (caused, e.g.. by the dot shape) [12].

Partial coherence

In the presence of strong Coulomb interaction double occupation of a quantum dot is prohibited and transport in the sequential tuneling regime is only partially coherent [6]. This is reflected in the visibility of the Aharonov-Bohm signal in an interferometer with an embedded dot. To understand the meaning and origin of partial coherence it suffices to consider a single dot connected to two leads. The three possible processes that transfer an electron through the dot are shown in Fig. 2.7. For brevity only processes in wich the electron injected from the source has spin up are discussed, since processes with spin down in the source are similar.

(a) The dot is initially empty. An electron (spin up in the figure) tunnels onto the dot, resulting in a virtual occupation and then leaves again.

In case the dot is initially occupied, the strong Coulomb interaction requires this electron to leave to the drain before a second electron can tunnel in from the source.

(b) If the dot is initially occupied with a spin up, since the spin of the entering electron is also directed up, the dot final state of the dot is indistinguishable from the initial state.

(c) If the initial state of the dot is a spin down state, the co-tunneling process will flip the spin, so that initial and final state are different.

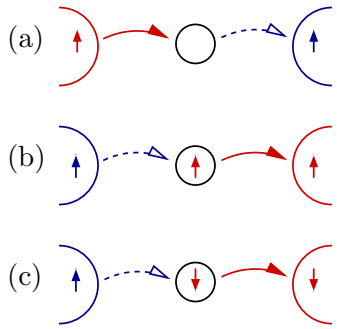

Figure 2.7: Transport through a quantum dot in the co-tunneling regime is only partially coherent. The solid lines indicate processes which happen before those indicated by dashed lines. While the processes shown in (a) and (b) are coherent, process (c) flips the spin on the dot, i.e., it leaves a "trace in the environment" and is thus incoherent.

In contrast to the first two processes (a) and (b) the spin flip process (c) leaves a "trace in the environment" (in the language of decoherence—here the environment is just the dot itself) and allows to distinguish between entering and leaving electron. It is thus incoherent.

In summary, all processes starting from an empty dot are coherent (a), while only half the processes starting from an initially occupied dot are coherent. The above argumentation was based on co-tunneling transport through a quantum dot. The situation in an interferometer with a quantum dot embedded in one arm is slightly different. Interference takes places between two amplitudes: one for transport through the dot and one for the reference arm. The contribution for transport through the dot is the amplitude belonging to a co-tunneling process and therefore exhibits the above-mentioned coherence effects. This means that the amplitude belonging to the incoherent processes cannot contribute to Aharonov-Bohm interference. As a result the amplitude of the conductance oscillations as a function of magnetic flux (the visibility) depends on whether the dot is singly occupied or empty.

Experimental results confirm this view [13]. Figure 2.8 shows the measured value of the Aharonov-Bohm visibility for two succesive Coulomb peaks. Both peaks are asymmetric: in the region between the peaks the dot is singly occupied and the visibility is reduced. The dip near the peak maximum is not related to partial coherence, but rather owed to the phase shift of π as the dot is tuned through resonance (Sec. 2.3.1).

In the absence of interaction more processes are possible if the dot is initially occupied: as intermediate state also double occupation of the dot is allowed. This gives rise to processes similar to (b) and (c). One of them is spin conserving, while the other flips the spin. Thus the number of incoherent processes on both sides of the Coulomb peak is the same and the visibility is the same.

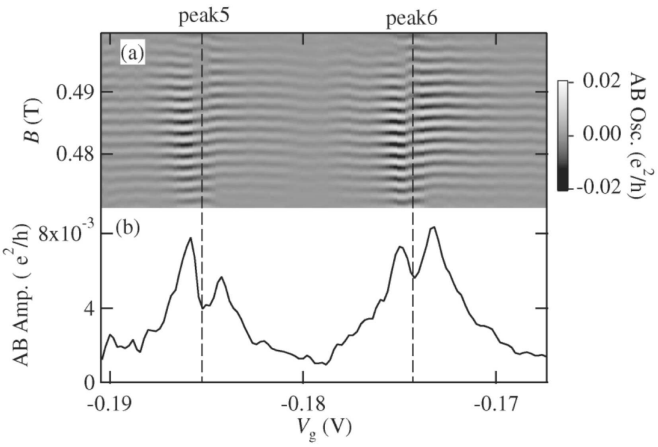

Figure 2.8: Visibility of the Aharonov-Bohm signal as a function of gate voltage as measured in Ref. [13] (b). Between the two Coulomb peaks (dashed lines), the interference is reduced since the dot is singly occupied. The upper panel (a) shows the oscillations over which the visibility was averaged to give the result shown in panel (b).

2.3.2 Interferometry with double dots

The second system studied in this thesis consist of an Aharonov-Bohm interferometer with one quantum dot embedded in each arm, also called a parallel double quantum dot. Double quantum dots are of interest in quantum computing, as will be discussed in the following section. Since two levels are coupled to the same drain, interference may result in completely blocked transport not only on behalf of the Aharonov-Bohm phase. Instead, coherent population trapping may occur, which is strongly reflected in the transport properties.

Entanglement generation

Since the proposal of Loss and DiVincenzo [14] quantum dots have been examined in the context of quantum computing. The spin of an electron on a quantum dot may serve as a representation of one qubit. The strength of this approach lies in its scalability: it is expected that without undue effort larger arrays of qubits can be manufactured, which is a requirement for a powerful quantum computer. Since for a quantum computer logical gates need to be implemented that control a single qubit but also several qubits at a time, the minimal system size consists of two qubits, i.e., a double quantum dot. In order for quantum computation to be possible it is not only required to have several qubits accessible, it is furthermore necessary to be able to bring these qubits into an entangled state. For parallel quantum dots is has recently been suggested how an entangled eletron pair can be generated in non-equilibrium situations [15, 16].

Two different setups have been proposed, in both of which the two dots are connected to one common lead. Coulomb interaction on each dot is assumed to be large, so that

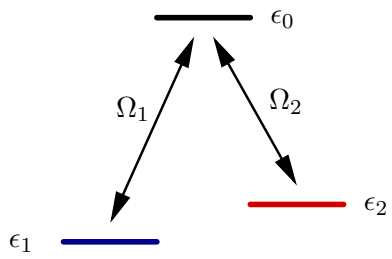

(a) Λ-type system for optical coherent population trapping.

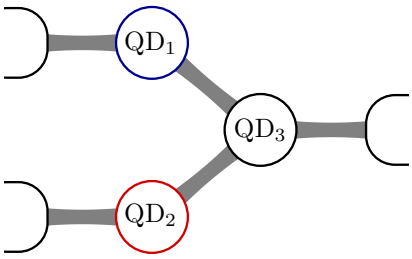

(b) All-electronic realization of coherent population trapping.

double occupation of each dot is prohibited. Naturally, no Coulomb interaction is assumed between the dots, so that double occupation of the system is possible if each dot contains one electron. Entanglement of these electrons is shown to be manifested in an increased population of the singlet state in comparison to the triplet states.

In the first scheme, the energy levels of both quantum dots are initially above the Fermi level of the single connected lead. The transient dynamics of the system state upon quickly pushing the levels below the Fermi energy are studied. Ideally, the double dot is then charged solely with a spin singlet. In case the dots are not equally coupled to the leads, are detuned in energy or there is a singlet-triplet relaxation mechanism the singlet probability is reduced and a finite probability of triplet occupation appears.

The second scheme consists in connecting each dot to one additional drain lead. This allows a current to be passed through the system. Analogous to the above situation, in the stationary limit singlet occupation is preferred over triplet occupation.

In summary, it is possible to generate an imbalance between singlet and triplet in a non-equilibrium situation by means of the interplay of coherent tunneling and Coulomb interaction. The mechanism is similar to coherent population trapping, which is described in the following section.

Coherent population trapping

The phenomenon of coherent population trapping (CPT) originates from quantum optics [17] but can occur in any quantum mechanical system with two coherent states. It is a quantum mechanical effect in which decay of the system from a specific state is prevented due to interference. The effect consists in the formation of a "dark" state, a coherent superposition of the system states that decouples from driven transitions. In the context of optics it appears in so called Λ-systems (Fig. 2.9(a)

The basic effect requires three states, two ground states ($|1\rangle$, $|2\rangle$) with energies $\epsilon_1, \epsilon_2 < 0$ and one excited state $|0\rangle$ with energy $\epsilon_0 = 0$ (Fig. 2.9(a)). In order to excite the transitions $|1\rangle \leftrightarrow |0\rangle$ and $|2\rangle \leftrightarrow |0\rangle$, the system is exposed to two classical, monochromatic fields of frequencies $E_i = e_i \cos(\omega_i t + \phi_i)$, $i = 1, 2$. These fields, however, are slightly detuned from resonance by an amount $\hbar\delta_i = \epsilon_i - \hbar\omega_i$. Employing the rotating wave approximation the transitions are then governed in the interaction picture by the Hamiltonian $H_I(t) = -\frac{1}{2}\sum_i \Omega_i e^{i(\delta_i t - \phi_1)} |0\rangle\langle i| + \text{H.c.}$ where the strength

of the coupling is defined by the Rabi frequencies Ω_i. Then, the following linear combination of the states $|1\rangle$ and $|2\rangle$ can be defined

$$|\text{dark}\rangle = \frac{1}{\sqrt{\Omega_1^2 + \Omega_2^2}} \left(\Omega_1 |1\rangle - e^{i\phi(t)} \Omega_2 |2\rangle \right) \text{ with } \phi(t) = (\omega_1 - \omega_2)t + \phi_2 - \phi_1. \quad (2.10)$$

It turns out that if both fields are detuned from resonance by an equal amount, $\delta_2 - \delta_1 = 0$, the state $|\text{dark}\rangle$ decouples from the light field, i.e., the system cannot be excited to $|0\rangle$.

An all-electronic realization of CPT was proposed in Ref. [18]. The three levels are naturally represented by three strongly interacting quantum dots in a Λ-configuration, i.e., one dot is coupled to a lead and the other two dots, while the other two dots are connected to a second lead (Fig. 2.9(b)). The inter- and intra-dot Coulomb interaction is assumed to be large enough that the entire system can be occupied by at most a single electron. Electrons entering the system from the source lead can enter the symmetric and antisymmetric combination of the dot levels, $|1\rangle \pm |2\rangle$. The antisymmetric combination corresponds to the "dark state": transitions to the third dot are prohibited by destructive interference. Transport in the opposite direction is always possible. This allows operation of the system as a rectifier.

The counting statistics of the triple dot CPT system have been calculated [19]. Noise is enhanced, since transport is interrupted once the dark state is occupied, so that the system exhibits bunching. A more detailed analysis can be found in Sec. 3.1.1. The influence of an Aharonov-Bohm phase on the transport properties has been discussed in Ref. [20]. There the two dots, which contain the dark state, were also connected directly. The dark state still forms, but the Aharonov-Bohm-phase allows to tune away the destructive interference, leading to periodicities in the counting statistics.

Phase locking

As has been discussed above for the single dot interferometer, the linear conductance of any two terminal interferometer is always an even function of magnetic flux, Eq. (2.9). There it was also mentioned that stronger statements can be made for systems with appropriate symmetries [6]. The double dot interferometer studied in this thesis has such a symmetry. The symmetry arises from a specific choice of the dot-lead coupling strengths: the coupling strengths between a given lead and each of the dots are equal, while the coupling strengths between the double dot and different leads are allowed to be different (Fig. 2.9). Furthermore the dot levels are assumed to be energetically degenerate. As can be seen from the figure, the system is symmetric with respect to a rotation about the horizontal axis. This results in the relation

$$I(V, \phi) = I(V, -\phi), \quad (2.11)$$

which means that the current is even in the magnetic flux. It is straightforward to extend this argument to higher cumulants of the current distribution, so that the entire probability distribution of charge transfer is symmetric under flux reversal.

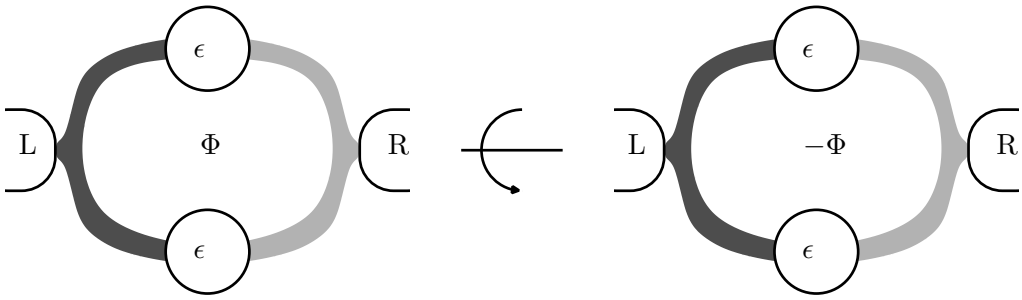

Figure 2.9: The double quantum dot interferometer is symmetric under rotation about the horizontal axis This allows to extend phase locking to arbitrary voltages. The different shading of the arms indicate different dot-lead coupling strengths.

3 Current fluctuations in nanostructures

Due to the granularity of the electronic charge any current measurement is subject to noise. The origins of noise are manifold and may lie in the measurement apparatus, but also in the system itself. Thus, even if the apparatus was working perfectly, the searched for effect might be covered by noise. This is the reason why noise is in general considered a nuisance and measures are taken to reduce its influence. While this is often justified, it overlooks the fact that in some kinds of noise information about the system is encoded. This information may augment information present in the current, so that system parameters are determined more precisely. It may also contain additional information not present in the current. For this reason current noise in mesoscopic systems has been extensively studied [21, 22, 23]. Below, some of the constituents of current noise are discussed. While the first are usually considered disturbances, the last example, the shot noise, contains information about the conduction process.

Current noise is related to the Fourier transform of the current autocorrelator by the Wiener-Khinchin theorem

$$S(\omega) = \frac{1}{2}\int \mathrm{d}t e^{i\omega t}\left\langle \Delta\hat{I}(t+t_0)\Delta\hat{I}(t_0) + \Delta\hat{I}(t_0)\Delta\hat{I}(t+t_0)\right\rangle , \tag{3.1}$$

where the symmetrization is necessary due to the quantum nature of the current operators, $\Delta\hat{I}(t) = I(t) - \langle\hat{I}\rangle$.

3.1 Types of current noise

Transport studies in condensed matter physics are often carried out in semiconductors, in which the generation-recombination or *random telegraph noise (RTN)* can occur. Its origin lies in fluctuations in the number of charge carriers, which are caused by the continuos generation and recombination of electron and hole pairs [24]. If the timescale at which this trapping occurs is labeled τ, the noise has a Lorentzian dependence on frequency, $S(\omega) \sim \tau/(1+\omega^2\tau^2)$ [25]. It can therefore be avoided by measuring at sufficiently high frequencies.

A more obstructive source of noise is the *flicker noise*, which is also called $1/f$*-noise* since it depends on frequency with a power law $S(\omega) = 1/\omega^\alpha$ with an exponent α close to unity. It is a very general form of noise, found not only in electronic systems, but in many physical, biological and even economic systems. The theories for its explanation are as numerous as the situations in which it appears [26]. A frequently applicable model assumes the current to continually switch between two states, caused by, e.g., motion of a scatterer between to stable positions or (de-)ionization of an impurity. Many such bistable impurities will then result in $1/f$-noise [27]. Flicker noise can

be avoided in experiments by measuring at frequencies even higher than necessary to avoid random telegraph noise.

A noise form of more fundamental physical origin is equilibrium noise or Johnson-Nyquist noise. Together with shot noise, it can be explained in terms of the scattering theory [28, 29, 31]. The basic assumption is that the conductor can be regarded as consisting of independent transmission channels, each with a transmission probability T_n. These are found as the eigenvalues of the product of the transmission matrix and its Hermitian conjugate, i.e., in a one-dimensional conductor the transmission T is just the absolute square of the transition matrix element, $T = |t|^2$. With this the conductance of a two terminal device can be written as the product of the transmission probability, the conductance quantum e^2/h and a factor two for spin. The total conductance of the device is then just the sum of the conductances of the independent channels,

$$G = 2\frac{e^2}{h}\sum_{n=1}^{N} T_n. \tag{3.2}$$

In a similar way, an expression for the noise can be calculated. It generally depends on temperature T and bias voltage V [30, 31, 32]:

$$S_{I^2} = 2\frac{e^2}{h}\sum_{n=1}^{N}\left[2k_BT\,T_n^2 \,+\, eV\coth\left(\frac{eV}{2k_BT}\right)T_n(1-T_n)\right]. \tag{3.3}$$

Therein the frequency dependence has been suppressed, as it will always be done in the following, by taking the noise at zero frequency.

The equilibrium contribution (at $V = 0$) was called "Wärmerauschen", i.e., thermal noise, by W. Schottky who first analyzed it during the study of electron noise in vacuum tubes. It is also known as *Johnson-Nyquist noise*, named after the experimentalist [33] and theorist [34], who first studied it in electric circuits. It is frequency independent (up to the quantum limit at k_BT/h) and related to the linear conductance G as $S_{I^2}(V = 0) = 4k_BTG$ according to the fluctuation-dissipation theorem. It is of purely classical origin: in absence of a transport voltage the charge carriers still possess thermal energy, which allows them to pass the junction in both directions. While this does not generate an average current, it still causes current fluctuations. Thermal effects also appear in higher even cumulants of the current distribution function, but not in the odd cumulants. In particular the third moment is insensitive to them.

At higher bias voltages, the influence of Johnson-Nyquist noise steps back behind the *shot noise* (called "Schrotrauschen" by Schottky). This term was coined since the origin of shot noise lies in the granularity of charge. The crossover, described by Eq. (3.3), is shown in Figure 3.1. At high voltages, the noise becomes proportional to the current, which allows to define the quotient of the two $F = S/2eI$, called the Fano-factor [35]. As can be seen from Eq. (3.3), within scattering theory the Fano-factor of a single channel conductor is $F = 1 - T$, i.e., noise is suppressed. This fact is also referred to as partition noise: additional order is introduced in the current, since the incoming electron stream is divided into a reflected and a transmitted part (cf. Fig. 3.2).

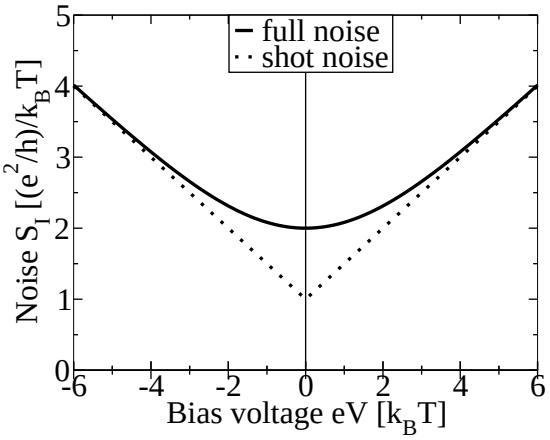

Figure 3.1: Noise of a non-interacting conductor of transmission $T = 1/2$ as obtained from Eq. (3.3). In absence of a bias voltage the equilibrium noise assumes a value of twice the conductance quantum divided by temperature due to spin degeneracy. For large voltages the equilibrium noise is unimportant and noise increases linearly, resulting in a constant Fano-factor $1 - T$.

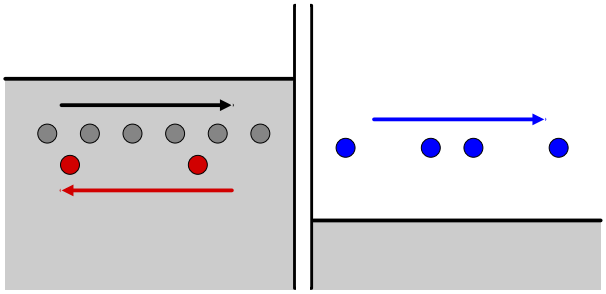

Figure 3.2: Shot noise for a barrier transparency $T = 2/3$, resulting in a Fano factor of $F = 1/3$

Experimental isolation of shot noise is challenging: on the one hand the measurement frequency has to be high enough to overcome $1/f$- and random telegraph noise, but on the other hand at higher frequencis the noise of the measurement apparatus becomes important and may obscure the system's behavior. The first successful measurements were by Reznikov and Kumnar in quantum point contacts [36, 37]. Due to conductance quantization, the transmission probabilities of practically all channels in a QPC are either close to zero or close to unity. Eq. (3.3) then predicts that noise is very strongly reduced. Later a more stringent test could be performed by Cron *et al.* in an aluminum break junction [38]. The junction was considerably narrower, so that only three channels contributed. The measurement conformed very well with the theoretical prediction based on the knowledge of the transmission $\{T_n\}$, known from the current voltage characteristic in the superconducting state.

As will be discussed later (Sec. 3.2.2), in double barrier structures noise is usually reduced, since while one electron occupies the intermediate region, the passage of other electrons is hindered. This effect indeed complicates the observation of full shot noise in mesoscopic, semiconductor based tunnel barriers: it is not unlikely that the tunnel junction contains a localized state (due to impurities or potential disorder). Since this state effectively forms a double barrier structure between the leads, for low transmission of the (intended) tunnel contact transport is dominated by the behavior of the localized state, which leads to noise suppression below the Poissonian value [39, 40] (the reverse may also be true, see below and [41, 42]). Recently however, full shot noise was also observed in semiconductor based barriers [43], simply by making the barriers very small, so that the probability of impurities appearing in the junctions is reduced.

An early success was achieved by Birk *et al.* in ungated structures consisting of nanoparticles between a STM tip and a substrate, nicely demonstrating the crossover from thermal to shot noise [44]. Recent results in self assembled InAs quantum dots also coincide well with theory both if several dots [45] or single dots are contacted [46]. Results for single electron transistors, i.e., gated double barrier structures, were found in carbon nanotubes [47], in a regime where co-tunneling plays an important role. In metallic SETs noise was measured both in high bias regimes [48] and at lower bias voltages, where the influence of Coulomb interaction was clearly visible [49].

3.1.1 Mechanisms of noise enhancement

Usually electronic noise is suppressed below its Poissonian value as mentioned above: the partition noise, caused by electrons being either reflected or transmitted at a junction of a given transmission reduces the Fano factor. The magnitude of suppression is quantified by the Fano factor $F = S/2eI$ (the factor of two arises due to contributions of negative and positive frequencies in Eq. (3.1)) [35]. In the case of uncorrelated events, such as in tunnel junctions of vacuum diodes, the Fano factor assumes the value 1. This is called the Poissonian value, since for a Poisson process all cumulants are equal, $\kappa_1 = \kappa_i$. The generating function is $S_{\mathrm{Poisson}} = t_0\kappa_1(e^{i\chi} - 1)$. A deviation from the Poissonian value is a hint to correlations between the individual transport events.

A suppression of the Fano factor is the usual case, which was also historically first

observed and understood; in general terms it corresponds to correlations due to increased order in transport. Correlations may be introduced by Coulomb repulsion between the charge carriers, but it is strongly screened in metals (and semiconductors). More important for the generation of correlations is the Pauli principle, which prevents double occupation of electronic states and gives rise to Fermi statistics in thermal equilibrium. In vacuum tubes and tunnel junctions it is not influential, since the average occupation of a state is too small. Otherwise, it causes antibunching of electrons - in contrast to photons, which tend to bunch together in the same state due to their Bose statistics. Both bunching for bosons and antibunching for fermions have been experimentally observed in Hanbury Brown-Twiss experiments, even within the same apparatus [50].

Entangled electrons

This does not mean that electrons may never appear in bunches. In fact, the requirement for the Fermi wave function to always be antisymmetric applies to the *total* wave function. Only the spatial component needs to be symmetric for bunching to be possible: If the spin part of the wave function was antisymmetric, the spatial part would automatically be symmetric, resulting in bunching. An antisymmetric spin wave function is realized in a two-particle singlet state $|\uparrow,\downarrow\rangle - |\downarrow,\uparrow\rangle$. Correspondingly singlet states tend to bunch together like bosons, while the other two-particle states, the triplets, show fermionic antibunching.

The effect was observed by injecting particles into a beam splitter and measuring the cross correlations of the outgoing beams [51, 52] and has been predicted to also be visible in the noise [53, 54]. More recently, it was discussed theoretically how the effect manifests itself in the counting statistics of electrons propagating along a single channel [55, 56, 57].

Quasiparticle transport

While the appearance of super-Poissonian noise due to the Pauli principle is rather subtle, more down-to-earth reasons can also result in enhanced noise. The most straighforward examples are those in which quasiparticles are transported that do not carry the elementary charge. In this case the Fano factor is directly related to the number of charges per elementary event. A prominent example of such quasiparticles are Cooper pairs consisting of two electrons such that the elementary transported charge is twice the electronic charge. The charge transferred in an individual transport event is reflected in the Fano-factor (cf. Sec. 3.2) and, indeed, in a superconducting quantum point contact Fano factors of 2 were measured [58] (Fig. 3.3).

However, not in all systems is the current carried by just a single type of charge carrier. It is known, that in superconductor-superconductor junctions multiple Andreev reflection occurs, which results in transmission of multiples of the elementary charge [59, 60]. Another example consists in quantum dots operated in the Kondo regime, where both single- and double-quasiparticle scattering occurs. Since both processes contribute, the Fano factor is neither 1 nor 2, but assumes the intermediate value of 5/3 [61, 62, 63].

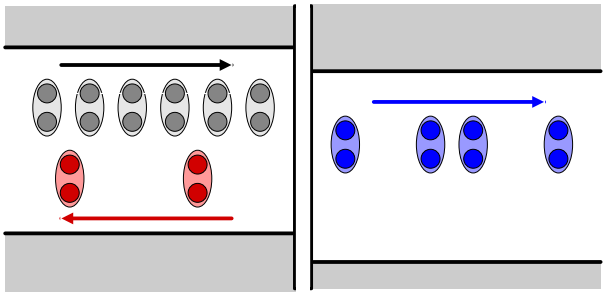

Figure 3.3: Bunching of cooper pairs leads to enhanced noise since the charge transferred in a single event is increased by a factor of two in comparison to electrons.

Interrupted transport

Bunching may also appear if correlations between electrons are not due to an external mechanism that modifies the effective charge, but are rather introduced in the transport process itself. A frequently found mechanism consists in a second level to the level through which transport occurs. The second level interrupts transport by means of Coulomb interaction, when it is occupied. A prototypical example has already been mentioned above: Djuric *et al.* [42] described a system in which one level is coupled to source and drain leads, but also to an additional, otherwise uncoupled level. While Rabi oscillations of a single particle are possible, occupation of both levels costs a charging energy. If the bias voltage supplies energy in excess of the charging energy, the Rabi oscillations become unimportant, since occupation of the lead-coupled dot is always possible. In this case the noise assumes the value expected for a double barrier structure. However, in the regime of single occupation, the noise is enhanced beyond the Poissonian value: The mechanism behind this is essentially that the electron occupying the two levels can not tunnel through the drain, while it occupies the second dot and - on the other hand - no other electron can pass through the lower dot, due to Coulomb interaction. Thus, transport is blocked. Since periods of zero current alternate with periods of finite current, the system exhibits bunching (Fig. 3.4). This kind of bunching is different from the form mentioned above in the context of superconductivity: While there the charge of quasiparticles was larger than the electronic charge, here the charge transferred in a single bunch is undefined and can vary from one to many. Similar effects were predicted in [64] and observed in Refs. [41, 65].

These systems represent the extreme case of systems in which several levels participate in transport with different coupling strengths: one level is completely decoupled. If both levels couple to the leads, transport is not completely interrupted, but occurs on different timescales for the two levels. Such a system has been described by Belzig [66] in an energetically degenerate single level quantum dot with energy conserving tunnel contacts. If the energetic level degeneracy is of the order of the temperature, the drain Fermi level may be tuned such that the two spin states couple with different rates to the drain, since they experience a different occupation of the lead states. Through calculation of the full counting statistics it was even possible to demonstrate that electron

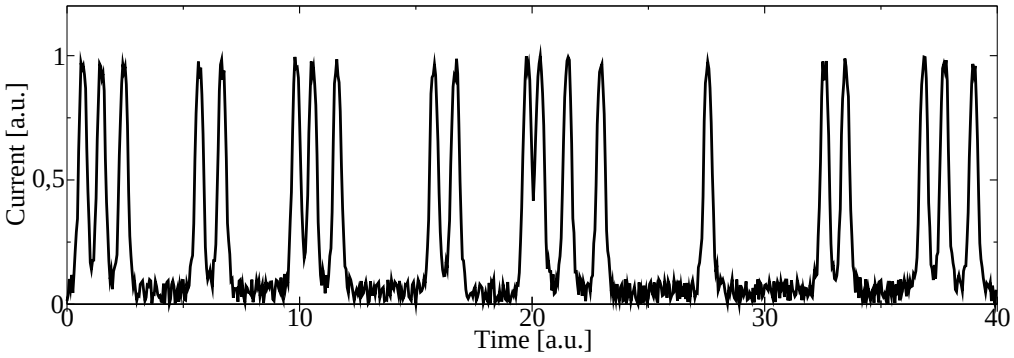

Figure 3.4: Transfer of electrons in bunches leads to super-Poissonian noise also if the bunches are not all of the same size. This contrasts the effect in Fig. 3.3, where quasiparticle transport leads to a Fano factor that equals the multiple of the elementary charge that constitutes a quasiparticle. In the artificially constructed example shown here, the value is only loosely related to the varying number of charges transferred in a bunch.

bunches contribute with any value of charge.

A very similar effect involving several states was observed by Gustavsson *et al.* [67]. In the experiment two levels with similar energies both lie in the thermal broadening of the Fermi distribution of the source lead. Since they are different orbital states and have different spatial extension, these levels couple differently to the leads. For the same reason they influence the tunneling rates for electrons to tunnel in a third state. For proper values of the tunneling rates this leads to the system eventually being trapped in one of the two almost degenerate states for a long time, so that transport is suppressed. Once this trapped state has decayed to the leads, electrons tunnel through the system until the next trapping occurs. This effect is reminiscent of the setup described in Ref. [68], where super-Poissonian statistics were found in a parallel double quantum dot. Similar effects can be expected whenever multiple levels participate in transport. As the internal dynamics get more involved (e.g., in molecules [69, 70]), more and more features appear in current and noise, requiring careful analysis.

Different coupling of specific states can also be obtained by attaching the dot to ferromagnetic leads: the spin-dependent density of states in the leads results in spin-dependent tunneling rates. Depending on the relative alignment and polarization of the lead magnetizations, super-Poissonian noise can occur both with one [71] and two [71, 72, 73] leads being ferromagnetic. In parallel double quantum dots connected to ferromagnetic leads, co-tunneling may result in super-Poissonian noise [74].

At this point it is already clear that the mechanisms for enhanced noise are plentiful and are not restricted to mere Coulomb interaction or different tunneling barriers. Indeed any mechanism that interrupts transport will do the job. Among the more exotic examples are bistabilities [75, 76]. These can for example be realized in nanoelectromechanical systems, such as a quantum shuttle. The system has two different transport

mechanisms: tunneling through the oscillating island and shuttling, i.e., the island's spatial oscillation between source and drain transfers the electrons. At the transition between the two regimes enhanced noise is expected [77]. A similar mechanism, related to phononic degrees of freedom is found in Franck-Condon blockade, where the the transition rates depend critically on the phononic state of the system. The system can be trapped in a low-lying phononic state, since the transition rates for electrons and phonons are suppressed. Once the system has left the ground state, these rates increase, so that, if phononic relaxation is weak, transport increases exponentially due to self-enhancement [78]. Only after relaxation to the ground state transport is suppressed again, so that electrons pass the system in "avalanches". The authors derived a fundamental relation that expresses the Fano factor in terms of the time between transfer of each bunch t and the number of electrons in each bunch N

$$F = \langle N \rangle \frac{\langle t^2 \rangle - \langle t \rangle^2}{\langle t^2 \rangle} + \frac{\langle N^2 \rangle - \langle N \rangle^2}{\langle N \rangle^2}. \tag{3.4}$$

This expression allows to understand the value of Fano factors in different systems. It has been applied in the context of a spin blockade mechanism that occurs in magnetic molecules [79]. It also explains noise enhancement in a system, where electrons are injected onto a quantum dot from a normal source lead, but leave to a ferromagnetic drain lead [71]. For high polarizations the electrons belonging to the minority electrons of the drain are trapped on the dot for a long time, while their probability to be injected is equal to that of the majority spins. Correspondingly the majority spins are transported in avalanches of N electrons with a probability $1/2^N$, giving rise to Fano factor of 3.

In serial double dots [80] an effect known as Pauli spin blockade reduces transport [81, 82]. The scheme is complicated but essentially relies on the fact that with two electrons occupying the double dot in a triplet state, decay to the drain lead is suppressed, while it is possible for the singlet. The studies did not focus on noise, but where rather trying to develop a method for spin to charge conversion, a technique required for spintronics and in quantum information processing. Still, the mechanism should also be able to generate super-Poissonian noise, the value of which is determined by the rate with which the triplet relaxes into a singlet. Furthermore, in serial double quantum dots coherence effects are known to produce enhanced noise [83, 84, 85]

In triple-dot geometries where the dots are set up in a triangular configuration coherent population trapping can occur. An electron can occupy a specific linear combination of two of the levels, the so called dark state. In the case of a symmetric system the dark state is just the antisymmetric combination of the levels. It is called dark since destructive interference prevents its decay into the third dot. In case the system occupies this state, transport is interrupted until the state decoheres. This mechanism was shown to also result in enhanced noise [19].

Enhanced noise in parallel double quantum dots

In parallel double quantum dots with normal leads enhanced noise was predicted by a number of authors who studied spinless electrons with Coulomb interaction between the

dots [86, 87, 88]. In all cases the noise enhancement can be understood by considering the symmetric and antisymmetric combination of the dot levels. The antisymmetric combination of the levels couples less strongly to the leads. Thus, if the antisymmetric state is occupied, Coulomb interaction prevents transport through the other state. This leads to an interruption of transport and, therefore, enhanced noise. In some of the studies the coupling of both states is finite [86, 88]. In contrast, in Ref. [87] the weakly coupled state decouples completely in the case of energetically degenerate dot levels and the Fano factor diverges.

For completeness it has to be mentioned that another author also studied spinless electrons with interdot Coulomb interaction [89] and predicts no super-Poissonian noise, but rather only enhanced normalized cumulants (in particular the third) in the regime of single occupation. The enhancement has to be understood relative to the value in a similar system in which interference is not possible.

Also through the mechanism of channel blockade, driven transitions between two levels may give rise to enhanced noise [90]. The same authors described an effect similar to that in Ref. [66] in parallel double dots, where asymmetric lead coupling due to thermal smearing gives rise to enhanced noise [91].

To the author's knowledge there is only one study predicting enhanced noise in parallel double quantum dots that takes into account the spin of the electron [92]. In this model interdot coupling was assumed. This leads to an energy splitting of the doubly occupied states: the singlet state is lowered in energy compared to the triplet states. For specific voltage settings this energy splitting results in different coupling strengths for singlet and triplet, which in turn result in super-Poissonian statistics. Note that the Fano factor remains finite, in contrast to the results presented in Sec. 6.

3.2 Theory of full counting statistics

The concept of full counting statistics has its origin in quantum optics. Mandel [98] and Cook [99] studied the emission of photons from an atom under the influence of a resonant field that stimulates emission. Later the concept was realized to be useful also in mesoscopic physics, where the transmission of single electrons through a conductor could be counted [100]. The motivation is that the counting statistics might reveal information not contained in the average current and autocorrelator.

Indeed this is possible in the case of diffusive conductors, features were predicted in the frequency dependent third cumulant at a frequency corresponding to the inverse of the diffusion time through the contact [93]. Similar predictions were made for the third cumulant of transport through chaotic cavities: a feature was found at the inverse dwell time of the cavity [94]. This is remarkable in so far as the second cumulant does not contain such information, it rather shows features only at the inverse RC-time of the cavity [95].

It has also been argued that the zero frequency third cumulant allows a more accurate determination of the transmitted charge q of a tunneling quasiparticle, to which it is related as $\kappa_3 = q^2\kappa_1$, also at high temperatures [96, 97].

A statistical process is fully characterized by its probability distribution. The full

counting statistics aims at the calculation of this distribution for the statistics of the charge transferred through a conductor. In this case the probability distribution is given as the probability $P(N,t)$ that N charges have passed the conductor after time t. A quantity that is often easier to calculate than the distribution $P(N,t)$, but contains the same information is the generating function[1][2]

$$S(\chi,t) = \ln\left[\sum_{N=-\infty}^{\infty} e^{iN\chi} P(N,t)\right]. \tag{3.5}$$

This generating function describes the distribution of transmitted particles, not charge. If the statistics of charge was sought for, the transformation kernel would have to be $e^{i\chi eN}$, since each electron carries the charge elementary charge e.

The generating function allows calculation of the n-th cumulant κ_n by taking the derivative with respect to the counting field χ at $\chi = 0$

$$\kappa_n(t) = \frac{\partial^n}{\partial(i\chi)^n} S(\chi,t)\bigg|_{\chi=0}. \tag{3.6}$$

The cumulants are related to the moments $\mu'_k = \overline{N^k}$ (not the centralized moments) by the following recursion formula

$$\kappa_n = \mu'_n - \sum_{k=1}^{n-1} \binom{n-1}{k-1} \kappa_k \mu'_{n-k}. \tag{3.7}$$

This implies that the first three cumulants coincide with the central moments $\mu_n = \overline{(N-\overline{N})^n}$, $n = 1,2,3$.

The first cumulant is just the average transmitted charge, i.e., current times counting time. It represents the peak position of the distribution in Fig. 3.5. The second cumulant of the charge fluctuations is similarly related to current fluctuations by $\kappa_2 = t\, S_{I^2}/e^2$. It represents the width of the distribution. The third cumulant, called skewness, describes the asymmetry of the distribution: The Poisson distribution has positive skewness, which means that the right tail (for larger N) is longer (in other words: the mean is greater than the median). The fourth cumulant is related to the normalized moments as $\kappa_4 = \mu_4 - 2\mu_2^2$. The fourth cumulant divided by the second cumulant κ_4/κ_2 is called kurtosis and measures the sharpness of the distribution's peak: the sharper the peak, the higher the curtosis. Knowledge of these cumulants alone is of limited value in the context of mesoscopic systems. If the charge transported in an elementary transport process is not the electron charge, this is one information that is contained in the low order cumulants: the Fano factor κ_2/κ_1 is proportional to that elementary charge–if only under the condition that the elementary charge is the same for each transport event.

[1] In this definition $S(\chi)$ has a different sign compared to some of the literature, e.g., [23].

[2] Both the cumulant generating function and the shot noise power (Eq. (3.1)) are conventionally labeled S. This convention is also followed in this thesis. Which of the quantities is meant, becomes clear from its arguments.

If several elementary processes with different charges exist, this information cannot be extracted directly from the cumulants, but it is contained in the generating function. since it allows to identify the underlying transport mechanisms. For instance, if the generating function can be written as a sum, all terms of the sum can be understood as generating functions for processes, which are independent from each other. This is readily understood by noting that the probability for the transfer of N charges can be decomposed into K charges having been transferred by process 1 and $N-K$ by process 2. If the two processes are independent, the joined probability is the product of the individual probabilities

$$P(N) = \sum_K P_1(K)\, P_2(N-K). \tag{3.8}$$

Fourier transformation results in the desired relation

$$S(\chi) = S_1(\chi) + S_2(\chi) \text{ with } S_i(\chi) = \sum_N e^{iN\chi} P_i(N). \tag{3.9}$$

A further quantity that is easily extracted from the generating function is the number or particles that are transferred in a single event. It is reflected in the periodicity of the generating function. Assume that only bunches of N_0 charges can be transferred. In other words, the probability for the transfer of any number of particles that is not a multiple of N_0 is zero, $P(N \neq kN_0) = 0$. The generating function can thus be written as

$$S(\chi) = \sum_k e^{i\chi k N_0} P(kN_0) = \sum_N e^{ik\chi N} P(N). \tag{3.10}$$

Correspondingly its periodicity is changed from 2π to $2\pi/k$.

The theoretical approaches for the calculation of counting statistics are to numerous to be mentioned here and only the result of a seminal work by Levitov *et al.* [100] will be discussed in Sec. 3.2.3. For the inclusion of the counting field the concept of a "Larmor clock" was introduced. It consists of a spin that precesses in the magnetic field which is caused by the fluctuating current. The coupling strength between this spin and the current turns out to enter the calculation as the counting field. Each passing electron causes the spin to rotate by a specific angle, so that the total precession angle is related to the number of electrons that have passed. Measurement of the precession angle thus allows access to the cumulant generating function. Within a scattering approach, the statistics of a single channel conductor are derived.

3.2.1 Single barrier: Poisson and binomial processes

Processes in which the system's behavior at a time t depends only on the state of the system at time t and not at earlier times are called Markov processes. Simplifying even further, such that the behavior does not even depend on the system state at time t results in the Poisson process. It is fully described by a rate Γ, with physical examples being vacuum diodes [101] and tunnel junctions.

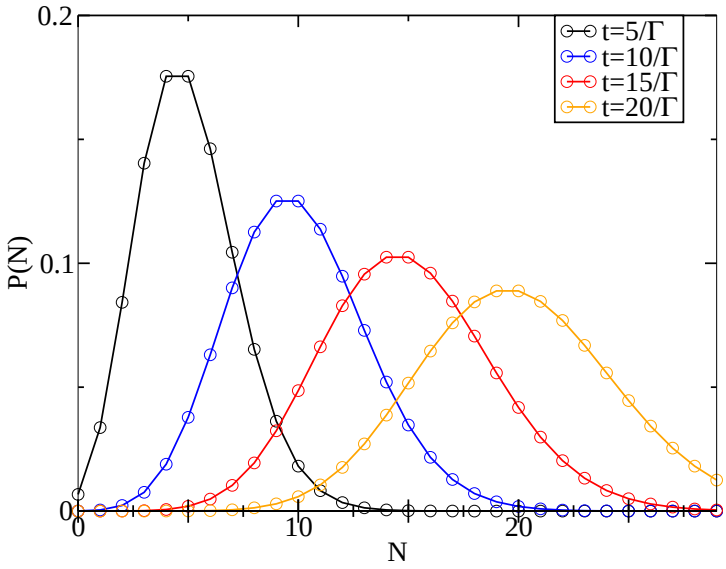

Figure 3.5: The distribution of the Poisson process shifts to higher values of transmitted charge as time increases. At the same time it spreads out and approaches a Gaussian shape due to the central limit theorem. The lines are guides to the eye only.

A master equation may then be formulated for the probability that N charges have been transferred at time t

$$\frac{\mathrm{d}}{\mathrm{d}t}P(N,t) = \Gamma\left[P(N-1,t) - P(N,t)\right]. \tag{3.11}$$

Assuming that transport (and counting) starts at time $t = 0$, the solution is

$$P(N,t) = \Gamma \int_0^t \mathrm{d}\tau e^{-\Gamma(t-\tau)} P(N-1,\tau) + e^{-\Gamma t} P(N,0). \tag{3.12}$$

Inserting the initial values $P(N,0) = \delta_{N,0}$ and $P(N<0,t) = 0$ (since particles are not transferred back) results in

$$P(N,t) = \frac{(\Gamma t)^N}{N!} e^{-\Gamma t} \tag{3.13}$$

This distribution is plotted in Figure 3.5. As time increases the distribution shifts towards higher N and spreads out. The shift occurs linearly with time, such that the maximum after time t lies at Γt.

Fourier transforming the probabilities gives

$$e^{S(\chi,t)} = e^{-\Gamma t} \sum \frac{(\Gamma t e^{i\chi})^N}{N!}, \tag{3.14}$$

so that the generating function is

$$S(\chi,t) = t\,\Gamma(e^{i\chi} - 1). \tag{3.15}$$

It is obvious that all cumulants are proportional to time and equal to each other,

$$\kappa_n = t\,\Gamma. \tag{3.16}$$

This explains the shift and spreading out of the distribution in Fig. 3.5. It implies that the cumulants, normalized to the average current, are all equal to unity, $\kappa_n/\kappa_1 = 1$. Since the Poisson process describes uncorrelated events, it serves as a useful reference point to characterize correlated events, for which noise may be in- or decreased.

Such correlations can be introduced by simply changing the number of particles transferred in a single event [102] (see also Sec. 3.1.1). An example is the fractional quantum Hall regime, in which the Fano factors 1/3 [103, 104] and 1/5 [105] have been reported. Other examples, in which noise is enhanced, have already been discussed in Section 3.1.1.

The Poissonian distribution is a special, limiting case of the binomial distribution. The binomial distribution describes the statistics of events with two outcomes, like tossing a coin, or–more physically–passing a barrier. While for the coin toss the two outcomes have equal probability, a barrier is described by probabilities for transmission $0 \leq T \leq 1$ and reflection $R = 1 - T$. This is reminiscent of the discussion of noise within the scattering theory in the previous section 3.1. Indeed, the partition noise $T(1-T)$ is also found as second moment of the binomial statistics.

The binomial distribution is

$$P(N) = \binom{M}{N} T^N (1-T)^{M-N}, \tag{3.17}$$

where $M = t\,eV/h$ denotes the number of attempts. Its expectation value is MT, its second moment $MT(1-T)$, in accord with the scattering theory results from above. The generating function of the binomial distribution is a bit harder to find than for the Poisson process, but readily written as

$$S(\chi) = M \ln\left[1 + T(e^{i\chi} - 1)\right] \tag{3.18}$$

It is clear that for small transmissions $T \ll 1$ the statistics of a tunnel process, i.e., Poissonian statistics should be recovered. While this relation is not at all clear from the distributions $P(N)$, is is easy to see from the generating functions: Merely expanding Eq. (3.18) does the job and results in Eq. (3.15), identifying $M = T\,\Gamma\,t$.

3.2.2 Double barrier: master equation description

The next question to ask after knowing the statistics of transport through a single barrier is how transport through a double barrier takes place. The simplest realization of a double barrier system is a single level quantum dot, which can be empty or occupied by a single particle. This system has been described in the literature in detail, even for spinful and interacting particles [111], but it is instructive to give a basic derivation here for non-interacting and spinless particles. Describing the occupations by a vector $\mathbf{P}(N,t) = (P_0(N,t), P_1(N,t))$ and assuming that the level is always only filled from

one lead with a rate Γ_L and emptied to another lead with rate Γ_R, a master equation can be formulated, this time in matrix form:

$$\frac{\mathrm{d}}{\mathrm{d}t}\mathbf{P}(N,t) = \begin{pmatrix} -\Gamma_L & 0 \\ \Gamma_L & -\Gamma_R \end{pmatrix} \mathbf{P}(N,t) + \begin{pmatrix} 0 & \Gamma_R \\ 0 & 0 \end{pmatrix} \mathbf{P}(N-1,t) \tag{3.19}$$

In order to find the solution of the equation it is helpful to perform a Fourier transformation with respect to the transferred charge N. This introduces the counting field χ in the kernel $\mathbf{W}$.

$$\begin{aligned} \frac{\mathrm{d}}{\mathrm{d}t}\mathbf{P}(\chi,t) &= \begin{pmatrix} -\Gamma_L & 0 \\ \Gamma_L & -\Gamma_R \end{pmatrix} \mathbf{P}(\chi,t) + e^{i\chi} \begin{pmatrix} 0 & \Gamma_R \\ 0 & 0 \end{pmatrix} \mathbf{P}(\chi,t) && (3.20) \\ &= \mathbf{W}(\chi)\,\mathbf{P}(\chi,t) \quad \text{with } \mathbf{W}(\chi) = \begin{pmatrix} -\Gamma_L & e^{i\chi}\Gamma_R \\ \Gamma_L & -\Gamma_R \end{pmatrix} && (3.21) \end{aligned}$$

The appearance of the counting factor $e^{i\chi}$ in the component responsible for the transition that leads to a change in the number of transferred particles justifies why later, in Sec. 4.2, the counting field is introduced in the tunnel matrix elements of the Hamiltonian.

The solution is easily found to be $\mathbf{P}(\chi,t) = e^{t\mathbf{W}(\chi)}\mathbf{P}_{\mathrm{in}}$, with the initial state $\mathbf{P}_{\mathrm{in}}$. The kernel $\mathbf{W}(\chi)$ can now be spectrally decomposed $\mathbf{W} = \sum_i \mathbf{p}_i \lambda_i \mathbf{q}_i^T$. In order to be physical, all eigenvalues have a negative real part, so that their contributions to $\mathbf{P}$ decay with time. For long times t the eigenvalue λ_0 with maximum absolute value of the real part dominates, so that the generating function can be obtained as

$$e^{S(\chi)} = \mathbf{e}^T\mathbf{P}(\chi) = \mathbf{e}^T e^{\mathbf{p}_0\, t\lambda_0\, \mathbf{q}_0^T}\mathbf{P}_{\mathrm{in}} \tag{3.22}$$

where $\mathbf{e}^T = (1,1)$. Since $\mathbf{p}_0$ and $\mathbf{q}_0$ are left and right eigenvectors, their outer product is a projector and the generating function becomes

$$S(\chi,t) = \ln\left(e^{t\lambda_0}\,(\mathbf{e}^T\cdot\mathbf{p})(\mathbf{q}_0^T\cdot\mathbf{P}_{\mathrm{in}})\right) = t\lambda_0 + \text{const.} \tag{3.23}$$

The constant is irrelevant for the calculation of the moments and thus the entire statistics. The eigenvalue of the two-dimensional matrix $\mathbf{W}(\chi)$ is straightforward to obtain,

$$S(\chi,t) = t\,\frac{\Gamma_L+\Gamma_R}{2}\left(1-\sqrt{1+\frac{4\Gamma_L\Gamma_R}{(\Gamma_L+\Gamma_R)^2}(e^{i\chi}-1)}\right). \tag{3.24}$$

The Fano-factor of transport through a double barrier thus is

$$\begin{aligned} \frac{\kappa_2}{\kappa_1} &= \frac{\Gamma_L^2+\Gamma_R^2}{(\Gamma_L+\Gamma_R)^2} && (3.25) \\ &= \begin{cases} \frac{1}{2} & \text{for } \Gamma_L = \Gamma_R \\ 1 & \text{for } \Gamma_L \gg \Gamma_R \text{ and } \Gamma_L \ll \Gamma_R \end{cases} && (3.26) \end{aligned}$$

The introduction of a second barrier thus leads to a reduction of the current noise. With each additional barrier, noise will be reduced further and further. This has been

exploited by various authors to calculate the noise of a disordered wire, treating the wire as an infinitely long chain of barriers [106, 107, 108], in which the Fano factor is known to assume the value 1/3 [109].

Equation (3.24) is essentially the shot noise limit of the generating function found as early as in 1996 by de Jong [110]. The difference lies in a factor of two, since de Jong assumed two independent (spin) channels. While here only transport from left to right lead was assumed, in the reference the generating function for a non-interacting tunnel coupled quantum dot was calculated allowing for arbitrary bias voltages. This results in a second term for transport in the opposite direction and "blocking factors" consisting of Fermi functions:

$$S(\chi,t) = t\,(\Gamma_L+\Gamma_R)\left(1-\sqrt{1+\frac{4\Gamma_L\Gamma_R}{(\Gamma_L+\Gamma_R)^2}\left[f_L(1-f_R)(e^{i\chi}-1)+(1-f_L)f_R(e^{-i\chi}-1)\right]}\right), \tag{3.27}$$

where the Fermi functions are taken at the energy of the dot level. This result was rederived by Bagrets *et al.* in Ref. [111] using a matrix technique that allowed also the description of strong Coulomb interaction on the dot.

The generating function of the double barrier system fulfills the fluctuation-dissipation relation that relates equilibrium noise and linear conductance:

$$\kappa_2(V=0) = \left.\frac{\partial\kappa_1}{\partial V}\right|_{V=0}. \tag{3.28}$$

3.2.3 Levitov formula

A different approach to FCS for non-interacting particles is based on the scattering theory [28, 29, 31]. While the noise calculations discussed earlier were based on the explicit evaluation of current autocorrelators, for the calculation of the counting statistics a different technique has to be developed: a detector has to be coupled to the conductor that counts each charge as it passes the system. Levitov *et al.* used a precessing spin for this purpose [100]: the spin is coupled to the current operator via a coupling parameter which turns out to be the counting field. With this it was possible to derive the generating function for transport of noninteracting electrons through an arbitrary two-terminal setup in terms of the energy-dependent transmission probability $T(\omega)$ per spin channel [100, 112],

$$\begin{aligned} S(\chi,t) &= 2t\int\frac{\mathrm{d}\omega}{2\pi\hbar}\ln\Big\{1+T(\omega)\Big[f_L(\omega)[1-f_R(\omega)](e^{i\chi}-1) \\ &\quad +[1-f_L(\omega)]f_R(\omega)(e^{-i\chi}-1)\Big]\Big\}, \end{aligned} \tag{3.29}$$

where $f_L(\omega)$ and $f_R(\omega)$ are the Fermi functions of the left and right leads, respectively. This result implies that electrons at different energies are independent, since the total generating function is just the integral of contributions for each energy. Since the spin channels are also independent, a factor of two appears outside the integral.

The first and second cumulant of this distribution are

$$\kappa_1 = 2t \int \frac{\mathrm{d}\omega}{2\pi\hbar} [T(\omega)(f_L(\omega) - f_R(\omega))] \tag{3.30}$$

$$\kappa_2 = 2t \int \frac{\mathrm{d}\omega}{2\pi\hbar} [T(\omega)\,(f_L(\omega)(1 - f_L(\omega) + f_R(\omega)(1 - f_R(\omega))] + T(\omega)(1 - T(\omega))[f_L(\omega) - f_R(\omega)]^2 \tag{3.31}$$

These are the same as obtained by direct calculation, (Eqns. (3.2),(3.3)). The first part of κ_2 constitutes the Johnson-Nyquist Noise, while the second part is the shot noise contribution.

The first cumulant of current is the ordinary result known from scattering theory: the current is proportional to the barrier transmission. The second cumulant also recovers a known result: the partition noise. Interesting properties appear at first in the third cumulant. In the shot noise regime ($f_L = 1$, $f_R = 0$) it reads

$$\kappa_3 = M\,T(1 - T)(1 - 2T) \tag{3.32}$$

where $M = t\frac{e}{h}V$ denotes the number of attempts under an applied voltage V. For transmissions larger than 1/2 the third cumulant becomes negative. While negative cumulants do not appear in a Poissonian process they are by no means unusual for other statistics. The fourth and higher cumulants of the double barrier system, for instance, becomes negative for specific parameter. Merely the second cumulant is positive in any system.

3.3 Measurement of full counting statistics

Noise measurements are always challenging due to unwanted contributions in the noise. Some of these, originating from the system itself have been discussed above (e.g., $1/f$-noise). Others may originate from the measurement setup, since current and voltage sources are unable to provide a stable signal. Matters are further complicated since practically all probability distributions converge towards a Gaussian distribution for large N. This means that high cumulants are suppressed and become increasingly hard to measure for long measurement times. Also, the condition $k_BT \ll eV$ requires that the sample remains cool while a high voltage is applied.

In the following sections three measurement schemes for higher cumulants will be reviewed. The first approach relies on conventional noise measurements. It runs into the problem of large feedback effects of the measurement apparatus on the sample which completely obscure the desired signal. The second section discusses the use of threshold detectors for current fluctuations and their realization in Josephson junctions. The third section finally discusses a series of experiments that have successfully measured the counting statistics of specific systems containing quantum dots, by observing the individual electrons passing the system in real time. It should be mentioned that a fourth approach is discussed in the literature, which relies on coupling the system under study to two level systems (double quantum dots). Also within this scheme feedback effects have been addressed.

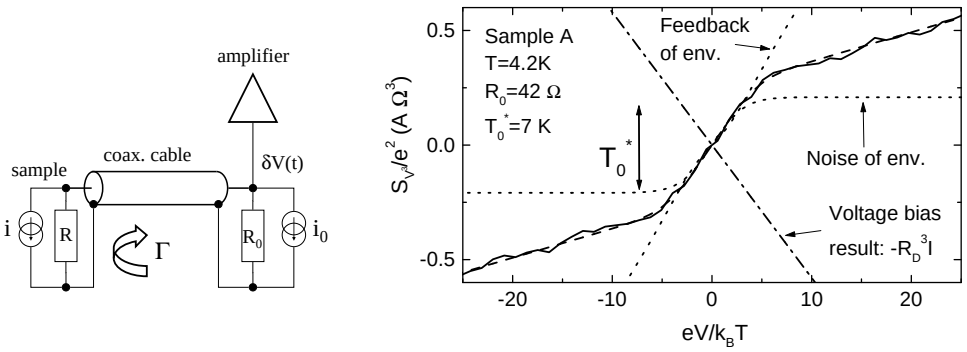

Figure 3.6: Replacement circuit for the experiment of Ref. [113] and third moment as a function of bias voltage for one of the measured samples.

3.3.1 Conventional noise measurements

An experiment that received much attention in its day, attempting to measure the third cumulant in a current biased tunnel junction, was carried out by Reulet [113]. As it turned out in the analysis, the sample could not be regarded as fully current biased, nor as voltage biased, which gives rise to complicated corrections. A tunnel junction was chosen, since its statistics are well known, so that the third moment that was to be extracted from the measurement was known. The idea was to apply a current bias to the sample and measure the voltage fluctuations. This does not result in the same statistics as a measurement under voltage bias [114, 115] for which Poissonian statistics are expected for a tunnel barrier. Instead, the voltage fluctuations under current bias follow a Pascal distribution. Still, the mean current and voltage are trivially related by Ohm's law and the second moments are related by a simple scaling factor, which depends on the device impedance. The third and higher cumulants, however, receive corrections that are related to lower cumulants. The origin of these contributions lies in the fact that the sample's own current fluctuations induce a current drop over the devices impedance, resulting in additional voltage fluctuations. The sample to be measured can be modeled as a resistor R in parallel with current generator i (Fig. 3.6). This current generator represents the fluctuations in current caused by the internal dynamics of the sample and thus i constitutes the quantity that is to be measured. In exactly the same way the measurement apparatus can be modelled by its finite impedance Z and a noise generator i_0 in parallel. Since these two devices are operated in parallel, the total impedance of the circuit is $R_D = ZR/(R+Z)$. Correspondingly the measured voltage V under current bias fluctuates as $\delta V = -R_D(i+i_0)$. This results in the voltage fluctuations being given as the rescaled current fluctuations (as mentioned above), plus an additional term for noise originating from the measurement device

$$S_{V^2} = R_D^2\left(S_{I^2} + S_{i_0^2}\right) \tag{3.33}$$

$$S_{V^3} = -R_D^3 S_{I^3} + 3R_D^4 S_{i_0^2}\frac{\mathrm{d}S_{I^2}}{\mathrm{d}V} + 3R_D^4 S_{I^2}\frac{S_I^2}{\mathrm{d}V} \tag{3.34}$$

The third moment of voltage fluctuations is related to current fluctuations by the same rescaling (first term), receives a term for voltage fluctuations induced by the environment as above (second term) and also a contribution for the sample's own current fluctuations (third term). The analysis is further complicated by the fact that signals in the coaxial cable, which connects sample and detector have a finite propagation time, which becomes important at the high measurement frequencies.

In total, the undesired contributions turned out to be considerably larger than the original signal, resulting in totally different behavior (the curve even has opposite slope for one sample!).

A later experiment by Bomze *et al.* was performed in the voltage biased regime (by increasing the junction resistance far beyond the input resistance) and was able to accurately measure Poissonian statistics [116]. This experiment was precise enough to be able to disprove predictions of a "quantum regime" for noise at low frequencies [117]. For this "quantum regime" it was predicted that, similar to the Johnson-Nyquist noise, zero point fluctuations should result in additional noise, which would—in contrast to thermal noise—affect also the third cumulant.

As a side remark it should be mentioned that it can easily be verified which moment of fluctuations is actually measured, since each moment has a unique dependence on the measurement bandwidth. Labeling the lower boundary frequency f_1 and the upper f_2, the second moment is just proportional to the bandwidth $f_1 - f_2$, while the third is proportional to $(f_1 - 2f_2)^2$.

3.3.2 Josephson junction detectors for higher cumulants

Tobiska and Nazarov suggested the use of threshold detectors for the measurement of counting statistics [118]. Higher moments have little influence on the distribution $P(N)$ in the vicinity of its peak, but rather affect the tails. Since the tails are exponentially suppressed, the measurement of higher moments requires the detection of very rare events. The idea is such that the detector gives a signal if the current exceeds a certain threshold value during the measurement time. Josephson junctions can fulfill this purpose. They consist of two superconductors in close proximity. A current lower than the critical current I_c can be passed through the junction without inducing a voltage drop. If the critical current exceeds this threshold value, the current is always associated with a voltage, which is given by Ohm's law for high currents. The system dynamics can be understood as a particle in a tilted washboard potential

$$U(\phi) = -E_J \cos\phi - (\hbar I/2e)\phi$$

with $\phi = \phi_1 - \phi_2$ being the phase across the junction [119].

The particle can be excited out of the potential wells, by application of a current to the junction higher than the critical current I_c. This leads to a voltage drop across the junction. Detection of the voltage drop thus indicates that the current exceeded a threshold. Such excitations originate naturally from a finite temperatures. Correspondingly the temperature of the sample can be measured by sweeping the bias current and recording the probability of a voltage pulse for each bias current. The same principle can of course be used to measure fluctuations of the bias current [120].

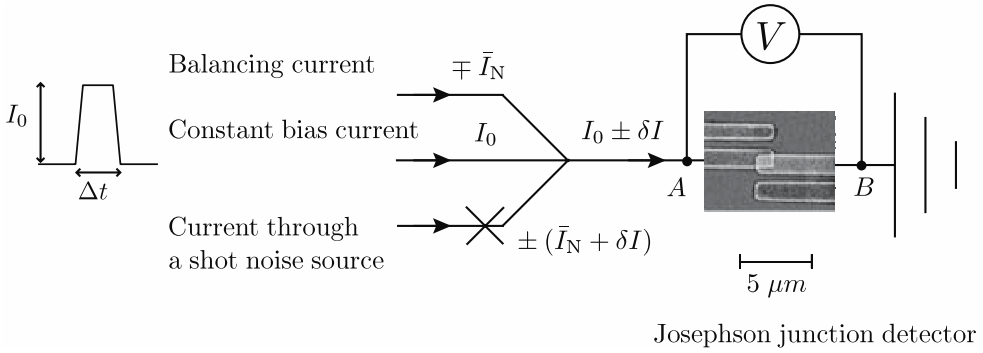

Figure 3.7: Setup of Ref. [124] for using a Josephson junction as a threshold detector for the fluctuations δI of the noise source.

In a different regime of the Josephson junction, the excitation above the barrier is less important and particles tunnel through the barrier instead of being excited over it. This effect is referred to as macroscopic quantum tunneling. The noise of the input current can be accessed since it affects the shape of the potential [121, 122].

A concrete setup is shown in Fig. 3.7. Three input currents are injected. The first one $I_N + \delta I$ originates from the conductor to be studied and delivers the current fluctuations. Since it also injects an average current I_N, the negative current $-I_N$ is also injected, such that (ideally) only the fluctuations remain. A third current I_0 is required to tune the junction close to its critical current such that the small fluctuations can excite a voltage pulse. The measurement scheme consists in applying several times a current I_0 for a certain duration and counting how often a voltage pulse occurs. This corresponds to probing one tail of the distribution. The opposite tail can be probed by reversal of I_0. Since odd cumulants affect the tails differently this allows extraction of the third cumulant, but also even cumulants can be measured with Josephson junctions [123].

3.3.3 Real-time detection of electrons by a QPC

Real-time detection of electrons in mesoscopic systems is a challenging task for two reasons. Firstly the electronic charge is very small, so that very precise detectors are required. Secondly electron dynamics are very fast, with timescales ranging between pico- and microseconds. Observation of electron transport in real time has nonetheless become possible in the last decade.

The historically first motivation for counting of single electrons was found in the context of metrology [125, 126]. For this purpose it was important to generate a stream of electrons as noiseless as possible. The ordered stream of electrons was created by a series of junctions through which electrons pass one after the other, so that they exit to the drain at a fixed frequency f. At this point, a single electron transistor (SET) takes over the actual measurement task by detection of each single electron. Since SETs are very sensitive to their electrostatic environment they allow very precise and fast detection of the electrons [127]. The current carried by these electrons is $I = ef$.

These experiments have little to do with noise measurements—in fact the reverse is true: measures where taken to actively reduce noise in the system under study: the stream of electrons. Yet, the experiments demonstrated the possibility to detect single electrons in real time (at frequencies up to 10 MHz).

The fact that a SET allows very accurate determination of the number of electrons on it has been exploited also in measuring the charge of a single quantum dot directly connected to source and drain [128]. Owing to the high bandwidth of the SET-detector, real-time detection of electrons passing the quantum dot was possible. While this setup is not relevant for metrology, it allowed extraction of the quantum dot's tunneling rate and occupation probabilities from the time trace of the dot's occupation, which were recorded with a bandwidth of still 1 MHz.

Despite the great success of SETs in the real-time detection of electrons, for the analysis of counting statistics a different detector device was used: the quantum point contact. It has been described as early as in 1989 [129] and realized in 1993 [130] how a quantum point contact side coupled to a quantum dot is able to detect the electronic state of the dot. The mechanism is similar to that of detection with SETs: The transmission of the QPC is very sensitive to its electric environment. It is usually tuned by adjusting the voltages on plunger gates that control the width of the constriction. However, not only the negative potential of the plunger gates affects the transmission—also charges in the vicinity, i.e., on a quantum dot, reduce the transparency of the QPC. If the gate voltages are tuned such that only one channel is open in the QPC and that this channel's transmission is near 1/2, the QPC current is very sensitive to additional charges, so that already a single electron will block transmission through the QPC. By observing the time trace of the QPC current it is thus possible to observe electrons charging and discharging the dot.

This technique has been used in the context of quantum information processing where single shot read-out of individual spins is of great importance [131, 132]. Nonetheless it is also useful for the measurement of full counting statistics: since the time evolution of the dot's occupation is known, it is possible to reconstruct the probability distribution of charge transfer. In order to be sure that electrons enter the dot always from one lead and leave always to the other it is advisable to apply a high bias voltage to the dot (In absence of a bias voltage, analysis of the time trace yields nothing but Johnson-Nyquist noise [67]). In the large bias regime however the statistics of the system can be reproduced from the time trace alone [133, 134]. What is more, this matching was achieved without fitting parameters, since the tunnel rates to source and drain can also be reconstructed from the time trace, by measuring the time spans between two consequent jumps of the current. These times correspond to the tunneling times and follow an exponential probability distribution [67, 133].

The restriction to the high bias regime was necessary since the QPC detects only that electrons occupy the dot but is insensitive to the direction from which they come or to which they leave. This restriction can be overcome, if a serial quantum dot is measured [135]. The QPC is placed so close to both dots that an electron occupying either of the dots influences the transmission. However, the dots affect the QPC transmission differently, resulting in the current taking on three distinct values: one for an electron in the first dot, another for an electron in the second dot and a third for both dots being

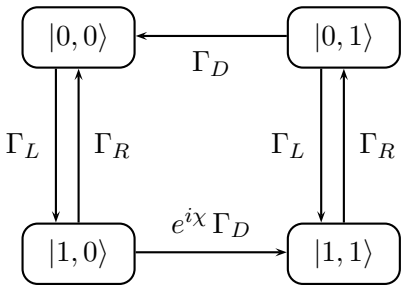

Figure 3.8: Motion of the finite-bandwidth detector.

empty. Since electrons tunnel from the lead only onto the nearest dot (co-tunneling through the dots is suppressed) it is known in which direction an electron traverses the system and the requirement of high bias voltages can be dropped.

QPC-charge detectors for counting statistics have also been employed to observe co-tunneling effects in serial double dots [136, 137]. In the latter case, the electrons could propagate along two different paths in the co-tunneling process, so that an Aharonov-Bohm effect could be observed. It has also been possible to realize a DQD detector for frequency selective photon-noise [138] as suggested in Ref. [139]. Furthermore it has been demonstrated how cross-correlation measurements can be used to reduce the QPC-current and still maintain the same signal-to-noise ratio [140]. This is feasible since it reduces the backaction of the QPC on the system. Finally, the same detector could be implemented in graphene [141].

Finite bandwidth detector

The noise measured by the QPC detector is slightly lower than expected. The reason lies in the finite bandwidth of the detector: if two tunneling events occur in quick succession, i.e., the dot state changes only for a very short time, the detector is too slow to notice and an electron has passed the system without being detected. In order to describe this effect the counting statistics has to be calculated with specific consideration of the detector [142, 143]. The key idea lies in doubling the system's Hilbert space by introducing states $|\alpha,\beta\rangle$, where α labels the states of the system under study and β labels the state of the detector. The high-current state corresponding to an empty dot is called $\beta = 0$, the low-current state with an electron on the dot $\beta = 1$. If additional detector states are needed (e.g., for the double dot system of Ref. [135]), they can be incorporated in the same way.

Modeling the detector motion requires the introduction of an additional rate Γ_D with which the detector follows the system state. For the quantum dot example of Ref. [143] the transitions are illustrated in Fig. 3.8. The dot is charged with rate Γ_L and discharged with rate Γ_R. This happens regardless of the detector state. In order to obtain the counting statistics of the detector, the transitions $|1,0\rangle \to |1,1\rangle$ are counted. These describe the detection of the occupied dot. Calculation of the counting statistics for this model can be carried out as usual.

The counting statistics obtained in this way for a quantum dot in the shot noise

regime do not coincide with Eq. (3.24):

$$S(\chi,t) = -t\,\frac{\Gamma_L+\Gamma_R+\Gamma_D}{2}\left(1-\sqrt{1+\frac{4\Gamma_D}{(\Gamma_L+\Gamma_R+\Gamma_D)^2}\frac{S_{\mathrm{dot}}(\chi,t)}{t}}\right) \tag{3.35}$$

where S_{dot} denotes the generating function of Eq. (3.24) [143, 144]. The moments of this distribution are suppressed in comparison to those of the ideal statistics expected for an errorless detector. This has also been experimentally verified in Ref. [144] for cumulants up to fifth order.

4 Counting statistics of tunnel coupled systems

This chapter introduces the techniques used in this thesis for the calculation of the counting statistics of tunnel coupled, interacting systems. Central to the approach is a real-time diagrammatic technique, which allows the description of non-equilibrium transport phenomena in nanoscale systems. The system is split up in reservoir regions and interacting regions (quantum dots), which are weakly coupled. The time evolution of the system is described by a generalized master equation for the reduced density matrix of the interacting region. The kernel of this integro-differential equation can be calculated by a systematic perturbation expansion in the tunnel coupling strength, as described in the first section of this chapter.

In the second section this approach is extended to be suitable for the calculation of full counting statistics. For this purpose all quantities are also made dependent on N, the number of transferred charges. Then, the generating function can be related to one of the eigenvalues of the the master equation's kernel. Since the eigenvalue is in general impossible to obtain analytically for matrices of dimensions higher than four[1], an alternative, recursive scheme for the calculation of the cumulants is introduced.

4.1 Real-time transport theory

The study of transport through interacting systems is not a simple task and calls for simplifications. It is generally useful to split the system up into an interacting and a non-interacting part. Depending on the coupling of these parts, different formalisms are applicable [146, 147, 148]. Both experimentally relevant and theoretically interesting is the case of weak, i.e., tunnel coupled leads, that inject and extract electrons into the interacting region. Under these circumstances the simplest approach is the golden rule theory, also called "orthodox theory". It is a lowest order perturbation theory, which captures only sequential tunneling (cf. Sec. 2.2)[2, 149, 150, 151, 152].

The orthodox theory reaches its limits when higher order processes play a role. This happens for larger tunnel couplings, e.g., when the Kondo effect comes into play, but also at intermediate coupling strength in the co-tunneling regime, when the lead potentials are not in resonance with the energy levels of the intermediate system, so that Coulomb blockade occurs. An extension to higher orders is required for the description of co-tunneling, asking for more advanced techniques. Additionally, also in lowest order perturbation theory the orthodox theory runs the risk of missing effects [153],

[1] The eigenvalues of five-dimensional matrices can be solved using Jacobi's theta function [145]. The solutions obtained in this way are of limited value for the calculation of counting statistics.

which, although present in the Hamiltonian [154] might not be expected to appear in lowest order perturbation theory.

The diagrammatic method introduced in this section allows to systematically extend the perturbation theory to higher orders of the coupling, e.g., the co-tunneling regime [16, 155, 156, 157]. Under specific circumstances even a resummation of diagrams for arbitrary orders in the coupling strength can be carried out. This is the case in the resonant tunneling approximation [158, 159] and in presence of superconducting leads with a large order parameter [160]. The approach starts from a formally exact equation for the reduced density matrix of the interacting region. In particular it describes the complete density matrix, i.e., also off diagonal elements [15, 153, 155, 161]. The kernel of this equation is expressed as a series of irreducible diagrams on the Keldysh contour and calculated via a set of rules that are specific to the system [162, 163, 164] For the calculation of the counting statistics they contain in particular prescriptions on how to include the counting factors. In absence of these component the kernel can be interpreted as generalized transition rates or self-energies.

In the following sections a Hamiltonian for several single level quantum dots tunnel-coupled to leads will be introduced, allowing also for additional direct coupling of the leads. The perturbative expansion of the generalized master equation is then performed and the set of rules is given.

4.1.1 Model for a quantum dot with two leads

Two systems are to be examined in this thesis, both consisting of (one or two) quantum dots connected to two electronic reservoirs. Therefor, for the introduction of the diagrammatic technique a model is chosen which allows to describe both. Despite this specification, the method can be applied to a broader range of systems including metallic islands [157], superconducting [160, 165] and ferromagnetic leads [153, 161] and transport regimes (e.g., pumping [166, 167, 168, 169]). Its key idea is to split the system into reservoirs and an (interacting) intermediate region and integrate out the reservoir degrees of freedom to obtain an exact kinetic equation for the density matrix of the intermediate system. The kernel of this integro-differential equation can then be calculated by means of a systematic perturbation expansion in the system-lead coupling [162, 163, 164].

Correspondingly the Hamiltonian is in general split up into three parts, describing leads (H_{res}), intermediate region (H_{sys}) and tunnel coupling (H_T):

$$H = H_{\mathrm{res}} + H_{\mathrm{sys}} + H_T \tag{4.1}$$

The first part H_{res} is a sum of contributions for each reservoir r. Each contribution H_r describes a reservoir of non-interacting electrons in thermal equilibrium

$$H_{\mathrm{res}} \sum_r H_r = \sum_r \sum_{k,\sigma} \epsilon_{rk\sigma}\, a^\dagger_{rk\sigma} a_{rk\sigma}\,, \tag{4.2}$$

where $a^\dagger_{rk\sigma}$ and $a_{rk\sigma}$ are creation and annihilation operators for electrons in reservoir r with momentum k, spin σ and energy $\epsilon_{rk\sigma}$.

The intermediate region in the present case consists of several single-level quantum dots, which are modeled by the Anderson Hamiltonian for a spin-degenerate level with Coulomb interaction

$$H_{\mathrm{sys}} = \sum_i \sum_\sigma \epsilon_i \, c_{i\sigma}^\dagger c_{i\sigma} + U_i n_{i\uparrow} n_{i\downarrow} \,, \tag{4.3}$$

where $c_{i\sigma}^\dagger$ and $c_{i\sigma}$ are the creation and annihilation operators for the dot. The energy levels ϵ_i are assumed to be spin independent. A further assumption is made with regards to the interaction: while electrons on the same quantum dot are subject to the Coulomb interaction U_i, electrons on different dots are regarded as non-interacting. In principle such an interaction could also be introduced. Since its impact on the further argumentation consists only in limiting the class of allowed diagrams and it leaves the general arguments unchanged, such an interaction is neglected, in particular since in the systems studied in Chapters 5 and 6 no such interaction is required.

The third part $H_T = H_{T_1} + H_{T_2}$ describes spin conserving tunneling of electrons between the reservoirs and the intermediate system

$$H_{T_1} = \sum_{r,i,k,\sigma} t_{rik} a_{rk\sigma}^\dagger c_\sigma \; + \mathrm{H.c.} \tag{4.4}$$

and direct tunneling between the leads (required for the single dot interferometer in Ch. 5)

$$H_{T_2} = \sum_{\substack{r \neq s \\ k_1, k_2, \sigma}} \tilde{t}_{rs} a_{rk_1\sigma}^\dagger a_{sk_2\sigma}. \tag{4.5}$$

The counting fields are introduced by replacing the tunneling amplitudes as $t_{rik} \to t_{rik} e^{\pm i\chi_{ri}}$ and $\tilde{t}_{rs} \to \tilde{t}_{rs} e^{\pm i\chi_{rs}}$. The sign of the counting field depends on the branch of the Keldysh contour on which the tunneling term appears. Details will be given in Sec. 4.1.3 on page 49. Details on the relation between the counting field for the junctions χ_r and the counting field χ for transport through the system as a whole can be found in Chapters 5 and 6.

In lowest order perturbation theory several golden rule transition rates can be constructed from these Hamiltonians. The lowest order for transport through the dot is described by the rate $\Gamma_{ri}/\hbar = 2\pi/\hbar \sum_k |t_{rik}|^2 \delta(\omega - \epsilon_{rk})$. Combining terms from Eq. (4.4) and Eq. (4.5) results in the lowest interfering order from Ch. 5, which has the rate $|t^{\mathrm{ref}}|\sqrt{\Gamma_r \Gamma_s}/\hbar$, with the dimensionless parameter $|t^{\mathrm{ref}}| = 2\pi|\tilde{t}|\sqrt{\rho_r \rho_s}$ and the density of states ρ_r.

4.1.2 Perturbation expansion in the tunnel coupling

Starting from these tunneling Hamiltonians a perturbative expansion in the tunnel coupling can be performed. For this purpose the tunneling part of the Hamiltonian is assumed to vanish for times earlier than an initial time t_0. Correspondingly the system's density matrix is assumed to factorize into parts for the reservoirs and the intermediate system

$$\rho_0 = \rho(t_0) = \rho_{\mathrm{sys}}(t_0) \prod_r \rho_r(t_0) \tag{4.6}$$

In the course of the argumentation t_0 will be sent to $-\infty$ and the tunneling Hamiltonian will be turned on adiabatically. Since the reservoirs are assumed to be so large that they are unaffected by tunneling in or out of (relatively few) electrons, they can be assumed to always remain in equilibrium. They are thus always described by the grand-canonical ensemble $\rho_{\mathrm{res}} = \exp\left(-\beta(H_{\mathrm{res}} - \sum_r \mu_r \hat{n}_r)\right)/Z_{\mathrm{res}}$ with the constant electrochemical potentials μ_r, inverse temperature $\beta = 1/(k_B T)$ and the number operator $\hat{n}_r$.

At the initial time t_0 the occupation of the intermediate system may be chosen arbitrarily (given the normalization condition $\sum_\mu \rho_\mu^\mu = 1$), since in the stationary limit, where t_0 is shifted to $-\infty$, all physical quantities become independent of the particular choice of ρ_0. For special systems whose Hamiltonian is charge and/or spin-conserving, if the initial density matrix is diagonal in charge and/or spin space this property is conserved for all times.

In the interaction picture, where operators evolve under the free Hamiltonian $H_0 = H_{\mathrm{sys}} + H_{\mathrm{res}}$, the expectation value of an operator evolves according to

$$\begin{aligned} \langle A(t)\rangle &= \mathrm{tr}\left(\rho_I A(t)_I\right) && (4.7)\\ &= \mathrm{tr}\left[\tilde{T}\exp\left(-i\int_{t_0}^{t} dt' H_T(t')_I\right)\rho_0 A(t)_I T\exp\left(i\int_{t_0}^{t} dt' H_T(t')_I\right)\right], && (4.8)\end{aligned}$$

with the time- and anti-time ordering operators T and $\tilde{T}$. With the help of the Keldysh technique, the two time integrals can be condensed into one, employing the Keldysh time ordering operator T_K

$$\langle A(t)\rangle = \mathrm{tr}\left[T_K \exp\left(-i\int_K dt' H_T(t')_I\right) A(t)_I \rho_0\right]. \qquad (4.9)$$

The Keldysh time ordering operator orders all following operators with respect to the Keldysh time, such that "earlier" operators appear to the left of operators "later" with respect to Keldysh time, without introducing sign changes. As indicated in Fig. 4.1, the Keldysh time starts at t_0, runs up to the time t along the upper contour and then back to t_0 along the lower contour. The Keldysh time ordering operator thus distributes operators on both parts of the contour.

Now, since the initial density matrix was assumed to separate into lead and system parts, the leads can be easily treated as equilibrium reservoirs by performing the trace over them, so that the expectation value becomes

$$\langle A(t)\rangle = \mathrm{tr}_{\mathrm{dot}}\left[\rho_0^{\mathrm{dot}}\,\Pi\, A(t')_I\right]. \qquad (4.10)$$

In doing so the propagator for the reduced system was introduced

$$\Pi = \left(\prod_r \mathrm{tr}_r\right) T_K \exp\left(-i\int_K dt' H_T(t')_I\right)\prod_r \rho_0^r. \qquad (4.11)$$

It consists of propagators forwards and backwards in time, which become connected by contractions of the lead operators in the tunneling Hamiltonian. Instead of this

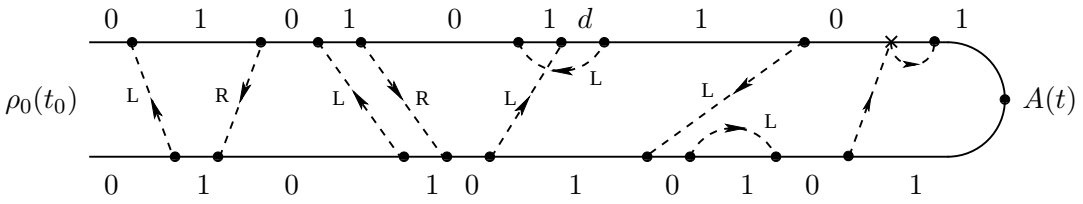

Figure 4.1: The Keldysh contour consists of a horizontal line running right from time t_0, changing direction at time t and running back left to t_0. Lead operators appear as dots and crosses (cf. p. 47). Their contractions are denoted by tunneling lines, while dot operatores cannot be contracted and are treated explicitly by labeling the contour segments with the dot occupation.

literal interpretation, it is more intuitive to think of the contour as describing the whole density matrix: In this case the diagram has to be read from left to right and at each (real) time t the system state is described by a density matrix $\rho_\mu^\nu = |\mu\rangle\langle\nu|$, where ν is the state on the upper and μ on the lower contour.

The expression for the reduced propagator serves as a starting point for an expansion in the tunnel coupling. For this purpose the exponential is expressed in terms of the tunnel coupling

$$T_K e^{-i\int_K dt' H_T(t')_I} \tag{4.12}$$
$$= \sum_{m=0}^{\infty} (-i)^m \int_K dt_1 \int_{\substack{K \\ t_1>t_2>\ldots>t_m}} dt_2 \ldots \int_K dt_m \; T_K\big[H_T(t_1)_I H_T(t_2)_I \ldots H_T(t_m)_I\big]$$

where $t_1 > t_2 > \ldots > t_m$ is to be understood in the Keldysh sense. This expansion can be symbolized by a Keldysh diagram:

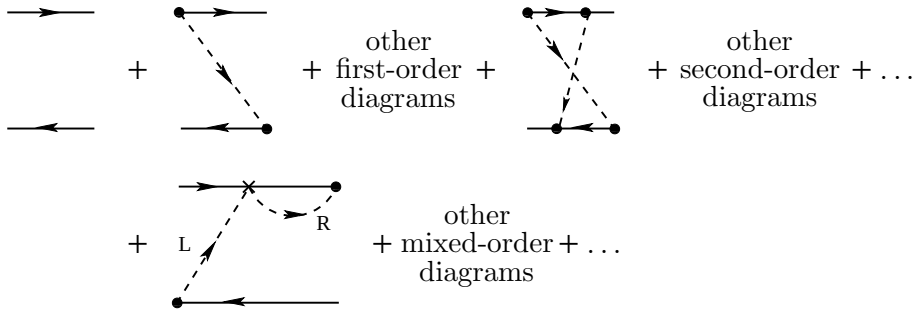

The horizontal lines represent forward (from t_0 to t) and backward (from t to t_0) propagators. On these time paths internal vertices from lead operators $a_r(t)$, $a_r^\dagger(t)$ in the tunneling Hamiltonian are arranged, represented by solid dots. These operators change the charge state of the dot. Another class of internal vertices, represented by crosses, represents terms of the Hamiltonian describing direct tunneling between the leads, Eq. (4.5). These operators do not affect the charge state of the dot.

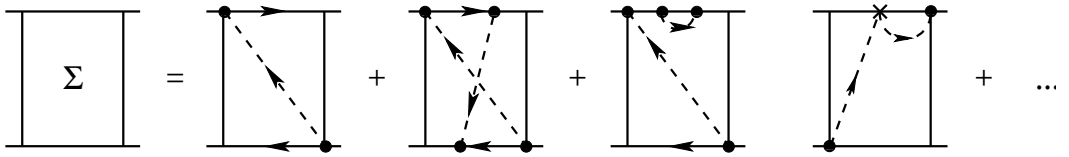

Figure 4.2: Diagram contributions to the self-energy. The leftmost diagram is of first order in the dot-lead coupling and describes sequential tunneling. The two diagrams to its right are of second order in the dot-lead coupling and describe co-tunneling. The two rightmost diagrams are of first order in both dot-lead and lead-lead coupling (the "cross"-vertex) and describe lowest-order interference between the path through the dot and direct tunneling between the leads.

Wick's theorem allows to contract pairs of lead operators. These contractions are represented by tunneling lines connecting destruction and annihilation operators. They are directed away from "dot"-vertices corresponding to an operator $a^\dagger_{rk\sigma}(t)c_\sigma(t)$ describing the tunneling of an electron from the dot to lead r and towards dot vertices correspoding to an operator $a_{rk\sigma}(t)c^\dagger_\sigma(t)$ for creation of an electron on the dot. The case of the "cross"-vertices is analogous: a "cross"-vertex corresponds to the operator pair $a^\dagger_r(t)a_s(t)$, so that due to the order of creation and annihilation operators the line entering the vertex (from lead s) must appear at an earlier Keldysh time. This may give rise to a crossing of tunneling lines (e.g., in the left diagram of Fig. 4.2). The number of tunneling lines present in a diagram corresponds to its order: the first line shows diagrams of conventional first and second order in Γ, the second line shows a lowest order diagram for mixed contributions of order $|t^{\mathrm{ref}}|\sqrt{\Gamma_L\Gamma_R}$.

Only the lead operators can be treated by Wick's theorem, as the operators for dot electrons appear as quartic terms in the Coulomb interaction term. They are taken care of by an exponential factor $e^{i\epsilon_\chi \Delta t}$ with ϵ_χ being the energy of the intermediate system's state and Δt the time interval during which this state exists on the Keldysh contour. Depending on the order of creation operators in the definition of a state containing multiple electrons further minus signs may be induced (e.g., in case $c_{i\overline{\sigma}}$ acts on the doubly occupied state defined as $c^\dagger_{i\sigma}c^\dagger_{i\overline{\sigma}}|0\rangle$).

Each tunneling line corresponds to the expectation value of a product of one creation and one annihilation operator

$$\left\langle a^\dagger_{rk\sigma}(t)a_{r'k'\sigma'}(t')\right\rangle = \delta_{kk'}\delta_{rr'}\; e^{i\epsilon_{rk\sigma}(t-t')}\; f^+_r(\epsilon_{rk\sigma}) \tag{4.13}$$

$$\left\langle a_{rk\sigma}(t)a^\dagger_{r'k'\sigma'}(t')\right\rangle = \delta_{kk'}\delta_{rr'}\, e^{-i\epsilon_{rk\sigma}(t-t')} f^-_r(\epsilon_{rk\sigma}) \tag{4.14}$$

with the Fermi function $f^+_r(\epsilon) = f(\epsilon-\mu_r)$ for reservoir r with chemical potential μ_r and $f^-_r(\epsilon) = 1 - f_r(\epsilon)$. Each crossing of tunneling lines yields a minus sign. Such crossings can in particular occur due to the requirement for lines to enter "cross"-vertices before they leave (w.r.t. Keldysh time).

4.1.3 Diagrammatic rules for counting statistics

It is more convenient to carry out the calculations in energy space. In order to perform the transformation from time to energy space, the vertices of a diagram are ordered from left to right and labeled by τ_j $(j = 1, 2, \ldots, n)$. Then the Keldysh contour integrals can be written as ordinary integrals, with a minus sign for each internal vertex on the backward propagator, so that expressions of the following type occur

$$\int_{-\infty}^{0} \mathrm{d}\tau_1 \int_{\tau_1}^{0} \mathrm{d}\tau_2 \ldots \int_{\tau_{m+n-2}}^{0} \mathrm{d}\tau_n \, e^{0^+\tau_1} e^{-i\Delta\epsilon_1(\tau_1-\tau_2)} e^{-i\Delta\epsilon_2(\tau_2-\tau_3)} \cdots e^{-i\Delta\epsilon_n\tau_n} = i^n \frac{1}{\Delta\epsilon_1 + i0^+} \frac{1}{\Delta\epsilon_2 + i0^+} \cdots \frac{1}{\Delta\epsilon_n + i0^+} \,. \tag{4.15}$$

Here $\Delta\epsilon_j$ is the difference of all energies going to the left minus all energies going to the right in the segment limited by τ_j and $\tau_j + 1$. This means the energies of upper and lower propagator as well as of tunneling lines. A convergence factor $e^{0^+\tau_1}$ was introduced to account for adiabatically switching on the tunneling Hamiltonian. In addition there are operators changing dot and lead states at the times τ_j.

Rules for the self-energy parts in energy space

Now rules can be formulated for the calculation of diagrams of arbitrary order. Since for the calculation of the counting statistics only the self energy is needed, we formulate the rules explicitly in absence of any operators $A(t)$.

1. Draw all topologically different diagrams with tunneling lines connecting vertices on either the same or opposite propagators. Assign to the four corners and all propagators the state indices (i, σ) (dot i is occupied with spin σ) and the corresponding energies $\epsilon_{i\sigma}$, as well as an energy ω_r to each tunneling line belonging to lead r.

2. For each time interval on the real axis confined by two neighboring vertices, assign the resolvent $1/(\Delta\epsilon + i0^+)$, where $\Delta\epsilon$ is the energy difference of left- minus right-going tunneling lines or propagators.

3. Add factors (-1) for each vertex connecting a multiply occupied state to a singly occupied one as required by the order of operators in the definition of the multiple occupation (e.g., in case $c_{\overline{\sigma}}$ acts on the doubly occupied state defined by $c_\sigma^\dagger c_{\overline{\sigma}}^\dagger |0\rangle$).

4. a) Assign to each tunneling line the factor

$$\frac{1}{2\pi} \rho_r f_r^{\pm}(\omega_r) \,. \tag{4.16}$$

with positive (negative) sign when the tunneling line is going backward (forward) with respect to the Keldysh contour. These factors come from the contraction of two lead operators in the tunnel Hamiltonian and resemble the transition rates predicted by Fermi's golden rule. Depending on the time ordering, the transition rate is proportional to the Fermi distribution f^+ for electrons or $f^- = 1 - f^+$ for holes.

b) Assign to each "dot" vertex on the upper contour a tunneling amplitude t_{ri}. For a "cross" vertex on the upper contour assign $\tilde{t}_{rs}$, if the line originating from lead s goes *into* the vertex and $\tilde{t}^*_{rs}$ if it goes *out*. For vertices on the lower contour the same rules apply, just taking the complex conjugates instead.[2]

c) Introduce the counting fields by replacing the tunneling amplitudes as $t_r \to t_r\, e^{\pm i\chi_r}$ and $\tilde{t} \to \tilde{t}\, e^{i(\pm\chi_L \mp \chi_R)}$, where the upper (lower) signs are taken on the upper (lower) contour.

d) Sum over the leads.

5. The diagram gets a prefactor of $(-1)^b(-1)^c$, where b is number of internal vertices on the backward propagator and c the number of crossings of tunneling lines. Note that c must also include crossings arising from the order of lines entering the "cross"-vertices.

6. Integrate over all energies ω_n of the tunneling lines.

In the sequential-tunneling regime for dot-lead coupling each diagram contains only one tunneling line. Therefore, only one energy integral appears, which can be calculated by using Cauchy's formula (the prime at the integral denoting Cauchy's principal value)

$$\int \mathrm{d}\omega \frac{f(\omega)}{\omega - \epsilon + i0^+} = -i\pi \int \mathrm{d}\omega \delta(\omega - \epsilon) f(\omega) + \int' \mathrm{d}\omega \frac{f(\omega)}{\omega - \epsilon}\,. \tag{4.17}$$

The lowest order for interference between dot-lead and lead-lead tunneling contains two resolvents. Examples of such diagrams are discussed in Appendix A.

4.1.4 Generalized master equation

For the calculation of the counting statistics, knowledge about the time evolution of the system is necessary, in particular the transition rates between different states are required. They are accessible by the diagrammatic technique discussed in the previous section. In order to access the density matrix of the system, these rates can be summarized in a formally exact master equation.

A component of the density matrix is expressed as

$$p^{\chi_1}_{\chi_2}(t) = \left\langle |\chi_2\rangle \langle\chi_1|\,(t)\right\rangle . \tag{4.18}$$

Its time evolution is described by the reduced propagator $\Pi^{\chi_1',\chi_1}_{\chi_2',\chi_2}(t',t)$, which describes the evolution of the dot subsystem in the Keldysh picture from state χ_1' at time t' forward to χ_1 at time t and then backwards from χ_2 at time t to χ_2' at time t',

$$p^{\chi_1}_{\chi_2}(t) = \sum_{\chi_1'\chi_2'} \Pi^{\chi_1\chi_1'}_{\chi_2\chi_2'}(t',t) p^{\chi_1'}_{\chi_2'}(t')\,. \tag{4.19}$$

[2] Rules 4 a) and b) together are equivalent to assigning Γ_{ri} for pairs of "dot" vertices as done in other works, e.g., [153, 162, 170]. However, here the phases of tunnel matrix elements are explicitly taken into account. This is necessary due to the special nature of the cross "vertex", which allows single, unpaired matrix elements to appear.

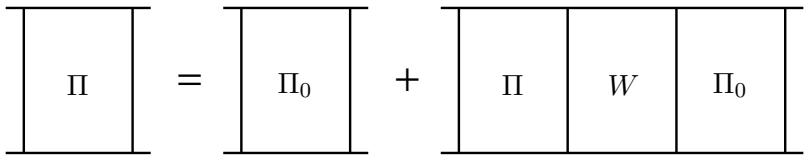

Figure 4.3: Dyson Equation for the reduced propagator.

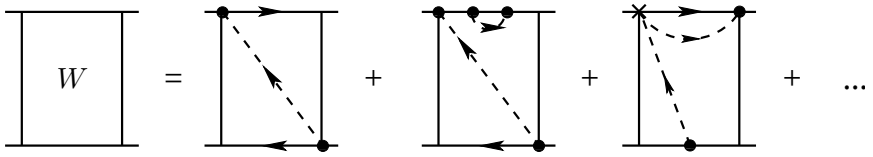

Figure 4.4: The self-energy is the sum over all irreducible diagrams in which any vertical cut intersects at least one tunneling line with the given states at the ends.

For the propagator a Dyson equation (Fig. 4.3) can be formulated, which relates it to the free propagator $\Pi^{(0)\chi_1}_{\chi_2}(t',t)$ of the isolated dot and the self energy $W^{\chi_1'\chi_1}_{\chi_2'\chi_2}(t_1,t_2)$:

$$\begin{aligned}\Pi^{\chi_1\chi_1'}_{\chi_2\chi_2'}(t',t) &= \Pi^{(0)\chi_1'}_{\chi_2'}(t',t)\delta_{\chi_1',\chi_1}\delta_{\chi_2',\chi_2} \\ &+ \sum_{\chi_1'',\chi_2''}\int_{t'}^{t} dt_2 \int_{t'}^{t_2} dt_1\, \Pi^{\chi_1\chi_1''}_{\chi_2\chi_2''}(t',t_1)\, W^{\chi_1''\chi_1}_{\chi_2''\chi_2}(t_1,t_2)\, \Pi^{(0)\chi_1'}_{\chi_2'}(t_2,t). \quad (4.20)\end{aligned}$$

In the diagrammatic language the self energy is the sum of all "connected" diagrams, where "connected" means that any vertical cut crosses at least one tunneling line (see Fig. 4.4), while the free propagator contains no tunneling lines.

Multiplying the Dyson equation with $P^{\chi_1'}_{\chi_2'}$, summing over the states χ_1', χ_2' and taking the time derivative results in the generalized master equation for the system's density matrix

$$\frac{d}{dt}p^{\chi_1}_{\chi_2}(t) + \frac{i}{\hbar}(E_{\chi_1} - E_{\chi_2})p^{\chi_1}_{\chi_2}(t) = \int_{t_0}^{t} dt' \sum_{\chi_1'\chi_2'} W^{\chi_1\,\chi_1'}_{\chi_2\,\chi_2'}(t',t)\; p^{\chi_1'}_{\chi_2'}(t')\,. \quad (4.21)$$

In case of a diagonal density matrix or energetic degeneracy of the states participating in the off-diagonal elements, the equation simplifies further since the energy difference $(E_{\chi_1} - E_{\chi_2})$ drops out.

4.2 Non-markovian counting statistics from a master equation approach

Among the large number of theoretical approaches to full counting statistics (cf. Sec. 3.2), many start from a master equation description [20, 66, 99, 111, 171, 173,

174, 175, 176, 177, 178]. They all share the central statement that the generating function is related to the eigenvalue of the master equation's kernel. One of these works, Ref. [173], has made a statement about the origin of non-Markovian effects: First, the full non-Markovian generating function was obtained in a way that in a second step it could be shown that the non-Markovian effects appear only in higher-than-lowest order in any small parameter. In this way a hierarchy of non-Markovian contributions could be established, each level corresponding to a certain order in the expansion. Since the present thesis is based on this approach, its central steps are repeated in the following sections.

The starting point is a master equation for the system's density matrix, which is assumed to be diagonal, so that its components can be arranged in a vector $\mathbf{p}(N,t) = (\rho_{\mu_1}^{\mu_1}, \rho_{\mu_2}^{\mu_2}, \ldots)$. In comparison to the previous section, the probabilities receive the additional variable N. It describes the number of charges that have passed the system after time t, so that $p_\mu^\mu(N,t)$ is the probability to find the system in state $|\mu\rangle$ after time t with N charges having been transferred. The probability for the transfer of N charges, regardless of the final system state, can then be expressed as $P(N,t) = \mathbf{e}^T \cdot \mathbf{p}$, with $\mathbf{e}^T = (1,1,\ldots,1)$. The Fourier transform of this probability is the cumulant generating function

$$S(\chi) = \ln\left[\sum_{N=-\infty}^{\infty} e^{iN\chi} P(N,t)\right]. \tag{4.22}$$

Now, the problem is broken down to finding $\mathbf{p}(N,t)$ after a given time. For the description of its time evolution Eq. (4.21) has to be extended to include the number of charges N. In a matrix notation it thus reads

$$\frac{d}{dt}\mathbf{p}(N,t) = \int \mathrm{d}t' \sum_{N'} \mathbf{W}(N-N',t',t)\mathbf{p}(N',t') \tag{4.23}$$

The kernel also receives a number dependence and describes transitions in which $N-N'$ charges are transferred. Without explicit time dependence of the system parameters the kernel only depends on the time difference $t-t'$ and the entire master equation can be Laplace transformed $\mathbf{W}(N,z) = \int_0^\infty \mathrm{d}t \exp(-zt)\mathbf{W}(N,t)$. Furthermore, the counting field can be introduced by a Fourier transform $\mathbf{p}(\chi,z) = \sum_N e^{iN\chi}\mathbf{p}(N,z)$ and $\mathbf{W}(\chi,z) = \sum_N e^{iN\chi}\mathbf{W}(N,z)$.

With these transformations the convolution in the master equation turns into a product

$$z\mathbf{p}(\chi,z) - \mathbf{p}^{\mathrm{in}} = \mathbf{W}(\chi,z)\cdot\mathbf{p}(\chi,z), \tag{4.24}$$

with $\mathbf{p}_{\mathrm{in}}$ denoting the initial state. The solution is the easily found to be $\mathbf{p}(\chi,z) = \sum_{n=0}^\infty (\mathbf{W}(\chi,z))^n/z^{n+1}\mathbf{p}_{\mathrm{in}}$. Assuming that the kernel decays in time faster than any power law, all derivatives $\partial/\partial z\mathbf{W}(\chi,z)$ exist and the kernel can be replaced by a Taylor series $[\mathbf{W}(\chi,z)]^n = \sum_{m=0}^\infty \partial_z^m\,[\mathbf{W}(\chi,z)]^n|_{z=0}\, z^m/m!$. Since the long-time behavior of $\mathbf{p}(\chi,z)$ is determined by its poles in z, the inverse Laplace transform can be carried out for large t

$$\mathbf{p}(\chi,t) = \sum_n \frac{1}{n!}\left[\partial_z^n \mathbf{W}^n e^{\mathbf{W}t}\right]_{z=0}\mathbf{p}_0. \tag{4.25}$$

Now a spectral decomposition of the matrix $\mathbf{W}(\chi, z)$ can be performed. In order for it to describe a physically reasonable system the real parts of all its eigenvalues must be negative. Due to the exponential dependence in Eq. (4.25) this means that the influence of all eigenvalues decays with time, so that in the long-time limit only the eigenvalue $\lambda(\chi, z)$ with smallest absolute value of the real part remains influential. To complete the spectral decomposition the corresponding left and right eigenvectors are needed, $\mathbf{W}(\chi, z)\mathbf{p}_0(\chi, z) = \lambda(\chi, z)\mathbf{p}_0(\chi, z)$ and $\mathbf{q}_0^T(\chi, z)\mathbf{W}(\chi, z) = \mathbf{q}_0^T(\chi, z)\lambda(\chi, z)$. Unitarity of $\mathbf{W}(0, z)$ implies that $\lambda(0, z) = 0$ for all z. This property ensures that the generating function fulfills probability normalization $S(0) = \ln \sum_N P(N) = 0$.

Knowing the $\mathbf{p}(\chi, t)$, the cumulant generating function can be found according to Eq. (4.22) as

$$S(\chi) = \ln \left[\sum_{n=0}^{\infty} \frac{1}{n!} \partial_z^n (\lambda^n(\chi, z) e^{\lambda(\chi,z)t + \mu(\chi,z)}) \right]_{z=0+}, \tag{4.26}$$

where the eigenvectors enter in the combination $\mu(\chi, z) = \ln(\mathbf{e}^T \cdot \mathbf{p}_0(\chi, z))(\mathbf{q}_0^T(\chi, z) \cdot \mathbf{p}_{\text{in}})$. Taking the time derivative the following relation, holding for arbitrary a and b, is applied, $\sum_{n=0}^{\infty} \frac{1}{n!} \partial^n(ab^{n+1}) / \sum_{n=0}^{\infty} \frac{1}{n!} \partial^n(ab^n) = \sum_{n=0}^{\infty} \frac{1}{n!} \partial^n(b^{n+1}) / \sum_{n=0}^{\infty} \frac{1}{n!} \partial^n(b^n)$. With this the final relation between generating function and the eigenvalue of the kernel λ of the master equation is established

$$S(\chi) = \left. \frac{\sum_{n=0}^{\infty} \frac{1}{n!} \partial_z^n [\lambda^{n+1}(\chi, z)]}{\sum_{n=0}^{\infty} \frac{1}{n!} \partial_z^n [\lambda^n(\chi, z)]} \right|_{z=0^+} t \; + \; const. \tag{4.27}$$

The integration constant is independent of time and can therefore be neglected in the long-time limit. Since in the long-time limit system properties must not depend on the initial conditions, the quantity μ which contains $\mathbf{p}_{\text{in}}$, drops out in the last step and the generating function depends only on the kernel's eigenvalue.

4.2.1 Non-Markovian Expansion

Memory effects are completely included in Eq. (4.27), since it was derived allowing for a time dependence of the kernel, whose only restriction was that it had to decay faster than any power law, so that all derivatives $\partial_z^n \lambda(\chi, z)$ exist. Since different orders of these derivatives enter the generating function, it is possible to define a hierarchy of memory effects in a non-Markovian expansion

$$S(\chi) = \sum_{n=0}^{\infty} S_n(\chi) = t \left\{ \lambda + \lambda \partial_z \lambda + \left[\frac{1}{2} \lambda^2 \partial_z^2 \lambda - 4\lambda \big(\partial_z \lambda\big)^2 \right] + \ldots \right\} \Bigg|_{z=0^+} \tag{4.28}$$

Each term S_n contains derivatives with respect to z, applied $n + 1$ factors of λ. The lowest order term S_0 contains no derivatives, so that it does not contain any time information of the kernel. It is the Markovian result

$$S_0(\chi) = t\, \lambda(\chi, z = 0). \tag{4.29}$$

The strength of the non-Markovian expansion becomes apparent when performing in addition an expansion in a small parameter, e.g., in the tunnel coupling as described

in the previous section. In this case the eigenvalue is expanded in the small parameter $\lambda(\chi, z) = \sum_{i=1}^{\infty} \lambda^{(i)}(\chi, z)$ and the lowest order contribution to the generating function is just the Markovian part $S_0(\chi) = t\lambda^{(1)}(\chi, 0)$. In order to capture non-Markovian effects, transport thus needs to be analyzed in higher-than-lowest order.

Still, also in higher orders of the small parameter an upper bound is put on the non-Markovian orders. It is clear from Eq. (4.28) that the current $I = \partial_{i\chi} S(\chi)|_{\chi=0}$ cannot contain non-Markovian effects, since the eigenvalue and all its z-derivatives vanish for $\chi \to 0$.

These two observations in combination allow to make the statement that the highest derivative of the eigenvalue that is needed to calculate the n-th moment in m-th order perturbation theory, $\partial_z^k \lambda(\chi, z)|_{z=0}$, is of the order $k = \min(m, n) - 1$. For the special case of second order the appearance of these derivatives has also been described in Ref. [69].

For the present work, since only transport in lowest order in the tunnel coupling is considered, the generating function is always given in the Markovian limit by the kernel's eigenvalue.

4.3 Perturbative approach to counting statistics

The technique described in the previous section is often hard to apply, since already for systems slightly more complex than a single level quantum dot, the density matrix grows in size very quickly. While exact solutions for eigenvalues of matrices up to the dimension four are known, for larger systems it is in general impossible to obtain an analytic form of the eigenvalue. For special cases efficient numerical techniques are known, but to analytically access the cumulants a different path can be taken. This approach was derived by Flindt *et al.* [171, 172] and consists in finding a formally exact expression for the generating function by Brillouin-Wigner perturbation theory. This expression can then be used to obtain analytic expressions for the cumulants in terms of the kernel $\mathbf{W}$ (which is regarded as the perturbation), its left and right eigenvectors $\langle 0|$ and $|0\rangle$ and its pseudoinverse $\mathbf{R}$. This technique allows the description of non-Markovian systems, but since the systems discussed here are Markovian (due to the lowest order expansion in tunneling) a simpler derivation which holds only for Markovian systems is given below.

The starting point is again the N-resolved master equation Eq. (4.23). Again, taking the Fourier transform with respect to N, the kernel can be split into a constant part $\mathbf{W} \equiv \mathbf{W}(\chi = 0)$ and a χ-dependent part $\mathbf{W}(\chi) = \mathbf{W} + \overline{\mathbf{W}}(\chi)$. The projectors $\mathbf{P} = |0\rangle\langle 0|$ and $\mathbf{Q} = 1 - \mathbf{P}$ are also needed.

The first step consists in realizing that the generating function $\lambda(\chi)$ is the eigenvalue to eigenvector $|0(\chi)\rangle$,

$$\mathbf{W}(\chi)|0(\chi)\rangle = \left[\mathbf{W} + \overline{\mathbf{W}}(\chi)\right]|0(\chi)\rangle = \lambda(\chi)|0(\chi)\rangle. \tag{4.30}$$

If the nullvectors are chosen to be normalized $\langle 0|0(\chi)\rangle = 1$ this implies

$$\langle 0|\left[\lambda(\chi) - \mathbf{W}\right]|0(\chi)\rangle = \lambda(\chi) = \langle 0|\overline{\mathbf{W}}(\chi)|0\rangle, \tag{4.31}$$

$$\mathbf{Q}\left[\lambda(\chi) - \mathbf{W}\right]|0(\chi)\rangle = \mathbf{Q}\overline{\mathbf{W}}(\chi)|0(\chi)\rangle. \tag{4.32}$$

The latter relation together with the fact that $\mathbf{W}$ and $\mathbf{Q}$ commute implies

$$\begin{aligned}\mathbf{Q}|0(\chi)\rangle &= \mathbf{Q}\left[\lambda(\chi) - \mathbf{W}\right]^{-1}\mathbf{Q}\overline{\mathbf{W}}(\chi)|0(\chi)\rangle &(4.33)\\ &= -\mathbf{R}\overline{\mathbf{W}}(\chi)|0(\chi)\rangle, &(4.34)\end{aligned}$$

where the pseudoinverse $\mathbf{R} = \mathbf{Q}\left[\mathbf{W} - \lambda(\chi)\right]^{-1}\mathbf{Q}$ was introduced. With $|0(\chi)\rangle = |0\rangle + \mathbf{Q}|0(\chi)\rangle$ this results in

$$|0(\chi)\rangle = |0\rangle - \mathbf{R}\overline{\mathbf{W}}(\chi)|0(\chi)\rangle. \tag{4.35}$$

By recursion this can be written as a geometric series

$$\begin{aligned}|0(\chi)\rangle &= \sum_n \left[-\mathbf{R}\overline{\mathbf{W}}(\chi)\right]^n |0(\chi)\rangle &(4.36)\\ &= \left[1 + \mathbf{R}\overline{\mathbf{W}}(\chi)\right]^{-1}|0(\chi)\rangle. &(4.37)\end{aligned}$$

Inserting this expression in Eq. (4.31), the eigenvalues $\lambda(\chi)$ (i.e., the generating function in the Markovian limit) is found to be

$$\lambda(\chi) = \langle 0|\overline{\mathbf{W}}\left[1 + \mathbf{R}\overline{\mathbf{W}}\right]^{-1}|0\rangle \tag{4.38}$$

From this equation the cumulants can be calculated as usual by taking derivatives w.r.t. χ (indicated by primes $'$), so that expressions for the cumulants κ_i can be found in terms of $|0\rangle$, $\langle 0|$, $\mathbf{R}$ and $\overline{\mathbf{W}}$.

$$\begin{aligned}\kappa_1 &= \frac{1}{i}\langle 0|\overline{\mathbf{W}}'|0\rangle &(4.39)\\ \kappa_2 &= \frac{1}{i^2}\langle 0|\mathbf{W}'' - 2\overline{\mathbf{W}}'\mathbf{R}\overline{\mathbf{W}}'|0\rangle &(4.40)\\ \kappa_3 &= \frac{1}{i^3}\langle 0|\overline{\mathbf{W}}''' - 3(\overline{\mathbf{W}}''\mathbf{R}\overline{\mathbf{W}}' + \overline{\mathbf{W}}'\mathbf{R}\overline{\mathbf{W}}'') - 6(\overline{\mathbf{W}}'\mathbf{R}(\mathbf{R}\overline{\mathbf{W}}'\mathbf{P} - \overline{\mathbf{W}}'\mathbf{R})\overline{\mathbf{W}}')|0\rangle &(4.41)\end{aligned}$$

Therein the derivative of the pseudoinverse $\mathbf{R}' = \mathbf{R}^2\,\partial_\chi\lambda(\chi)|_{\chi=0}$ was expressed in terms of the second cumulant and $\mathbf{P}$.

The power of this approach extends beyond what is needed in this thesis: it also allows a quick and stable numerical calculation of high order moments.

5 Single dot Aharonov-Bohm interferometer

The current of electrons through a closed interferometer shows characteristic Aharonov-Bohm oscillations. It follows from Onsager relations that the phase dependence of these oscillation is even, if a non-interacting, single level quantum dot is embedded into one arm of the interferometer. Since Onsager relations hold only for non-interacting systems, the picture changes in the presence of Coulomb interaction, which gives rise to a large charging energy in the quantum dot.

It has been predicted [6] and experimentally confirmed [13] that the interference signal probed by the linear conductance is partially reduced in the parameter regime where the quantum dot is predominantly singly occupied. The reason is that those electrons transferred through the dot that flip their spin with the spin of the quantum-dot electron do not contribute to the interference signal, while the nonspin-flip processes do contribute.

It is therefore natural to expect that the full counting statistics will also display this partial reduction of the interference signal due to spin-flip processes. In addition to this it will be demonstrated that resonant processes that give rise to an *odd* ϕ-dependence of the cumulant generating function occur and that even the FCS of the processes with *even* flux dependence, present in the non-interacting case, is not bidirectional Poissonian any more. Onsager relations are not violated since these resonant processes do not contribute to the linear conductance (and equilibrium noise). These processes have the interesting property that, for asymmetric tunnel couplings of the quantum dot to the left and right lead, they display enhanced generalized Fano factors that can be associated with the transfer of double charges.

The chapter starts with a specification of the model. The full counting statistics of this model are then calculated in two ways: First the charges are counted as they pass through the interfaces between dot and leads. In this case a number of interesting properties of the interacting system are found. The third section analyses the counting statistics of a different detector model where the charge state of the dot it monitored. This is shown to affect the statistics both in the interacting and in the non-interacting case.

5.1 Hamiltonian, density matrix and generating function

The system shown in Fig. 5.1 is described by a Hamiltonian consisting of parts for dot, leads and tunneling along each path:

$$H = H_{\text{dot}} + H_{\text{leads}} + H_{T,\text{dot}} + H_{T,\text{ref}}\,. \tag{5.1}$$

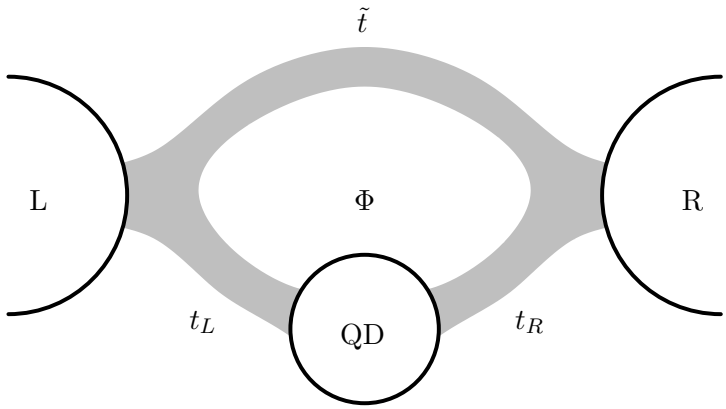

Figure 5.1: The single quantum dot Aharonov-Bohm Interferometer consists of a quantum dot tunnel coupled to two leads (with matrix elements $t_{L,R}$). The leads are directly coupled (tunnel matrix element $\tilde{t}$, so that two paths connect the leads. These paths enclose a magnetic flux Φ.

The quantum dot, $H_{\rm dot} = \sum_\sigma \varepsilon\, c_\sigma^\dagger c_\sigma + U n_\uparrow n_\downarrow$, is described as an Anderson impurity with a spin-degenerate electronic level ϵ and charging energy U for double occupation. Both limits of strong ($U \gg k_B T, \Gamma$) and vanishing ($U = 0$) charging energy will be discussed in the following.

In accordance with Section 4.1 the leads are described as reservoirs of noninteracting fermions $H_{\rm leads} = \sum_{r,k,\sigma} \varepsilon_{rk\sigma}\, a_{rk\sigma}^\dagger a_{rk\sigma}$ with indices for lead $r \in \{L, R\}$, momentum k and spin $\sigma \in \{\uparrow, \downarrow\}$.

The two parts of the tunneling Hamiltonian are:

$$H_{T,\rm dot} = \sum_{rk\sigma} t_r\, c_\sigma^\dagger a_{rk\sigma} + \text{H.c.}, \tag{5.2}$$

$$H_{T,\rm ref} = \sum_{kk'\sigma} \tilde{t}\, a_{Rk\sigma}^\dagger a_{Lk'\sigma} + \text{H.c.}. \tag{5.3}$$

The first part describes tunneling between dot and leads, while the second accounts for the reference arm. By appropriate choice of gauge the AB-phase $\phi = 2\pi\Phi/\Phi_0$ is incorporated in the phase of the tunneling amplitude of the reference arm $\tilde{t} = |\tilde{t}|\, e^{i\phi}$.

The strength of the tunnel coupling to the dot is characterized by the transition rates $\Gamma_r(\omega)/\hbar = 2\pi/\hbar \sum_k |t_{rk}|^2\, \delta(\omega - \epsilon_{r,k})$. For simplicity, the density of states ρ_r and the tunneling amplitudes t_r are assumed to be independent of energy, which implies constant tunneling rates $\Gamma_r/\hbar$. Furthermore, the total dot-lead coupling is defined as $\Gamma = \Gamma_L + \Gamma_R$. The coupling of the leads via the reference arm is described by the dimensionless parameter $|t^{\rm ref}| = 2\pi|\tilde{t}|\sqrt{\rho_L \rho_R}$.

In the case of small dot-lead coupling, $\Gamma_r \ll k_B T$, all quantities may be expanded to first order in the tunnel couplings $\Gamma_{L,R}$. Interference effects are included in lowest order by continuing the expansion to the order $|t^{\rm ref}|\Gamma_{L,R}$. In order to be consistent the order $|t^{\rm ref}|^2$ which describes transport through the reference arm only has to be also included:

$$S(\chi) = S^{(\Gamma)}(\chi) + S^{(|t^{\rm ref}|\Gamma)}(\chi, \phi) + S^{(|t^{\rm ref}|^2)}(\chi)\,. \tag{5.4}$$

The first and the third part describe tunneling through only the quantum dot and only the reference arm, respectively. Interference is described by the second, flux-dependent term.

It has been shown that non-Markovian corrections do not enter the cumulant generating function for the lowest-order term of a perturbation expansion in any small parameter [173]. Since all three terms of Eqn. (5.4) are of lowest order in parameters Γ, $|t^{\mathrm{ref}}|\sqrt{\Gamma_L\Gamma_R}$ and $|t^{\mathrm{ref}}|^2$, respectively, the entire generating function $S(\chi)$ is Markovian [173].

To obtain the generating function Eqn. 5.4 the master equation's kernel has to be calculated to the orders Γ and $|t^{\mathrm{ref}}|\Gamma$. This only allows to rigorously obtain the first two terms. The last term which corresponds to the reference arm is accessible within the diagrammatic approach, although it is not related to a change in the dot state (cf. Appendix A). The diagrammatic results coincides with common knowledge that transport through a tunnel barrier obeys Poissonian statistics [179]. The generating function for arbitrary voltages describes left- and right-going tunneling events

$$S^{(|t^{\mathrm{ref}}|^2)}(\chi) = t_0\,|t^{\mathrm{ref}}|^2 \int \mathrm{d}\omega \big[f_L(\omega)(1-f_R(\omega))\big](e^{i\chi}-1) + \big[(1-f_L(\omega))f_R(\omega)\big](e^{-i\chi}-1). \tag{5.5}$$

The prefactor consists of the probability for transfer of a single charge $|t^{\mathrm{ref}}|^2$ multiplied by the number electrons impinging during the measurement time t_0.

The other terms $S^{(\Gamma)}$ and $S^{(|\mathrm{ref}|\Gamma)}$ must be calculated from the aforementioned master equation (cf. Section 4.1.4). For this purpose the dot state is correctly described by the occupation probabilities p_0 for an empty dot, $p_\uparrow$ and $p_\downarrow$ for single occupation with spin up and down. Double occupation (p_d) is forbidden for large charging energy and has to be considered only for $U = 0$. The probabilities are arranged in a four-component vector $\mathbf{p}(N,t) = (p_0, p_\uparrow, p_\downarrow, p_d)^T$, where the p_i depend on the number of electrons N that have passed the system after time t. Since the generating function is related to the eigenvalues of the kernel matrix, it is desirable to keep the kernel dimensions as low as possible to minimize the algebraical complexity. Owing to spin symmetry ($p_\uparrow = p_\downarrow$) the dimensionality can be reduced from four ($U = 0$) and three ($U = \infty$) to two:

- The non-interacting system can be thought of as two independent spin channels, each of which is described by an occupation vector $(p_0, p_1)^T$. The corresponding kernel reads

$$\mathbf{W}_{U=0} = \begin{pmatrix} W_{0\leftarrow 0} & W_{0\leftarrow 1} \\ W_{1\leftarrow 0} & W_{1\leftarrow 1} \end{pmatrix} \tag{5.6}$$

  The generating function obtained from this kernel also describes only a single channel, but since the channels are independent and have equal properties, the full generating function is obtained by simple doubling of the result.

- The occupation of the interacting system is best described by a three-dimensional vector $(p_0, p_\uparrow, p_\downarrow)^T$, where the singly occupied charge state further specified by the spin of the electron. Since the Hamiltonian is spin symmetric, the transition rates are the same as those used above in the non-interacting case. The kernel

therefore reads:

$$\mathbf{W}_{U=\infty} = \begin{pmatrix} 2W_{0\leftarrow 0} & W_{0\leftarrow 1} & W_{0\leftarrow 1} \\ W_{1\leftarrow 0} & W_{1\leftarrow 1} & 0 \\ W_{1\leftarrow 0} & 0 & W_{1\leftarrow 1} \end{pmatrix} \tag{5.7}$$

These kernels can now be calculated, starting from the Hamiltonian in Eq. (5.1) using the diagrammatic real-time technique discussed in Sec. 4.1. Appendix A illustrates the calculation of the diagrams for transport involving the reference arm with the help of examples. For clarity the kernels are presented in the three-dimensional basis $(p_0, p_\uparrow, p_\downarrow)^T$. The kernel for a quantum dot without the reference arm $W^{(\Gamma)}$ has been previously obtained (see Refs. [111, 173]) and is repeated here

$$\mathbf{W}^{(\Gamma)} = \sum_{r=L,R} \Gamma_r \begin{pmatrix} -2f_r(\epsilon) & [1-f_r(\epsilon)]e^{i\chi_r} & [1-f_r(\epsilon)]e^{i\chi_r} \\ f_r(\epsilon)e^{-i\chi_r} & -1+f_r(\epsilon) & 0 \\ f_r(\epsilon)e^{-i\chi_r} & 0 & -1+f_r(\epsilon) \end{pmatrix} \tag{5.8}$$

The counting fields χ_r are incorporated by replacing the tunnel matrix elements in the Hamiltonian as $t_r \to t_r\, e^{\pm i\chi_r/2}$ and $\tilde{t} \to \tilde{t}\, e^{i\tilde{\chi}}$ with $\chi_L = -\chi_R = \tilde{\chi}/2 = \chi/2$, where the positive (negative) sign is taken for vertices on the upper (lower) branch of the Keldysh contour. This corresponds to a factor $e^{i\chi}$ for electrons passing through the dot from left to right lead and a factor $e^{-i\chi}$ for the opposite direction.

The kernel part describing interference consists of two parts:

$$\begin{aligned} \mathbf{W}^{(t^{\mathrm{ref}}\Gamma)} = \quad & |t^{\mathrm{ref}}|\sqrt{\Gamma_L\Gamma_R}\cos\phi \begin{pmatrix} 2A(\chi) & 0 & 0 \\ 0 & A(\chi) & 0 \\ 0 & 0 & A(\chi) \end{pmatrix} \\ & +|t^{\mathrm{ref}}|\sqrt{\Gamma_L\Gamma_R}\sin\phi \begin{pmatrix} -2B(\chi) & D(\chi) & D(\chi) \\ C(\chi) & B(\chi) & 0 \\ C(\chi) & 0 & B(\chi) \end{pmatrix} \end{aligned} \tag{5.9}$$

where the following abbreviations were used

$$A(\chi) = \int' \frac{\mathrm{d}\omega}{\pi} \frac{f_L(\omega)[1-f_R(\omega)]}{\epsilon-\omega}(e^{i\chi}-1) + \frac{[1-f_L(\omega)]f_R(\omega)}{\epsilon-\omega}(e^{-i\chi}-1) \tag{5.10}$$

$$B(\chi) = f_L(\epsilon)[1-f_R(\epsilon)]\, e^{i\chi} - [1-f_L(\epsilon)]f_R(\epsilon)\, e^{-i\chi} \tag{5.11}$$

$$C(\chi) = f_L(\epsilon)[1-2f_R(\epsilon)]e^{i\frac{\chi}{2}} - [1-2f_L(\epsilon)]f_R(\epsilon)e^{-i\frac{\chi}{2}} \tag{5.12}$$

$$D(\chi) = [1-2f_L(\epsilon)][1-f_R(\epsilon)]e^{i\frac{\chi}{2}} - [1-f_L(\epsilon)][1-2f_R(\epsilon)]e^{-i\frac{\chi}{2}}\,. \tag{5.13}$$

The processes appearing in the flux dependent part can be divided into two classes: Processes changing the dot state [$C(\chi)$ and $D(\chi)$] and processes that transfer charges without changing the dot state. The latter may possess either off-resonant [$A(\chi)$] or resonant [$B(\chi)$] nature and these differ in their dependence on magnetic flux. In contrast to the sequential-tunneling term, counting fields appear on the diagonal of the kernel since there are processes that transfer charges through the entire interferometer while leaving the dot state unchanged.

The kernel part describing direct, lowest order tunneling through the reference arm is diagonal, since these processes do not affect the dot state.

$$\mathbf{W}^{(|t^{\mathrm{ref}}|^2)} = |t^{\mathrm{ref}}|^2 \int \mathrm{d}\omega \Big\{ \big[f_L(\omega)(1-f_R(\omega))\big](e^{i\chi}-1) + \big[(1-f_L(\omega))f_R(\omega)\big](e^{-i\chi}-1) \Big\} \times \begin{pmatrix} 1 & 0 & 0 \\ 0 & 1 & 0 \\ 0 & 0 & 1 \end{pmatrix} \tag{5.14}$$

Since it is diagonal, its contribution to the eigenvalue is just additive and the eigenvalue (i.e., the generating function for transport through the reference arm $S^{(|t^{\mathrm{ref}}|^2)}$) itself is just one of the components, $|t^{\mathrm{ref}}|^2 \int \mathrm{d}\omega \Big\{ \big[f_L(\omega)(1-f_R(\omega))\big](e^{i\chi}-1) + \big[(1-f_L(\omega))f_R(\omega)\big](e^{-i\chi}-1) \Big\}$.

5.1.1 Physical interpretation of the transition rates as co-tunneling amplitudes

The transition rates in Eqns. (5.10-5.13) are calculated with the real time diagrammatic technique as discussed in Appendix A. This technique allows to rigorously include the counting fields. Alternatively the rates can be obtained by golden rule arguments. In lowest order for dot and reference arm this is straightforward, so that here only the interfering order is discussed.

The special order of diagrams describing the interference processes turns out to be composed of one amplitude for direct tunneling and one amplitude for tunneling via an intermediate state. Calculation of the latter requires the use of second order perturbation theory [7]. In perturbation theory the probability of transition $\mathrm{d}w_{fi}$ from an initial state i to a final state f, defined per density of final state $\mathrm{d}\rho_f$, through an intermediate state ν is given as

$$\mathrm{d}w_{fi} = \frac{2\pi}{\hbar} \left| V_{fi} + \int \mathrm{d}\nu \frac{V_{f\nu}V_{\nu i}}{E_i - E_\nu} \right|^2 \delta(E_f - E_i)\mathrm{d}\rho_f$$

where the integral $d\nu_f$ runs over all possible intermediate states and V_{ba} are transition matrix elements for a transition from state a to state b [7]. The system may either perform the transition directly (V_{fi}) or via an intermediate state (the integral term).

In the system at hand both kinds of transitions appear. Consider processes transferring electrons from the left to the right lead (these constitute the diagonal of the kernel of the master equation). An example in which the dot is empty in the initial and final state is shown below:

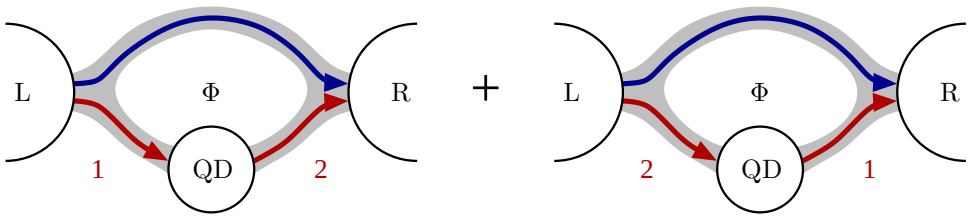

There are two such processes, differing in the intermediate state: Indicated in blue is a direct transition along the reference arm, while the transition in red passes through an intermediate state on the quantum dot. The numbers $1, 2$ indicate the order in which these processes appear: In the left diagram the dot is initially filled, while in the right diagram it is initially empty. The rates of the processes can be calculated in perturbation theory by evaluating the absolute square of the sum of the transition amplitudes for the interfering paths:

$$\int \mathrm{d}\omega_L \rho_L \int \mathrm{d}\omega_R \rho_R \, \delta(\omega_L - \omega_R) \left| V_{RL} + \frac{V_{RD} V_{DL}}{\epsilon - \omega_R + i\delta} \right|^2 + \int \mathrm{d}\rho_R \left| V_{RL} + \frac{V_{DL} V_{RD}}{\omega_R - \epsilon + i\delta} \right|^2 \tag{5.15}$$

The tunnel matrix element $V_{RL} \propto \tilde{t}$ stems from transitions through the reference arm (blue), while $V_{RD} \propto t_L$ and $V_{DL} \propto t_R$ describe transitions involving the quantum dot (red). The integration over ω_R is the integration over the final state, while that over ω_L runs over the initial states.

The direct transition via the reference arm does not require an intermediate state. The other path's initial state in the left lead has energy ω and due to energy conservation this is also the energy of the final state in the right lead. Here, an intermediate state is required: In the left process the dot is intermediately populated with an extra electron, while in the right process an electron is removed from the dot and populates the right lead. Since the two intermediate states differ, the denominators appear with exchanged energies. However, in both cases there is just a single intermediate state, so that the integration over intermediate states $\int \mathrm{d}\nu$ can be dropped.

Since the particular order $\tilde{t} t_L t_R$ is of interest, only terms of the desired order have to be retained in the evaluation of the modulus squared, i.e., only terms which contain products of all three tunnel matrix elements. These products of tunnel matrix elements give rise to products of Fermi functions $f_L(\omega)(1 - f_R(\omega))$ and the integration over final states $\int \mathrm{d}\rho_f$ is transformed into an energy integration $\int \mathrm{d}\omega$. The interpretation of the Fermi functions is clear: For the process to be possible, electrons must be available at this energy in the left lead $[f_L(\omega)]$, while the right lead must be unoccupied $[1 - f_R(\omega)]$. An additional minus sign is introduced in the right term due to the ordering of electron operators in the tunnel matrix elements.

Taking all this into account the integral can be evaluated and results in a delta function and a Cauchy-principal value contribution:

$$\begin{aligned} W_{0 \leftarrow 0} &= |t^{\mathrm{ref}}| \sqrt{\Gamma_L \Gamma_R} \left(-\sin\phi \, f_L(\epsilon)(1 - f_R(\epsilon)) + \cos\phi \int' \frac{\mathrm{d}\omega}{\pi} \frac{f_L(\omega)(1 - f_R(\omega))}{\epsilon - \omega} \right) \\ &\quad + (L \leftrightarrow R, \phi \leftrightarrow -\phi) \end{aligned} \tag{5.16}$$

The reverse process for transport from right to left has been included by exchanging the indices L and R and reversing the sign of the magnetic flux. This result coincides with the rate found in Section 5.1, Eqn. 5.9, identifying $A(\chi)$ with the Cauchy part and $B(\chi)$ with the resonant term. The counting fields are naturally missing in this calculation and would have to be added by hand.

Looking back at the diagrams, it becomes clear that the terms $A(\chi)$ and $B(\chi)$ have to be thought of as consisting of the interference between an amplitude for first order

tunneling through the reference arm and an amplitude for co-tunneling through the dot.

All other kernel elements of Eq. (5.9) can be derived in a similar way, also the off-diagonal ones. These transfer charges while changing the dot state. Correspondingly their diagrams look different: the example below shows the case where the dot is initially occupied and finally empty:

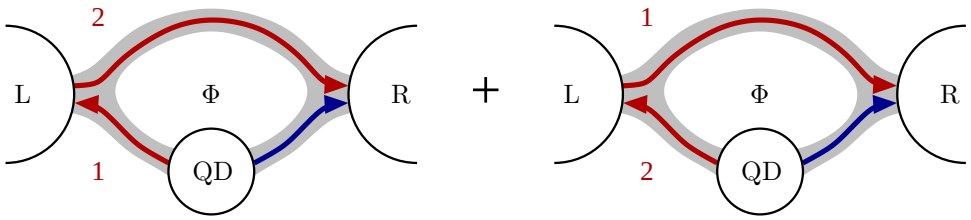

Again, the direct transition is indicated in blue, but this time it passes through the interface between dot and right lead. The process involving an intermediate state (red) passes through the left lead.

The corresponding transition rate therefore has the structure

$$\int \mathrm{d}\omega_R \rho_R \, \delta(\omega_L - \omega_R) \left\{ \left| V_{RD} + \int \mathrm{d}\omega_L \rho_L \frac{V_{RL} V_{LD}}{\omega_L - \epsilon + i\delta} \right|^2 + \left| V_{RD} + \int \mathrm{d}\omega_L \rho_L \frac{V_{LD} V_{RL}}{\omega_L - \epsilon + i\delta} \right|^2 \right\} \tag{5.17}$$

In contrast to the charge conserving rates the energy of the intermediate states is not fixed since it lies in the left lead. Instead, since the energy of the final state is fixed due to the direct tunneling from dot to right lead, the integration over the final state $\int \mathrm{d}\rho_R$ is reduced to a single term fixing the energy of the Fermi function of the right lead to ϵ. With the same arguments as above it is then possible to reproduce the remaining rates of Eq. (5.9).

It is thus supported by a simple perturbation calculation, that all rates of the master equation (and thus the relevant transport processes) consist of interference between an amplitude for first order direct tunneling and an amplitude for a conventional co-tunneling process via an intermediate state. If this intermediate state lies on the dot, the process has an even flux dependence, if it lies in one of the leads, the dependence on flux is odd. Despite being of higher than lowest order, the processes are not full co-tunneling processes and do not lead to level broadening and renormalization effects.

5.2 Interface current detector

In order to calculate the statistics of the entire system the counting fields are introduced at the junctions (see Ch. 4 and Fig. 5.2). This corresponds to errorless detection of all charges as they pass through the interfaces. For reasons of gauge invariance the detector may be thought of as detecting the charges entering the drain contact although technically the counting fields are attached to all interfaces. Until now it has not been experimentally possible to measure the full counting statistics by detecting

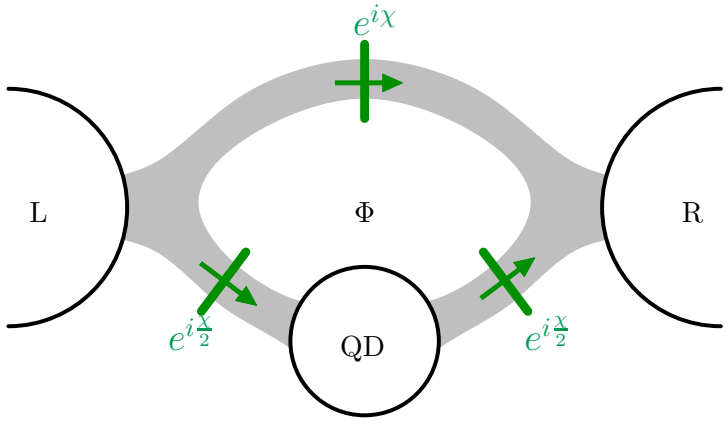

Figure 5.2: Interface current detector: The counting fields are attached to the tunnel matrix elements. This corresponds to counting electrons as they pass through the interfaces.

electrons while they pass the interface and experiment relying on noise measurements have proven too complicated for the detection of higher moments. Still, a number of theoretical predictions have been made for the detection of higher cumulants. In a later section the behavior of the system will be discussed in the presence of a counting statistics detector that has already been experimentally realized. This detector does not detect charges at the interfaces, but rather on the dot.

5.2.1 Transport in the non-interacting case

For reference, the statistics in the absence of Coulomb interaction are first summarised here. As mentioned above, the master equation needed to describe non-interacting electrons is two-dimensional and the eigenvalue of its kernel Eq. (5.6) is easily calculated.

As expected, the lowest order contribution in Γ, which describes transport through the quantum dot in absence of the reference arm, is given by the Bagrets-Nazarov formula [111]

$$S^{(\Gamma)}(\chi) = t_0 \frac{\Gamma_L + \Gamma_R}{2}\left(1 - \sqrt{\mathcal{D}_0(\chi)}\right) \tag{5.18}$$

$$\mathcal{D}_0(\chi) = 1 + \frac{4\Gamma_L\Gamma_R}{(\Gamma_L+\Gamma_R)^2}\left[f_L(1-f_R)(e^{i\chi}-1) + (1-f_L)f_R(e^{-i\chi}-1)\right] \tag{5.19}$$

where the Fermi-functions are taken at the level energy ϵ. The statistics contains terms for left- and right-moving electrons ($e^{\pm i\chi}$, respectively), but since it does not factorize, these cannot be regarded as independent.

Expanding the eigenvalue to lowest order in $|t^{\mathrm{ref}}|$, the interfering part of the statistics if found to be

$$S_0^{(\Gamma|t^{\mathrm{ref}}|)}(\chi,\phi) = t_0|t^{\mathrm{ref}}|\sqrt{\Gamma_L\Gamma_R}\cos\phi\, A(\chi), \tag{5.20}$$

where $A(\chi)$ consists of the same off-resonant, Poissonian processes as in Eq. (5.10). This is in accordance with Ref. [6], where the current of this system was calculated and found to be an even function of magnetic flux. [1]

The transport processes giving rise to the flux dependence are interference contributions of direct tunneling between the leads and elastic (i.e., energy- and spin-conserving) co-tunneling through the single-level quantum dot. The co-tunneling contribution causes the appearance of principal value integrals. They are proportional to the transmission amplitude through the reference arm and to the transmission rate through the quantum dot. Arguments backing up this interpretation were collected in the previous section 5.1.1. The main properties of the noninteracting case (to be contrasted later with results in the presence of electron correlations) are:

(i) The statistics is *bidirectional Poissonian*. This indicates that the individual transport processes are independent from each other, which is consistent with the notion that elastic co-tunneling through the quantum dot does not change its state.

(ii) The cumulant generating function is an *even* function of the Aharonov-Bohm phase ϕ. Onsager relations [182] require the linear conductance of a two-terminal device to be even in the magnetic field. For noninteracting electrons, the transmission for each energy, that could be probed by the linear conductance at low temperature, is independent from the other energies. Therefore, in the absence of Coulomb interaction, the cumulant generating function has to be an even function of ϕ in leading order of the transmission.

(iii) As the amplitude for transmission through the quantum dot is determined by co-tunneling, the energy ω of the incoming electron does not have to match the energy ϵ of the quantum level. Therefore the processes are of *off-resonant* nature.

Generating function of the non-interacting dot via Levitov-formula

In the absence of interaction a single-particle treatment of noninteracting electrons can be used. The full counting statistics for transport of noninteracting electrons through an arbitrary two-terminal setup is given by the Levitov-Lesovik formula [100],

$$\begin{aligned} S(\chi) &= 2t_0 \int \frac{\mathrm{d}\omega}{2\pi\hbar} \ln\Big\{1 + T(\omega)\Big[f_L(\omega)[1-f_R(\omega)](e^{i\chi}-1) \\ &\quad + [1-f_L(\omega)]f_R(\omega)(e^{-i\chi}-1)\Big]\Big\} \end{aligned} \tag{5.21}$$

which expresses the cumulant generating function in terms of the energy-dependent transmission probability $T(\omega)$ per spin channel, where $f_L(\omega)$ and $f_R(\omega)$ are the Fermi functions of the left and right leads, respectively. The factor 2 outside the integral describes the fact that two independent spin channels contribute.

[1] The occupation probabilities are independent of the reference arm and thus also flux, i.e., they are those of a simple quantum dot.

The transmission probability is the modulus squared of the transmission amplitude that, for the quantum-dot ABI, is the sum of the amplitudes for transmission through the reference arm and through the arm containing the quantum dot, respectively. For the symmetric case $\Gamma_L = \Gamma_R = \Gamma/2$ the exact transmission is known to be [183, 184]:

$$T(\omega) = \frac{(2|t^{\mathrm{ref}}|\omega/\Gamma - \cos\phi)^2 + \sin\phi^2}{\left[(2 + \frac{1}{2}|t^{\mathrm{ref}}|^2)\omega/\Gamma - \frac{1}{2}|t^{\mathrm{ref}}|\cos\phi\right]^2 + 1} \tag{5.22}$$

Inserting this in the Levitov-formula and expanding the resulting expression yields the generating function. Since only the lowest orders in Γ and $|t^{\mathrm{ref}}|$ are needed, the transmission itself can be expanded:

$$T^{(\Gamma)}(\omega) = \frac{(\frac{\Gamma}{2})^2}{(\frac{\Gamma}{2})^2 + (\omega - \epsilon)^2} \tag{5.23}$$

$$T^{(\Gamma|t^{\mathrm{ref}}|)}(\omega) = \sqrt{\Gamma_L\Gamma_R}|t^{\mathrm{ref}}|\,\cos\phi \int' \mathrm{d}\omega \frac{1}{\epsilon - \omega} \tag{5.24}$$

$$T^{(|t^{\mathrm{ref}}|^2)}(\omega) = |t^{\mathrm{ref}}|^2 \tag{5.25}$$

The non-interfering transport contributions are immediately understood: The transmission for transport through a dot, Eq. (5.23), is given by a Breit-Wigner resonance. The well known generating function of a single level in the limit of weak coupling [111] does not immediately follow from mere insertion in the Levitov-formula. It is rather necessary to define a χ-dependent current $I(\chi) = (ie/t_0)\partial S/\partial\chi$, as has been described in Ref. [111]. If the resonant level is placed between the energy levels of the leads, the main contribution to the integral in the Levitov-formula comes from the sharp (since $\Gamma \ll k_B T$) Lorentz peak. Closing the integration contour in the upper (lower) half plane, only the pole $\epsilon \pm i\sqrt{\mathcal{D}_0(\chi)}/2$ contributes [with $\mathcal{D}_0(\chi) = 1 + f_L(1 - f_R)(e^{i\chi} + (1 - f_L)f_R(e^{-i\chi} - 1)$] and the χ-dependent current is

$$I(\chi) = \frac{1}{2}\Gamma\left[f_L(1 - f_R)e^{i\chi} - (1 - f_L)f_R e^{-i\chi}\right]/\sqrt{\mathcal{D}_0(\chi)}$$

Integrating this over χ results in the generating function Eq. (5.18).

The transparency of the reference arm, Eqn. 5.25, is constant with respect to energy, which means that a Taylor expansion of the Levitov-formula leads to Poissonian statistics. The integral sums up all independent energy channels that lie in the bias window:

$$S^{(|t^{\mathrm{ref}}|^2)}(\chi) = t_0|t^{\mathrm{ref}}|^2 \int \frac{\mathrm{d}\omega}{\pi\hbar} f_L(1 - f_R)(e^{i\chi} - 1) + (1 - f_L)f_R(e^{-i\chi} - 1) \tag{5.26}$$

In the interfering contribution, the second term of Eq. (5.24), the integral of the Levitov-formula is transformed into a Cauchy principal value. Inserting Eqn. 5.24 in the Levitov-formula, together with an expansion in the small parameters yields again the generating function Eq. (5.20) previously obtained within the master equation approach. Thus, the correspondence between two different approaches to the FCS of non-interacting systems, the master equation approach and the Levitov-formula, has been shown.

5.2.2 Additional contributions to the statistics for an interacting dot

For interacting electron systems, the notion of a transmission probability $T(\omega)$ that contains all information about the full counting statistics via the Levitov-Lesovik formula is, in general, not applicable anymore. Incidentally such a notion still works for the lowest-order contribution $S^{(\Gamma)}(\chi)$. In fact, the non-interfering CGF for the interacting case can be reproduced by using that of the noninteracting one but with rescaled coupling parameters:

$$\Gamma_{L,R} \to \frac{\Gamma_L+\Gamma_R}{2}(F+1)\left(1 \pm \sqrt{1-\frac{8\Gamma_L\Gamma_R}{(\Gamma_L+\Gamma_R)^2}\frac{1}{(F+1)^2}}\right). \tag{5.27}$$

For the interference part $S^{(t^{\rm ref}\Gamma)}(\chi)$, however, one could define a transmission probability $T(\omega)$ by writing the current in the form $I=(e/h)\sum_\sigma \int d\omega T(\omega)[f_L(\omega)-f_R(\omega)]$, but plugging this transmission probability into the Levitov-Lesovik formula would not reproduce the higher cumulants.

An additional effect of Coulomb interaction was also discussed in Sec. 2.3.1: In a closed geometry the current must be an even function of the magnetic flux in linear response [6, 180]. This phenomenon is known as phase-locking. Beyond linear response phase locking may in general be broken [181]. It has been shown that the current of the single dot ABI indeed has a $\sin(\phi)$-contribution for finite voltages [6]. The statistics will therefore also have a contribution with odd flux dependence.

The low-order contributions to the cumulant generating function $S_\infty(\chi)=S^{(\Gamma)}(\chi)+S^{(|t^{\rm ref}|\Gamma)}(\chi,\phi)+S^{(|t^{\rm ref}|^2)}(\chi)$ are found to be

$$\begin{aligned}
S^{(\Gamma)}(\chi) &= -t_0\frac{\Gamma_L+\Gamma_R}{2}(F+1)\left(1-\sqrt{\mathcal{D}_\infty(\chi)}\right) && (5.28)\\
\frac{S^{(|t^{\rm ref}|\Gamma)}(\chi,\phi)}{t_0|t^{\rm ref}|\sqrt{\Gamma_L\Gamma_R}} &= \cos\phi\, A(\chi)\,\frac{2}{F+1} \\
&\quad -\frac{1}{2}\,\cos\phi\, A(\chi)\left[1-\frac{1}{\sqrt{\mathcal{D}_\infty(\chi)}}\right]\frac{1-3F}{F+1} \\
&\quad -\frac{1}{2}\,\sin\phi\, B(\chi)\left[1-\frac{1}{\sqrt{\mathcal{D}_\infty(\chi)}}\right] && (5.29)\\
S^{(|t^{\rm ref}|^2)}(\chi) &= t_0\,|t^{\rm ref}|^2\int {\rm d}\omega\big[f_L(\omega)(1-f_R(\omega))\big](e^{i\chi}-1) \\
&\quad +\big[(1-f_L(\omega))f_R(\omega)\big](e^{-i\chi}-1). && (5.30)
\end{aligned}$$

with the following definitions

$$\begin{aligned}
\mathcal{D}_\infty(\chi) &= 1+8\frac{\Gamma_L\Gamma_R}{(\Gamma_L+\Gamma_R)^2}\,\frac{1}{(F+1)^2} \\
&\quad \times\left[f_L(1-f_R)(e^{i\chi}-1)+(1-f_L)f_R(e^{-i\chi}-1)\right] && (5.31)\\
F &= \frac{\Gamma_L f_L(\epsilon)+\Gamma_R f_R(\epsilon)}{\Gamma_L+\Gamma_R} && (5.32)
\end{aligned}$$

The second term, Eq. (5.29) contains the central new results, while the first [111, 173] and third terms are well known. The first term is the Bagrets-Nazarov formula for an interacting quantum dot [111]. The third line, which describes transport through the reference arm only is naturally unaffected by dot properties and therefore the same as in the non-interacting case, Eq. (5.26).

As has already been argued, there are two kinds of terms in the interfering part of the generating function, differing in their flux dependence. Additionally they show a different voltage dependence, being resonant and off-resonant. The first type of processes are those associated with interference between co-tunneling through the dot and direct tunneling from left to right $[A(\chi)]$. These processes are of off-resonant nature and carry an even flux dependence. They are described by the first two terms in $S^{(t^{\mathrm{ref}}\Gamma)}(\chi)$. The first part looks similar to the CGF of the noninteracting problem. The only change is the appearance of the factor $1/(F+1)$. This factor describes partial reduction of the interference due to spin-flip processes.

This can be understood as follows: In a co-tunneling picture it is clear that transport of an electron through the initially occupied dot may or may not flip the dot spin. A spin flip process leaves a trace in the environment and is thus incoherent. Since the spin conserving processes are coherent, the flux dependence is not completely destroyed, but rather partially suppressed. This partial suppression depends on whether spin flip processes are possible and thus on the dot occupation. This dependence has already been shown to modify the current by a prefactor $1/(F+1)$ [6], with $F(\epsilon) = [\Gamma_L f_L(\epsilon) + \Gamma_R f_R(\epsilon)]/(\Gamma_L + \Gamma_R)$. Its influence on the statistics is found to be more complicated: Due to the second term in the CGF for these off-diagonal processes, described by the second line of Eq. (5.29), the statistics is not bidirectional Poissonian anymore. This means that the Coulomb interaction introduces correlations between left and right going processes. Although it is not totally unexpected that interaction induces correlations, it is still remarkable, since the processes involved are off-resonant and change the dot state only virtually. It should be noted that this term enters neither current nor noise in linear response.

The most significant effect of Coulomb interaction is, however, the appearance of a second type of transport processes, described by the third line of Eq. (5.29). Contributions of this kind are completely absent in the non-interacting case. They are of on-resonant nature, and they carry an odd flux dependence. As can be seen from the rates, Eq. (5.9), some of them are related to a change in the dot state, in contrast to the off-resonant co-tunneling terms that only occupy the dot virtually. A more detailed analysis in the shot noise regime, where the properties of sine and cosine terms become more peculiar, follows in Section 5.2.4.

5.2.3 Onsager relations for the generating function near equilibrium

Onsager relations require the linear conductance to be an even function of magnetic flux [6]. The idea behind the argument is that the system has to be time invariant in linear response. Here these arguments are extended to comprise the entire counting statistics.

The argument relies on a symmetry property of the system, illustrated in Fig. 5.3.

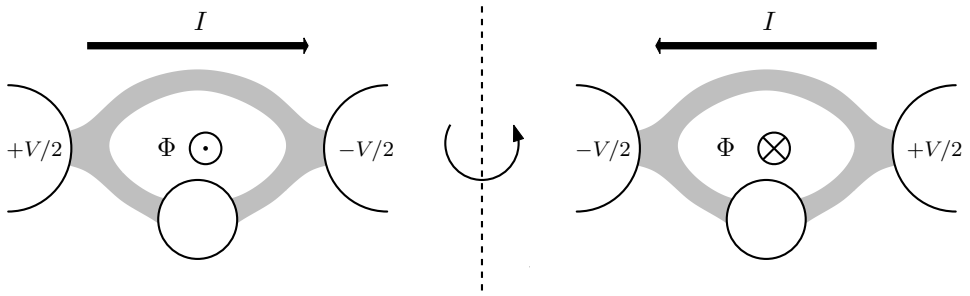

Figure 5.3: Symmetry operation to apply Onsager relations. Rotation of the system about the dashed axis corresponds to a time reversal operation ($V \to -V$, $I \to -I$, $\Phi \to -\Phi$).

Applying the time reversal operation on the system means that current I, bias voltage V and AB-phase ϕ are reversed. As can be seen from the figure this does not change the system, it merely corresponds to a spatial rotation. This means for the current, that

$$I(V,\phi) \quad = \quad -I(-V,-\phi). \tag{5.33}$$

By taking the derivative with respect to the transport voltage in equilibrium, the Onsager relation for the linear conductance is derived:

$$\frac{\partial}{\partial V} I(V,\phi)\bigg|_{V=0} \quad = \quad \frac{\partial}{\partial V} I(V,-\phi)\bigg|_{V=0}. \tag{5.34}$$

Strictly speaking this argument holds only for $\Gamma_L = \Gamma_R$, since otherwise the exchange of source and drain contact would be noticable. However, for the lowest interfering order, which is proportional to $|t^{\mathrm{ref}}|\sqrt{\Gamma_L \Gamma_R}$, this is irrelevant, since both source and drain contact participate in the transport processes. Correspondingly, the linear conductance is even in magnetic flux, i.e., the sine-contributions start in order V^2.

The fluctuation-dissipation theorem [185, 186] relates linear conductance and equilibrium noise:

$$\langle I^2 \rangle\big|_{V=0} = 4 k_B T \left.\frac{\partial I}{\partial V}\right|_{V=0} \tag{5.35}$$

Since the linear conductance is even in the magnetic flux, this implies that the $\sin(\phi)$-contribution to the generating function does not produce equilibrium noise. What is more, the argument can be extended to all of the even moments in linear response: The n-th cumulant is given as the sum of expectation values of products of up to n current operators, such that in each addend the total number of current operators coincides with the order of the cumulant, e.g., $\kappa_4 \sim \langle I^4 \rangle - 3(\langle I^2 \rangle)^2$. To each of these terms the relation Eq. (5.33) can be applied. Taking the limit $V \to 0$ shows that the order n determines the flux symmetry

$$[I(0,\phi)]^n \quad = \quad (-1)^n \, [I(0,-\phi)]^n \, . \tag{5.36}$$

As a result, the even order cumulants contain no sine-contribution, while the odd order cumulants contain no cosine contribution in equilibrium:

$$\kappa_{2n}^{\sin}(V=0)=0 \tag{5.37}$$
$$\kappa_{2n+1}^{\cos}(V=0)=0 \tag{5.38}$$
$$\tag{5.39}$$

This may also be directly derived from the generating functions Eq. (5.29). A generating function with vanishing even moments κ_{2n} has to be even in χ, while for the odd moments κ_{2n+1} to vanish it has to be odd in χ. The sine and cosine parts of Eq. (5.29) indeed fulfill these conditions:

$$S_{\cos}^{(|t^{\mathrm{ref}}|\Gamma)}(\chi)\Big|_{V=0} = S_{\cos}^{(|t^{\mathrm{ref}}|\Gamma)}(-\chi)\Big|_{V=0} \tag{5.40}$$
$$S_{\sin}^{(|t^{\mathrm{ref}}|\Gamma)}(\chi)\Big|_{V=0} = -S_{\sin}^{(|t^{\mathrm{ref}}|\Gamma)}(-\chi)\Big|_{V=0} \tag{5.41}$$

where $S_{\sin\,/\,\cos}$ denote the parts of the generating function proportional to $\sin(\phi)$ and $\cos\phi$, respectively. The time inversion is in this case simply performed by inverting the sign of the bias voltage, magnetic flux and of the counting field (instead of the current).

5.2.4 Signature of double particle effects in the shot noise regime

The properties of the modifications introduced by Coulomb interaction become more apparent in the shot noise regime, $\pm eV = \mu_L - \mu_R \gg k_B T$. In this case the transport voltage dominates over thermal fluctuations such that $f_L(\epsilon) = 1$ and $f_R(\epsilon) = 0$ and transport occurs mainly from left to right lead both for resonant and non-resonant processes[2]. In the following the additional assumption of strongly asymmetric left and right tunnel couplings, described by the ratio $\gamma = \Gamma_L/\Gamma_R \gg 1$ or $\gamma \ll 1$, is made. This means that, for transport through the QD alone, the bottleneck is given by the left ($\gamma \ll 1$) or the right ($\gamma \gg 1$) barrier. As mentioned above, the flux-dependent contributions can be studied individually. For this purpose the cumulants $\kappa_{\cos,\sin}^{(n)}$ are defined separately as the parts of the cumulant with flux dependence $\cos\phi, \sin\phi$. Then generalized factors can be defined as the quotients $\kappa_{\cos,\sin}^{(n)}/I_{\cos,\sin}$ with $I_{\cos,\sin} \equiv \kappa_{\cos,\sin}^{(1)}$ being the $\sin\phi$- and $\cos\phi$-dependent part of the current, divided by the elementary charge e.

Figure 5.4(a) shows the cosine-dependent generalized Fano factors as a function of $\Gamma_L/\Gamma_R = \gamma$. In the extremely asymmetric case where one arm is almost pinched off $\gamma \gg 1$ or $\gamma \ll 1$, the noise becomes Poissonian: $\kappa_{\cos}^{(n)} = I_{\cos}$.

This is not the case for the sine-dependent generalized Fano factors, Fig. 5.4(b). They are enhanced and approach $\kappa_{\sin}^{(n)}/I^{\sin} = 2^n - 1$ for $\gamma \gg 1$ or $\gamma \ll 1$. For $n = 2$, the Fano factor is 3. The transfer of q charges in one or a sequence of multiple elementary transport events is associated [187, 188, 103, 104] with a Fano factor $\kappa^{(2)}/\kappa^{(1)} = q$ and similar for higher cumulants ($\kappa^{(3)}/\kappa^{(1)} = q^2$) [97]. Within the framework of counting

[2] This is obvious for the resonant terms, but also holds for the off-resonant terms.

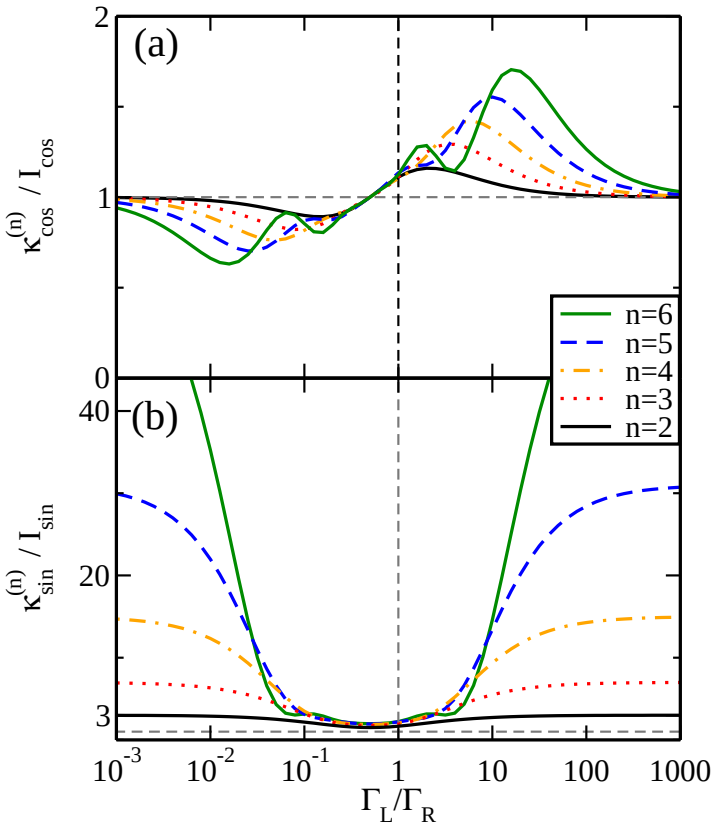

Figure 5.4: Generalized Fano factors $\kappa^{(n)}_{\mathrm{cos,sin}}/I_{\mathrm{cos,sin}}$ in the shot noise regime $\mu_L \gg \epsilon \gg \mu_R$. $\kappa^{(n)}_{\mathrm{cos,sin}}$ is the $\cos\phi/\sin\phi$-dependent part of the n-th cumulant ($n = 2$: noise, $n = 3$: skewness, etc.). (a) Cosine-dependent generalized Fano factors, determined by off-resonant processes. The value 1 is assumed at $\Gamma_L/\Gamma_R = 1/2$. (b) Sine-dependent generalized Fano factors, determined by on-resonant processes. They approach $2^n - 1$ for $\Gamma_L \gg \Gamma_R$ or $\Gamma_L \ll \Gamma_R$, while the minimum lies at $\Gamma_L/\Gamma_R = 1/2$ and has the value $(2^n - 1)/2^{n-1}$.

statistics, such transport processes with q_i charges carry counting factors $e^{iq_i\chi}-1$. The appearance of multiple counting factors with different q_i implies that transport occurs through several elementary events with different charges [59, 60, 66]. In our case, the Fano factor of 3 does not hint at three charges per event, rather a combination of single and double charges are involved. Expanding the cumulant generating function in terms of $\gamma \ll 1$ reveals counting factors for single and double charge transfers:

$$\begin{aligned} S_\infty(\chi) &= t_0\, 2\Big[\gamma\Gamma_R\,(e^{i\chi}-1) \\ &\quad +|t^{\mathrm{ref}}|\Gamma_R\,\gamma^{\frac{3}{2}}\,\sin\phi\; e^{i\chi}(e^{i\chi}-1) \\ &\quad +|t^{\mathrm{ref}}|\Gamma_R\sqrt{\gamma}\cos\phi\;\frac{e^{i\chi}-1}{F+1}\frac{1}{\pi}\ln\left|\frac{\mu_L-\epsilon}{\mu_R-\epsilon}\right| \\ &\quad +eV|t^{\mathrm{ref}}|^2(e^{i\chi}-1)\Big]\,. \end{aligned} \tag{5.42}$$

The first term describes transport trough the quantum dot in absence of the reference arm. Transport behavior is dominated by the smaller tunnel barrier $\Gamma_L = \gamma\Gamma_R$ and transport becomes Poissonian. The last line describes transport through the reference arm in absence of the dot and is also Poissonian. The cosine part of the interference term (third term) is, for very asymmetric tunnel couplings, Poissonian as well.

The sine part of the interference term, however, is different. It contains a counting factor of $e^{i2\chi}$, which is responsible for the enhanced generalized Fano factors. It should be noted that this contribution is proportional to $\gamma^{3/2}$, i.e., one order higher in the asymmetry γ than the cosine term.

One could hope to identify the appearence of the $e^{i2\chi}$ term not only in the higher cumulants but also directly in the probability distribution $P(N,t_0)$ as an even-odd feature. But once t_0 is large enough to get a reasonable number of transferred charges to identify the probability distribution, then the even-odd features from the sine part will be washed out by the other contributions in Eq. (5.42).

The statements made in this section might also be of experimental relevance: The $\sin\phi$- and $\cos\phi$-dependent parts can be easily distinguished from each other, either by performing a Fourier analysis for the cumulants or by tuning the flux such that only processes of one kind contribute to transport.

5.3 Dot charge detector

The full counting statistics of quantum dot systems have been measured with great success with the help of a detector, which measures the charge on (one of) the quantum dots in the system [67, 134, 135]. Under the assumption of large bias voltages, the temporal changes of this charge are related to the full counting statistics (see Sec. 3.3.3). Inspired by these experiments this section discusses in how far the statistics of the single dot Aharonov-Bohm interferometer can be measured by charge detection.

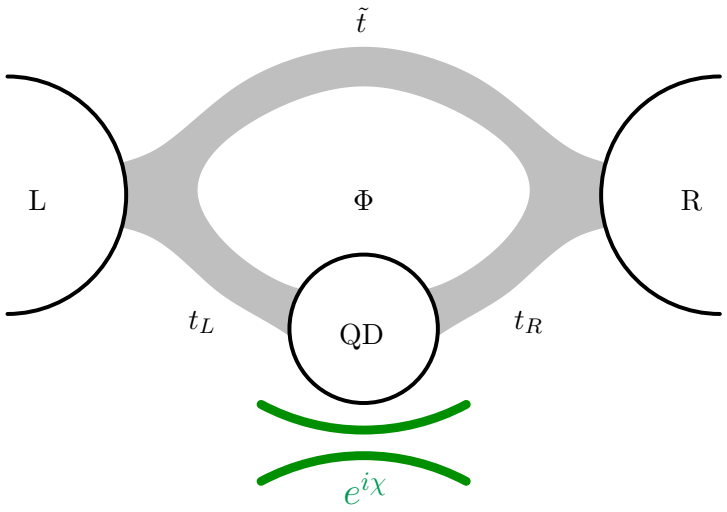

Figure 5.5: Dot charge detector: the transmission of the quantum point contact is strongly affected by the charge on the quantum dot in close vicinity. The change in the QPC-current allows to reconstruct the generating function of transport through the dot. See also Section 3.3.3.

5.3.1 Detector model

The detector has already been discussed in Section 3.3.3. In the experiments [67, 134, 135] it consisted of a quantum point contact in vicinity of a quantum dot. Charging the quantum dot with an additional electron increases the potential of the QPC's constriction and thus reduces the current. The switching of the QPC between a low and high current state is then detected, which yields the counting statistics of the dot.

Strictly speaking the counting statistics obtained in this way are those for the occupation of the quantum dot. Due to the assumption of large bias voltages, these statistics correspond to those of transport *through* the dot: Electrons entering the dot will always come from the left lead and electrons leaving the dot will always go to the right lead.

One may be worried that interference is destroyed by detecting the electrons on the dot. This is, however, only true for an open quantum-dot ABI for which measuring the dot charge provides a which-path information [189]. In closed interferometers (cf. Sec. 2.3.1) a measurement of the dot charge does not yield path information, because paths encircling the flux several times are possible [190, 191]. Furthermore, even without allowing for such higher winding numbers the knowledge of the electrons being on the quantum dot does not include the knowledge of the path along which it leaves: The electron might tunnel directly to the drain lead or first go back to the source virtually and then tunnel to the drain via the reference arm. These processes are exactly those described by the resonant terms $C(\chi)$ and $D(\chi)$.

Modeling of the detector requires adding a second index to the occupation probabilities [142, 143]: $\mathbf{p} = (p_{00}, p_{\uparrow 0}, p_{\downarrow 0}, p_{01}, p_{\uparrow 1}, p_{\downarrow 1})$. The first index $n = 0, \uparrow, \downarrow$ denotes the state of the dot and the second $m = 0, 1$ describes the state the detector believes the

dot to be in. Upon change of the dot state the detector follows with a rate Γ_D. This is described by a master equation for the probabilities $p_{n,m}$:

$$\frac{d}{dt}\mathbf{p}(t) = \begin{pmatrix} W_{0,0} & W_{0,\uparrow} & W_{0,\downarrow} & \Gamma_D & 0 & 0 \\ W_{\uparrow,0} & W_{\uparrow,\uparrow} - \Gamma_D & 0 & 0 & 0 & 0 \\ W_{\downarrow,0} & 0 & W_{\downarrow,\downarrow} - \Gamma_D & 0 & 0 & 0 \\ 0 & 0 & 0 & W_{0,0} - \Gamma_D & W_{0,\uparrow} & W_{0,\downarrow} \\ 0 & \Gamma_D e^{i\chi} & 0 & W_{\uparrow,0} & W_{\uparrow,\uparrow} & 0 \\ 0 & 0 & \Gamma_D e^{i\chi} & W_{\downarrow,0} & 0 & W_{\downarrow,\downarrow} \end{pmatrix} \mathbf{p}(t). \quad (5.43)$$

The rates $W_{i,j}$ are the rates of the system in absence of the detector. For the system at hand they are given by Eqns. (5.8) and (5.9) taken in the shot noise regime and for vanishing counting field $W_{i,j} = \left[W_{i,j}^{(\Gamma)} + W_{i,j}^{(|t^{\mathrm{ref}}|\Gamma)}\right]_{\substack{eV \gg kT \\ \chi=0}}$. The counting factor $e^{i\chi}$ is introduced for the transition from $p_{1,0}$ to $p_{1,1}$, i.e., when the charge on the dot is detected. The counting statistics for the detector motion can be obtained in the same way as before by taking the eigenvalue with the lowest negative real part.

5.3.2 Counting statistics for the detector motion

The lowest-order generating function for the detector motion without interaction on the quantum dot has been calculated before [143]. There it was also discussed that in the limit of infinite bandwidth $\Gamma_D \to \infty$ the generating function for a quantum dot [111] is recovered. Since the models for zero and strong interaction differ only by a factor of two in the rates for filling of the dots (Eq. (5.7)), the counting statistics also only differ by this factor. This means Γ_L has to be replaced by $2\Gamma_L$ in the interacting case. This changes the inverse lifetime of an electronic state on the dot $\Gamma = \Gamma_L + \Gamma_R$ to $\Gamma_\infty = 2\Gamma_L + \Gamma_R$:

$$S_0^{(\Gamma)}(\chi) = -t_0 \frac{\Gamma + \Gamma_D}{2} \left(1 - \sqrt{1 + \frac{4\Gamma_D}{(\Gamma + \Gamma_D)^2} S_0^{\mathrm{dot}}(\chi)}\right) \quad (5.44)$$

$$S_\infty^{(\Gamma)}(\chi) = -t_0 \frac{\Gamma_\infty + \Gamma_D}{2} \left(1 - \sqrt{1 + \frac{4\Gamma_D}{(\Gamma_\infty + \Gamma_D)^2} S_\infty^{\mathrm{dot}}(\chi)}\right) \quad (5.45)$$

The generating function for the ABI in absence of the detector $S_{0,\infty}^{\mathrm{dot}}(\chi)$ (Eq. (5.18) and Eq. (5.28), respectively) is dressed by terms depending on both detector rate $\Gamma_D/\hbar$ and the inverse lifetime $\Gamma\Gamma_\infty/\hbar$. This dressing describes a reduction of all moments due to the finite bandwidth Γ_D. This reduction is intuitively understandable: Owing to its finite bandwidth the detector misses some events, which naturally leads to a reduced current and thus also to reduced cumulants. What is more, not only the unnormalized cumulants are reduced for all values of Γ_D, but also the normalized cumulants $\frac{\kappa_n(\Gamma_D)}{\kappa_1(\Gamma_D)} < \left.\frac{\kappa_n}{\kappa_1}\right|_{\Gamma_D \to \infty}$.[3] For a non-interacting quantum dot the lower bound

[3] In the case $\Gamma_D \ll \Gamma$ both normalized and unnormalized cumulants are also reduced. This limit corresponds to a detector of vanishing bandwidth and is thus not physically meaningful.

for the Fano-factor was found to be 3/8 [143]. Here, for the AB interferometer, such a lower boundary cannot be easily given, due to the influence of the reference arm, which was included perturbatively and may in- and decrease the boundary, depending on the value of the magnetic flux. Still, changes are of the order of $|t^{\mathrm{ref}}|$ and thus only a small perturbation to the value 3/8.

In the limit of an infinite detector bandwidth $\Gamma_D \gg \Gamma, \Gamma_\infty$ all tunneling events are detected and the generating function of the interface detector is reproduced:

$$S^{(\Gamma)}_{0,\infty}(\chi) \quad \xrightarrow{\Gamma_D \to \infty} \quad S^{\mathrm{dot}}_{0,\infty}(\chi) \tag{5.46}$$

Since the detector localizes the electrons on the dot, it could be expected that it destroys coherence. However, this is not rue: While the position of the electron is known, it remains unknown along which path it got onto the dot and along which path it will leave. Consequently interference is not destroyed and a flux-dependent correction appears.

Still, the detector is not equivalent to the interface current detector: Processes that do not change the dot state cannot be detected. The diagonal parts of the kernel, which are nothing but the resonant contributions of co-tunneling through the dot, can therefore not be detected. This means in particular that no $\cos(\phi)$-terms appear. The terms which do appear are related to the off-diagonal parts of the kernel and thus the entire interfering part of the statistics has to be proportional to $\sin(\phi)$.

The interfering part of the generating function turns out to be more complicated, but simplifies greatly for a perfect detector:

$$\begin{aligned} S^{(|t^{\mathrm{ref}}|\Gamma)}_{\infty}(\chi,\phi) \quad &= \quad -t_0\,|t^{\mathrm{ref}}|\sqrt{\Gamma_L\Gamma_R}\sin\phi\left\{2\frac{\Gamma_L-\Gamma_R}{\Gamma_\infty}\frac{e^{i\chi}-1}{\sqrt{\mathcal{D}_\infty}}\frac{1}{G}\right. \\ &\quad \left. +\frac{1}{2}\left(1-\frac{1}{\sqrt{\mathcal{D}_\infty}}\frac{1}{G}-\frac{\Gamma_\infty}{\Gamma_D}\frac{1}{G}\right)\right\} \qquad (5.47) \\ &\xrightarrow{\Gamma_D\to\infty} \quad -t_0\,|t^{\mathrm{ref}}|\sqrt{\Gamma_L\Gamma_R}\sin\phi\left\{2\,\frac{\Gamma_L-\Gamma_R}{\Gamma_\infty}\frac{e^{i\chi}-1}{\sqrt{\mathcal{D}_\infty(\chi)}}\right. \\ &\quad \left. +\frac{1}{2}\left(1-\frac{1}{\sqrt{\mathcal{D}_\infty(\chi)}}\right)\right\} \qquad (5.48) \end{aligned}$$

The term $G = \sqrt{1+4\frac{\Gamma_D}{(\Gamma_D+\Gamma_\infty)^2}\mathcal{D}^{\mathrm{dot}}_\infty(\chi)}$ appearing in the expression for finite bandwidth simplifies to $G(\chi)\to 1$ for a perfect detector with $\Gamma_D \to \infty$.

This result has the following properties. First, cosine terms do not appear for both $U = 0$ and $U = \infty$. This is clear, because the detector is insensitive to the off-resonant co-tunneling processes $A(\chi)$ which go along with only a virtual occupation of the dot. In addition, the detector is insensitive to the resonant contribution $B(\chi)$ to the co-tunneling processes, as they also preserve the dot state. Correspondingly, the same statistics can be obtained if $A(\chi)$ and $B(\chi)$ are replaced by by $A(0)$ and $B(0)$ in Eq. (5.9) instead of solving the detector model Eq. (5.43). In this case it becomes apparent that the flux-dependent contribution may be understood as a correction to

the tunneling rates $\Gamma_{L,R}$: The rates in the kernel Eqns. (5.8) become

$$W_{1,0} = \Gamma_L + |t^{\mathrm{ref}}|\sqrt{\Gamma_L\Gamma_R}\sin\phi \tag{5.49}$$

$$W_{0,1} = \Gamma_R - |t^{\mathrm{ref}}|\sqrt{\Gamma_L\Gamma_R}\sin\phi. \tag{5.50}$$

Expanding the non-interfering generating function for a QD with these rescaled rates in terms of $|t^{\mathrm{ref}}|$ yields the first part of Eqns. (5.47,5.48). In the case of detection at the interfaces (Sec. 5.2), these terms did not appear, since they were cancelled by the resonant contributions of the charge conserving processes $B(\chi)$.

$$\begin{aligned} S_0^{(|t^{\mathrm{ref}}|\Gamma)}(\chi,\phi) &= -t_0\,|t^{\mathrm{ref}}|\sqrt{\Gamma_L\Gamma_R}\sin\phi\frac{\Gamma_L-\Gamma_R}{\Gamma}\frac{\Gamma_D}{\Gamma+\Gamma_D} \\ &\quad\times\frac{e^{i\chi}-1}{\sqrt{\mathcal{D}_0(\chi)}}\frac{1}{\sqrt{1+\frac{4\Gamma_D}{(\Gamma+\Gamma_D)^2}S_0^{\mathrm{dot}}(\chi)}} \end{aligned} \tag{5.51}$$

$$\xrightarrow{\Gamma_D\to\infty} -t_0\,|t^{\mathrm{ref}}|\sqrt{\Gamma_L\Gamma_R}\sin\phi\frac{\Gamma_L-\Gamma_R}{\Gamma}\frac{e^{i\chi}}{\sqrt{\mathcal{D}_0(\chi)}} \tag{5.52}$$

Moreover, Coulomb interaction also influences the sine-terms: It causes the second term of Eq. (5.48). In Fig. (5.6) the flux-dependent corrections to the cumulants are plotted. Their only interesting feature is a sign change for specific values of Γ_L/Γ_R – the enhanced moments for extreme asymmetry are lost.

In conclusion, is is found that measuring the quantum-dot charge by a nearby QPC does, indeed, provide some information of the FCS of the transport through the quantum-dot ABI. Naturally, interference processes that do not change the occupation of the dot remain undetected. This includes the off-resonant interference contributions with an even flux dependence and part of the on-resonant contributions with an odd flux dependence. The on-resonant interference processes that are accompanied with a change of the dot state, though, can be detected in that way. As not all processes are detected, the counting statistics of the sine-processes are not the same as in the interface detector model and the double particle features are lost.

Additionally, it is predicted that $\sin(\phi)$ terms appear also in the counting statistics of an non-interacting dot. It might appear that this violates the symmetry relations discussed in Section 5.2.3. However, this is not true, since the symmetry arguments were formulated for the system in absence of the detector. The occurrence of these terms depends crucially on an asymmetry of the coupling rates $\Gamma_L \neq \Gamma_R$. The very same term appears also in the interacting system (although in this case there is also the term known from the interface detector model). This suggests that introduction of the detector which distinguishes between filling and emptying universally introduces this term, regardless of the dot properties.

5.4 Chapter summary

In this chapter the counting statistics of an Aharonov-Bohm interferometer with a quantum dot embedded in one of its arms have been analyzed. In particular the effects of strong Coulomb interaction on the dot were discussed.

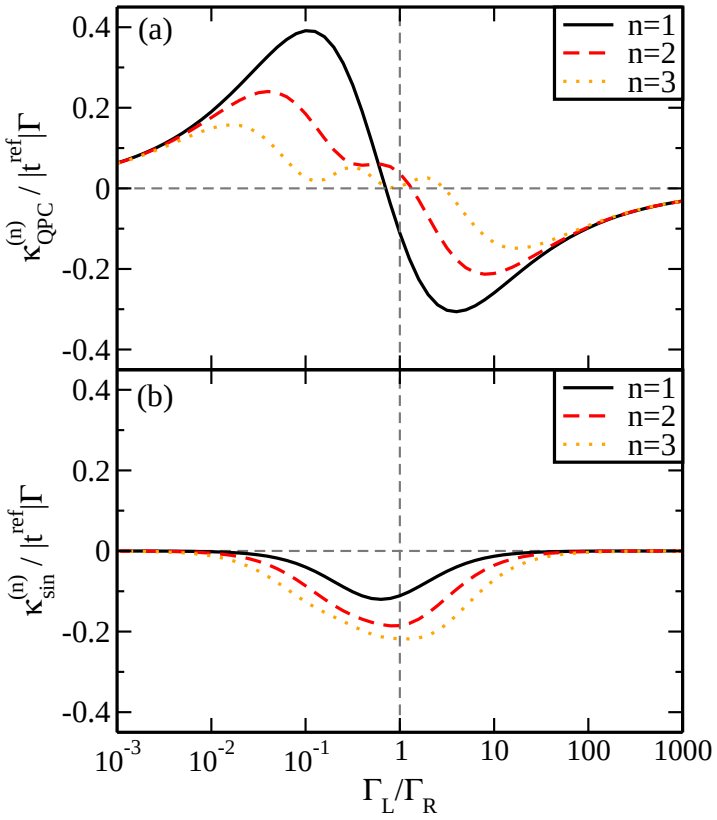

Figure 5.6: Logarithmic plots of the n-th cumulants $\kappa^{(n)}_{\rm QPC}$ (in presence of a perfect QPC-detector, solid, from Eq. (5.48)) and $\kappa^{(n)}_{\rm sin}$ (without the QPC-detector, grey, from Eq. (5.42)) in the shot noise regime $\mu_L \gg \epsilon \gg \mu_R$ (such that $f_L = 1, f_R = 0$). The value 1 is plotted for reference.

The rates of change of the quantum dot state (as they appear in the master equation) of a single dot Aharonov-Bohm interferometer are found to be the unaffected by Coulomb interaction: There are contributions both even and odd in the magnetic flux. Both of these arise due to interference of one amplitude for direct tunneling and one amplitude for co-tunneling via an intermediate state.

As required by Onsager relations the $\sin\phi$-terms do not appear in the statistics of a non-interacting dot. Rather the interfering part of the statistics is composed of Poissonian off-resonant terms with an even flux dependence.

In case of large charging energy on the dot, the picture changes. Firstly coherence is partially reduced due to spin-flip processes, which is reflected in a prefactor $1/(F+1)$. Secondly correlations between the off-resonant processes are introduced, so that their statistics is no longer Poissonian. Finally $\sin\phi$-terms appear in the statistics for finite bias. In the case of strongly asymmetric coupling of the dots to the leads, the moments of their statistics turn out to be strongly super-Poissonian, i.e., growing with increasing order of the moment. This is striking, since all other processes become Poissonian in this limit as events are determined by the smaller of the two rates and therefore become uncorrelated. The form of the generating function suggests that the $\sin\phi$-processes are related to double particle events in this limit.

In the last part of the chapter it was examined which of these features are detectable by measuring the charge of the quantum dot. Since the $\cos\phi$-processes leave the charge of the dot unchanged, such a detector is blind to them. Regrettably the interesting physics of the sine-processes in the interacting case is also lost. Instead, since the detector introduces an asymmetry between filling and emptying of the dot (by distinguishing these processes), some of the properties of the interacting case (in which the asymmetry between filling and emptying is inherently introduced in the rates) are carried over into the non-interacting statistics: A characteristic term with odd-flux dependence is introduced.

6 Tunable channel blockade in double dot Aharonov-Bohm interferometers

In this chapter the counting statistics of a parallel double quantum dot (DQD) as shown in Fig. 6.1 are analyzed. The dots are weakly coupled to two leads, operated in the shot-noise regime, with an Aharonov-Bohm flux Φ enclosed by the two paths. For sufficiently large separation of the dots, no interdot charging effects and interdot tunneling are possible. Assuming strong intradot interaction, the system can accommodate at most two electrons.

While sometimes neglected in transport studies [86, 192], the electron's spin can play a crucial role in this setup. Recently a scheme was pointed out how entangled electron pairs are generated by transport through a DQD [15, 16]: depending on the Aharonov-Bohm phase decay of the singlet to the drain is supressed. This resembles coherent population trapping, an effect originally described in quantum optics [17] that has become important also in condensed matter physics [19, 20, 193, 194]. In other words, the system contains a slowly and a quickly decaying state. It is known that this may lead to bunching and thus the singlet-triplet imbalance should be reflected in current noise and higher cumulants.

Indeed bunching behavior is found, strongly dependent on the magnetic flux. Its origin lies in the Hilbert space's decomposing into two parts when the flux assumes integer multiples of the flux quantum – one for the singlet and one for the triplets. Each subspace has its own transport statistics and the transition between the two parts is mediated by the magnetic flux.

In order to describe the system dynamics not only the doubly occupied singlet and triplet states need be appropriately described, also the singly occupied state demands some attention: Since the system consists of two levels, it is fully described only by a non-diagonal density matrix, whose off-diagonal components may be interpreted as an isospin. The second section therefore deals with the question of how to calculate the counting statistics of systems with off-diagonal components in the density matrix.

6.1 Hamiltonian and density matrix

The double dot interferometer shown in Fig. 6.1 is described by the following Hamiltonian

$$H = H_{\mathrm{u}} + H_{\mathrm{d}} + H_L + H_R + H_T\,. \tag{6.1}$$

Each of the two leads is described as a reservoir of non-interacting fermions $H_{\mathrm{r}} = \sum_{k\alpha} \varepsilon_{rk\sigma}\, a^\dagger_{rk\sigma} a_{rk\sigma}$ with indices for lead $r \in \{L, R\}$, momentum k and spins σ (see Sec. 4.1). The tunneling Hamiltonian H_T consists of parts $H_{T,r}$ for tunneling between

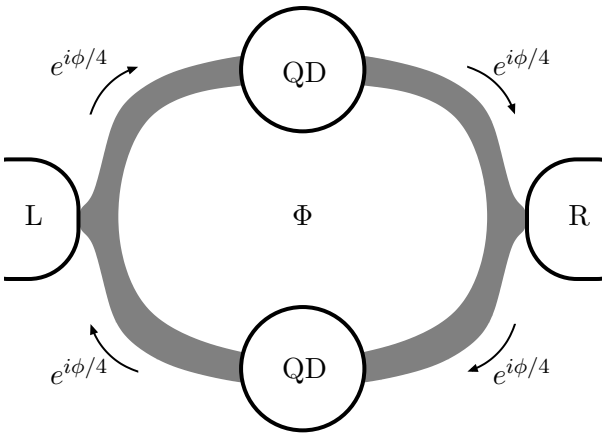

Figure 6.1: The double dot Aharonov-Bohm interferometer consists of two quantum dots (u and d) connected to two leads in parallel. The paths through the dots enclose a magnetic flux Φ, giving rise to Aharonov-Bohm interference.

each dot i and each lead r

$$H_{T,ri} = \sum_{k,\sigma} |t|_k^r \, e^{\pm i\phi/4} a_{rk\sigma}^\dagger c_{i\sigma} + \text{H.c.}, \tag{6.2}$$

with the flux dependence included in the phase factors $e^{\pm i\phi/4}$ according to Fig. 6.1. The phase ϕ is related to the magnetic flux Φ through the ring as $\phi = 2\pi\Phi/\Phi_0$. This setup is related to a quantum-dot spin-valve, identifying the two spin states on the dot with the dots in the two arms and the AB-phase with the phase factors originating from a finite angle between the lead polarizations [73]. The tunneling rate through interface r is quantified by $\Gamma_r(\omega)/\hbar = 2\pi \, |t_r|^2 \, \rho_r/\hbar$. The rates are assumed to be the same for tunneling to upper and lower dot from lead i. For simplicity, the densities of state ρ_r and the tunneling amplitudes t_r are assumed to be independent of energy, which implies constant tunneling rates.

Both quantum dots, $H_\text{i} = \sum_\sigma \varepsilon_i \, c_{i\sigma}^\dagger c_{i\sigma} + U_i n_{i\uparrow} n_{i\downarrow}$ with $i = u, d$, are described as Anderson impurities with spin-degenerate electronic levels $\epsilon_u = \epsilon_d = \epsilon$ and charging energy $U_{u/d}$ for double occupation. Only the regime of strong Coulomb interaction (U_i greater than all other energies) is of interest here. This implies that only single occupation of each dot is allowed.

In addition to strong on-site Coulomb repulsion, no interdot interaction is assumed, so that the entire system can be occupied by at most two electrons. The Hilbert space thus consists of the states $|\mu_u, \mu_d\rangle$ with $\mu_{u,d} \in \{0, \uparrow, \downarrow\}$ describing the occupation of dot i. It is more intuitive to express the density matrix in a different basis, which is introduced in the following. The probabilities $p_0 = \langle |0\rangle \langle 0| \rangle$ and $p_1 = p_u + p_d$ for an empty and a singly occupied dot are an obvious choice ($p_u = \sum_\sigma \langle |\sigma, 0\rangle \langle \sigma, 0| \rangle$ and $p_d = \sum_\sigma \langle |0, \sigma\rangle \langle 0, \sigma| \rangle$). However, the singly occupied state is more complex: Charging the empty system with one electron of spin σ from the left lead results in the state $c_{L,\sigma}^\dagger |0\rangle \equiv (e^{i\frac{\phi}{4}} c_{u\sigma}^\dagger + e^{-i\frac{\phi}{4}} c_{d\sigma}^\dagger) |0\rangle = e^{i\frac{\phi}{4}} |\sigma, 0\rangle + e^{-i\frac{\phi}{4}} |0, \sigma\rangle$. This state is not fully

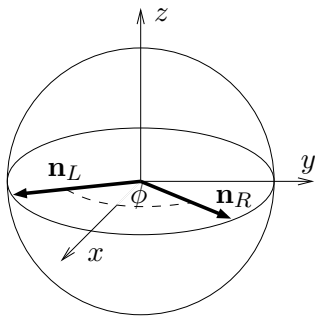

Figure 6.2: Isospin polarization directions of left (right) lead $\mathbf{n}_{L(R)}$. The isospins enclose an angle ϕ which is given by the Aharonov-Bohm phase $2\pi\Phi/\Phi_0$. The choice of coordinates is such that the state with one electron in the upper dot corresponds to an isospin fully aligned in $+z$-direction.

described by the probability of single occupation p_1, it rather needs to be further specified by off-diagonal elements of the density matrix $p_\nu^\mu = \langle |\mu\rangle \langle \nu| \rangle$ where μ and ν label the dot states. These off-diagonal elements are summarized as an isospin in the two-dimensional Hilbert-space of the two dot levels $\mathbf{I}_\sigma/2 = (I_{\sigma,x}, I_{\sigma,y}, I_{\sigma,z})/2 = (\frac{p_d^u+p_u^d}{2}, \frac{p_d^u-p_u^d}{2i}, \frac{p_u-p_d}{2})/2$. In this basis the state reached by tunneling in from the left lead is isospin-polarized along $\mathbf{n}_L = (\cos\phi/2, \sin\phi/2, 0)$. The right lead is correspondingly isospin-polarized along $\mathbf{n}_R = (\cos\phi/2, -\sin\phi/2, 0)$ (see Fig. 6.2).

Due to strong Coulomb interaction on the dots double occupation of the system is allowed only if one electron is found on each dot. Addition of a second electron from the left reservoir leads to the doubly occupied state $c_\sigma^\dagger(e^{i\frac{\phi}{4}} |\sigma, 0\rangle + e^{-i\frac{\phi}{4}} |0, \sigma\rangle)$. Since double occupation of individual dots is prohibited, this equals $|S\rangle = (|\uparrow,\downarrow\rangle - |\downarrow,\uparrow\rangle)/\sqrt{2}$, which means that by filling from the source lead only the singlet state $|S\rangle$ is accessible. The three triplets $|T_+\rangle = |\uparrow,\uparrow\rangle$, $|T_-\rangle = |\downarrow,\downarrow\rangle$, $|T_0\rangle = (|\uparrow,\downarrow\rangle + |\downarrow,\uparrow\rangle)/\sqrt{2}$ can be accessed only indirectly by removing one electron from the singlet state. The resulting isospin need not point in $+x$-direction so that filling with a second electron can result in a triplet. Spin symmetry of the Hamiltonian requires all triplets to be occupied with equal probability $p_{T_+} = p_{T_-} = p_{T_0} = p_T$. For this reason all other spin indices are dropped in the following.

In summary, there are seven non-vanishing elements of the density matrix: four probabilites and three off-diagonal components, expressed as an isospin $\mathbf{I}$. For the calculation of the counting statistics it is helpful to arrange these elements in a vector

$$\boldsymbol{\pi} = (p_0, p_1, p_S, p_T, I_x, I_y, I_z)^T . \tag{6.3}$$

Then, the master equation can be written in matrix form although the density matrix is not diagonal:

$$\frac{\partial}{\partial t}\boldsymbol{\pi}(N,t) = \mathbf{W}(N,t) \cdot \boldsymbol{\pi}(N,t) \tag{6.4}$$

The kernel $\mathbf{W}$ can now be calculated, starting from the Hamiltonian in Eq. (6.1)

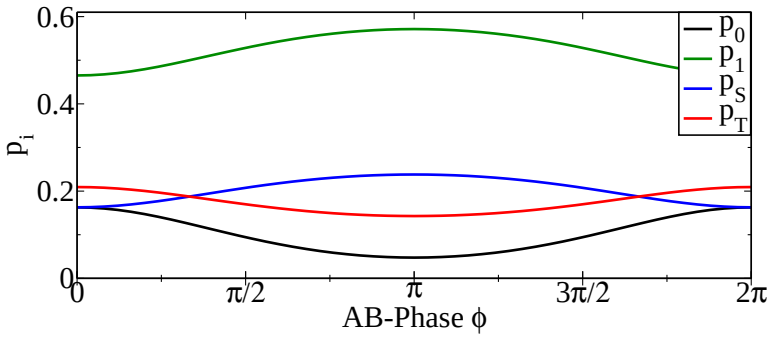

Figure 6.3: Occupation probabilities as a function of magnetic flux for a symmetric system in the shot-noise regime $f_L = 1, f_R = 0$. The oscillations do not follow a cosine law.

using the diagrammatic real-time technique discussed in Sec. (4.1). While for the calculation of the counting statistics the matrix form Eq. (6.4) is used, the master equation is presented here using a more intuitive notation distinguishing between occupation probabilities $\mathbf{p} = (p_0, p_1, p_S, p_T)$ and isospin $\mathbf{I}$.

$$\begin{aligned}\frac{d}{dt}\mathbf{p} &= \sum_{r=L,R} \Gamma_r \begin{pmatrix} -4f_r & e^{-i\chi_r}(1-f_r) & 0 & 0 \\ e^{i\chi_r} 4f_r & -(1+f_r) & e^{-i\chi_r} 2(1-f_r) & e^{-i\chi_r} 2(1-f_r) \\ 0 & e^{i\chi_r} \frac{1}{2} f_r & -2(1-f_r) & 0 \\ 0 & e^{i\chi_r} \frac{3}{2} f_r & 0 & -2(1-f_r) \end{pmatrix} \cdot \mathbf{p} \\ &\quad + \Gamma_r \begin{pmatrix} e^{-i\chi_r} 2(1-f_r) \\ -2(1-2f_r) \\ e^{i\chi_r} f_r \\ -e^{i\chi_r} 3f_r \end{pmatrix} \mathbf{I} \cdot \mathbf{n}_r \end{aligned} \tag{6.5}$$

$$\begin{aligned}\frac{d}{dt}\mathbf{I} &= \sum_{r=L,R} \Gamma_r \left[e^{i\chi_r} 2f_r p_0 + (1-f_r)p_1 + e^{-i\chi_r}(1-f_r)p_S - e^{-i\chi_r}(1-f_r)p_T \right] \mathbf{n}_r \\ &\quad - \Gamma_r (1+f_r)\mathbf{I} \end{aligned} \tag{6.6}$$

The power of this notation lies in the intuitive meaning of the isospin, which behaves analogous to the spin in a magnetic field. The double dot Aharonov-Bohm interferometer thus becomes similar to a quantum dot spin valve [153]. The main difference (and as will be seen later also the most interesting properties) is caused by the more complex structure of the doubly occupied state. Still, the analogy reaches so far, that the transmission through the system is larger if the (iso)spin polarizations of the leads are parallel than when they are anti-parallel.

The master equation will only be analyzed in the shot noise regime $f_L(\epsilon) = 1$, $f_R(\epsilon) = 0$ in the following. The stationary occupation probabilities are shown in Fig. 6.3 for a symmetric system, $\Gamma_L = \Gamma_R$.

6.2 Counting statistics for a system with a non-diagonal density matrix

The singly occupied subspace requires for a complete description not only its occupation probability p_1, but also an isospin $\mathbf{I}$, i.e., off-diagonal elements of the density matrix. So far it has only been formulated how to obtain the counting statistics from a master equation for a diagonal density matrix (cf. Ch. 4). In this case the master equation was formulated in matrix form

$$\frac{d}{dt}\rho(N,t) = \int \mathrm{d}t' \sum_{N'} \mathbf{W}(N-N', t-t')\rho(N', t') \tag{6.7}$$

with $\rho = (\rho_{\mu_1}^{\mu_1}, \rho_{\mu_2}^{\mu_2}, \ldots)$ denoting a vector of the diagonal elements of the density matrix. The generating function is then related to these probabilities

$$S(\chi) = \ln \sum_N e^{iN\chi} P(N,t), \text{ with } P(N,t) = \mathbf{e}^T \cdot \rho(N,t) \tag{6.8}$$

where $\mathbf{e}^T = (1, 1, \ldots, 1)$ is a vector of ones, summing responsible for summation of the diagonal elements of ρ. Its exact definition does not matter, since it appears in the calculation only in the combination $\ln(\mathbf{e}^T \cdot \mathbf{p_0})(\mathbf{q_0^T} \cdot \mathbf{p}_{\mathrm{in}})$ (in Eq. (4.26)), which drops out in the final expression for the generating function Eq. (4.27).

As mentioned above, the master equation can also be written in matrix form, if a vector $\pi(N,t)$ is defined to consist of the diagonal elements of the density matrix first, followed by the non-diagonal entries:

$$\pi(N,t) = (\rho_1^1, \rho_2^2, \ldots, \rho_n^n, \rho_{\mu_1}^{\nu_1}, \rho_{\mu_2}^{\nu_2}, \ldots, \rho_{\mu_m}^{\nu_m}) \text{ with } \mu_i \neq \nu_i. \tag{6.9}$$

Then the probability $P(N,t)$ that N charges passed the system after time t is obtained by summing over the first n components only, i.e., the vector $\mathbf{e}^T$ has to be redefined

$$\mathbf{e}^T = (\underbrace{1, \ldots, 1}_{n \text{ times}}, 0, \ldots, 0). \tag{6.10}$$

With this the generating function is correctly defined. However, since $\mathbf{e}^T$ does not appear in the final expression, the generating function is related to the eigenvalue of the master equation's kernel $\mathbf{W}$ in the same way as before.

Additionally, if the system states are not energetically degenerate, the master equation may contain a term $\frac{i}{\hbar}(E_{\chi_1} - E_{\chi_2})\rho_{\chi_2}^{\chi_1}(t)$. It is local in time and can be absorbed in the kernel as a contribution proportional to $\delta(t-t')$.

It should be noted, that now the kernel also describes the evolution of the off-diagonal elements of the density matrix. Therefore information about the off-diagonal elements also enters the generating function, although it does not depend on the exact definition of $\mathbf{e}^T$. In other words, the generating function can be calculated in the same way as in the case of diagonal density matrix.

Also for the perturbative calculation scheme for the cumulants described in Sec. 4.3 no modifications are required, since the role of $\mathbf{e}^T$ is taken over by the left nullvector

of $\mathbf{W}$. This can be seen from probability conservation $0 = \sum_\mu W_{\mu\nu}$, which can also be written as $0 = \mathbf{e}^T\mathbf{W}$, with $\mathbf{e}^T$ as above. It is therefore clear that there must always be at least one left nullvector and that it must always coincide with $\mathbf{e}^T$. In case a second left (and therefore also right) nullvector exists, the counting statistics can be calculated neither with the perturbative approach, nor via the eigenvalues (cf. next section).

6.3 Dynamical channel blockade for vanishing flux $\phi = 0$

In the limit of vanishing flux the master equation decouples into a part containing the singlet and a part containing the triplet occupation. This can be understood by visualizing the mechanism for charging the dots: the initially empty dot is first populated with an electron from the source, resulting in a state with isospin $|+\rangle_L$. The second electron entering from the source always results in a singlet state. Correspondingly the triplet and isospin $|-\rangle_L$ belong to a different subspace. Since the subspaces decouple and have different counting statistics an effect similar to bunching gives rise to noise enhancement for $\phi = 0$.

6.3.1 Separation of subspaces

When the Aharonov-Bohm flux assumes multiples of the flux quantum $\phi = 2\pi m$ and the master equation (6.5,6.6) separates into two blocks. This has been discussed in Refs. [15, 16]. This decoupling is related to the fact that starting from an empty dot not all system states are accessible by filling from the left lead. The first electron charging the system is isospin-polarized along the source direction $\mathbf{n}_L$, i.e., the system is in a state $|+\rangle_L$ with $p_1 = 1$ and $\mathbf{I}\cdot\mathbf{n}_L = 1/2$ (In absence of a flux, the isospin polarization is such that the electron is equally distributed between the two dots). Charging the system with a second electron results in the singlet state (as discussed above). Correspondingly the states $|0\rangle$, $|+\rangle_L$, $|S\rangle$ form a separate subspace.

The corresponding occupation probabilities can be expressed in terms of the isospin by noting that the projector $|+\rangle_{LL}\langle+|$ can be written as $|+\rangle_{LL}\langle+| = (|1,0\rangle\langle 0,1| + |0,1\rangle\langle 0,1|)/2 + (|1,0\rangle\langle 0,1| + |0,1\rangle\langle 1,0|)/2 = p_1/2 + \mathbf{I}\cdot\mathbf{n}_L$. This motivates to transform the master equation with $\mathbf{S}$, so that $\mathbf{S}\,\mathbf{p} = (p_0, \frac{p_1}{2} + \mathbf{I}\cdot\mathbf{n}_L, p_S, \frac{p_1}{2} - \mathbf{I}\cdot\mathbf{n}_L, p_T, \mathbf{I}\cdot(\mathbf{n}_z \times \mathbf{n}_L), I_z)$, in order to make visible the different subspaces. This means that in the first three components it is summarized what from now on will be referred to as the $+$-subspace, named after the isospin component it contains. The fourth and fifth component contain the $-$-subspace (consisiting of $|-\rangle_R$ and $|T\rangle$), while the last two components describe the remaining directions of the isospin, which are orthogonal to $|+\rangle_L$ and $|-\rangle_R$ and are thus referred to as the $\perp$-subspace. The density matrix elements are thus arranged in the vector $\mathbf{Sp} = (\mathbf{p}_+, \mathbf{p}_-, \mathbf{p}_\perp)$ with the following defintions:

$$\mathbf{p}_+ = \begin{pmatrix} p_0 \\ \frac{p_1}{2} + \mathbf{I}\cdot\mathbf{n}_L \\ p_S \end{pmatrix}, \quad \mathbf{p}_- = \begin{pmatrix} \frac{p_1}{2} - \mathbf{I}\cdot\mathbf{n}_L \\ p_T \end{pmatrix}, \quad \mathbf{I}_\perp = \begin{pmatrix} \mathbf{I}\cdot(\mathbf{n}_z \times \mathbf{n}_L) \\ I_z \end{pmatrix}. \quad (6.11)$$

With these definitions the master equation can be written as

$$\begin{aligned}
\frac{d}{dt}\mathbf{p}_+ &= \mathbf{W}_+\,\mathbf{p}_+ \qquad (6.12)\\
&\quad + e^{i\frac{\chi}{2}}\frac{1-\cos\frac{\phi}{2}}{2}\begin{pmatrix} 2\Gamma_R & 0 \\ 0 & 2\Gamma_R \\ \Gamma_L & 0 \end{pmatrix}\mathbf{p}_- + \sin\frac{\phi}{2}\begin{pmatrix} e^{i\frac{\chi}{2}}2\Gamma_R & 0 \\ -\Gamma_L+\Gamma_R & 0 \\ -e^{i\frac{\chi}{2}}\Gamma_L & 0 \end{pmatrix}\mathbf{I}_\perp\\
\frac{d}{dt}\mathbf{p}_- &= \mathbf{W}_-\,\mathbf{p}_- \qquad (6.13)\\
&\quad + e^{i\frac{\chi}{2}}\frac{1-\cos\frac{\phi}{2}}{2}\begin{pmatrix} 4\Gamma_L & 0 & 2\Gamma_R \\ 0 & 3\Gamma_L & 0 \end{pmatrix}\mathbf{p}_+ + \sin\frac{\phi}{2}\begin{pmatrix} -\Gamma_L-\Gamma_R & 0 \\ e^{i\frac{\chi}{2}}3\Gamma_L & 0 \end{pmatrix}\mathbf{I}_\perp\\
\frac{d}{dt}\mathbf{I}_\perp &= \sin\frac{\phi}{2}\left[\begin{pmatrix} -e^{i\frac{\chi}{2}}2\Gamma_L & -\frac{\Gamma_L+\Gamma_R}{2} & e^{i\frac{\chi}{2}}\Gamma_R \\ 0 & 0 & 0 \end{pmatrix}\mathbf{p}_+ \right. \qquad (6.14)\\
&\quad \left. + \begin{pmatrix} -\frac{\Gamma_L+\Gamma_R}{2} & -e^{i\frac{\chi}{2}}\Gamma_R \\ 0 & 0 \end{pmatrix}\mathbf{p}_-\right] - (2\Gamma_R+\Gamma_R)\mathbf{I}_\perp,
\end{aligned}$$

with $\mathbf{W}_+$ and $\mathbf{W}_-$ given by

$$\mathbf{W}_+ = \begin{pmatrix} -4\Gamma_L & e^{i\frac{\chi}{2}}2G_R^+ & 0 \\ e^{i\frac{\chi}{2}}4G_L^+ & -\Gamma_L(2-\cos\frac{\phi}{2})-\Gamma_R(1+\cos\frac{\phi}{2}) & e^{i\frac{\chi}{2}}2G_R^+ \\ 0 & e^{i\frac{\chi}{2}}G_L^+ & -2\Gamma_R \end{pmatrix}, \qquad (6.15)$$

$$\mathbf{W}_- = \begin{pmatrix} -\Gamma_L(2+\cos\frac{\phi}{2})-\Gamma_R(1-\cos\frac{\phi}{2}) & e^{i\frac{\chi}{2}}2G_R^+ \\ e^{i\frac{\chi}{2}}3G_L^+ & -2\Gamma_R \end{pmatrix}. \qquad (6.16)$$

Therein the definitions $G_r^\pm = \Gamma_r\frac{1\pm\cos\frac{\phi}{2}}{2}$ have been used.

It turns out that for zero flux the master equation assumes block diagonal form and the +- and −-subspaces decouple. The +-subspace is found in the upper-left 3×3 block. In presence of a flux it is coupled by tunneling, i.e., a change in the charge state, to the 2×2-dimensional −-subspace located in the middle. However, this coupling cannot be described simply by a rate $\Omega_{+\leftrightarrow-}$. Instead there are six possible transition paths which occur with four different rates. The paths and rates can be read off from the 2×3- and 3×2-matrices in Eqns. (6.12) and (6.13)

As for $\phi = 0$ the system decomposes into two uncoupled subsystems it is no longer possible to calculate its counting statistics as described in Ref. [173]. There are two independent stationary solutions of the master equation (6.5,6.6) – one for each subspace. The full stationary solution would obviously be a linear combination of the two, with the coefficients given by the initial occupations of the subspaces, i.e., the stationary state depends on the initial conditions. For the same reason it is unclear how the counting statistics have to be defined: There are two eigenvalues that vanish for $\chi \to 0$ and a simple linear combination of them, like for the stationary occupation, does not do the job: As discussed in the following sections, the statistics which are obtained as analytic continuation from $\phi \neq 0$ differ from those that would be obtained from

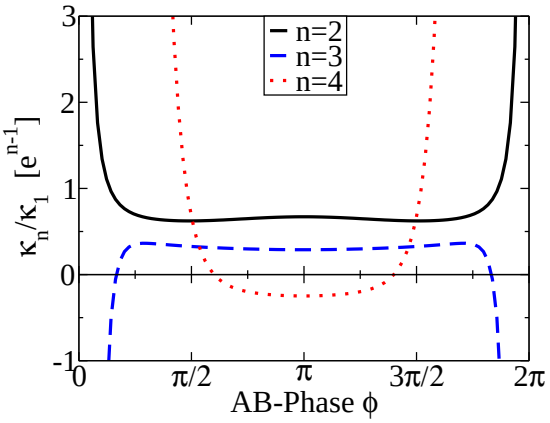

Figure 6.4: The normalized n-th cumulants κ_n/κ_1 diverge for $\phi \to n\pi$ in a symmetric system ($\Gamma_L = \Gamma_R$), due to the competition of two channels belonging to different system states. The width of the divergence is governed by the relaxation rate between these two states.

a linear combination of two generating functions, regardless of the initial conditions. Also the perturbative method described in Sec. 4.3 runs into problems: While usually the correct subspace is determined automatically by multiplication with left and right nullvector, in the case of decoupled subsysytems there are also two different sets of nullvectors (one for each subspace) and it remains unclear, how the recursive equation Eq. (4.38) has to be solved.

We do not investigate further how the counting statistics of a system in which the stationary state, depends on the initial condition, can be calculated. It can be expected that any physical system is subject to some mechanism that lifts the degeneracy and couples the subspaces. One such mechanism is already inherent in the present system: by excluding the points $\phi = 2\pi m$ from the calculation the subspaces are always coupled and the counting statistics at the degeneracy points can be obtained by continuation of the solutions found in the vicinity. In Section 6.5 a number of different mechanisms resulting in a coupling of the subspaces are discussed.

6.3.2 Super-Poissonian statistics

The separation of the system's Hilbert space into two separate subspaces has consequences for the transport statistics: The subspaces have different transport properties, such that the system continually switches between a high and a low voltage state, which leads to enhanced noise, similar to bunching. There are two factors determining the magnitude of noise enhancement: The larger the difference in the currents of the two states is, the more enhanced is the noise. As the rate with which the system switches between the states is decreased, the noise is expected to be enhanced further. In the system discussed, the coupling can be decreased to zero by tuning the magnetic flux such that the phase assumes multiples of 2π. In this case the subspaces decouple and all normalized cumulants diverge as $\kappa_n/\kappa_1 = (1/\sin\phi/2)^{2(n-1)}$ (Fig. 6.4). It should

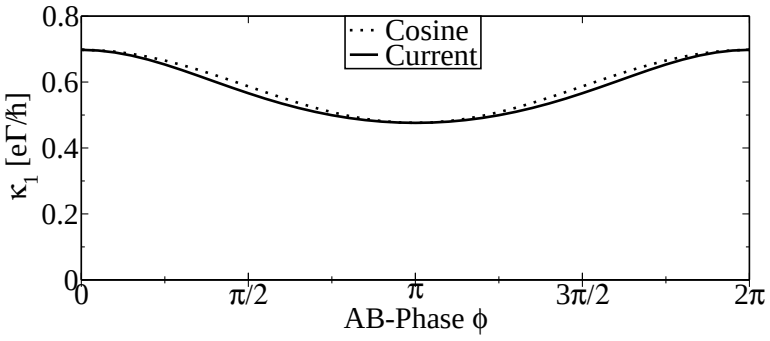

Figure 6.5: The current through the double dot system is subject to Aharonov-Bohm oscillations. These are not following an exact cosine law.

be emphasized that the divergence of the normalized cumulants is not caused by a vanishing current, whose dependence on flux is approximately cosine-like (Fig. 6.5), i.e., maximal at $\phi = 0$.

To specify the picture outlined above the properties of the subspaces are analyzed separately. For this purpose the generating functions associated with the 3×3- and 2×2-subspaces containing singlet and triplet, $\mathbf{W}_+$ and $\mathbf{W}_-$, respectively, are calculated (see Eq. (6.15)).

The generating function for the $-$-subspace Eq. (6.17) resembles that for a quantum dot, as could be expected, since the subspace is spanned by only two states,

$$S_- = -t_0 \frac{3\Gamma_L + 2\Gamma_R}{2} \left(1 - \sqrt{1 + \frac{4(3\Gamma_L)(2\Gamma_R)}{(3\Gamma_L + 2\Gamma_R)^2}(e^{i\chi} - 1)} \right). \tag{6.17}$$

The transition rates are $3\Gamma_L$ for filling and $2\Gamma_R$ for emptying. This can be understood by counting the possible realizations of each state: If the dot is in a triplet state, taking away either of the two eletrons results in single occupation. On the other hand, starting from a singly occupied state there are three triplets which can be accessed by tunneling into the system.

While the generating function for the $+$-subspace can be easily obtained, it is too complex to be shown here. It describes a three state system, with transition rates as can be read off from Eq. (6.15). The lower part of Fig. 6.6 shows these rates.

There are numerous examples in the literature, in which super-Poissonian noise is caused by different states participating in transport. They comprise, e.g., two levels with different coupling to the source [66] and different coupling to source and drain with an additional inter-level coupling [67]. A model closer to a real telegraph model was discussed in Ref. [42]: Transport occurs through a single level, but occasionally a side-coupled level is charged, so that transport is temporarily suppressed due to Coulomb blockade.

The complex internal dynamics distinguish the double quantum dot discussed here from these in two ways: Firstly the two states are not just differing in current, but are each characterized by their own distribution function. Secondly the transitions

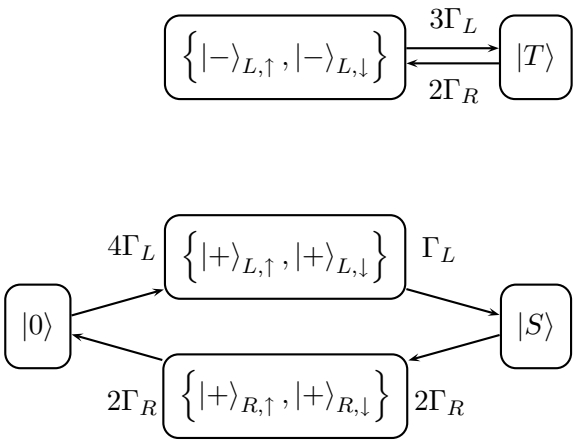

Figure 6.6: Rates connecting the different states in the triplet (top) and singlet (bottom) subspaces. Note that for $\phi = 2\pi m$ the singly occupied states are equal, $|\pm\rangle_L = |\pm\rangle_R$.

between the subsystems cannot just be described by simple rates $\Gamma_{+\leftrightarrow-}$. Instead there are many coupling paths, which are described by the matrices in in Eqns. (6.12)-(6.14).

6.3.3 Statistics for strongly asymmetric coupling $\Gamma_L \gg \ll \Gamma_R$

The subspace dynamics depend on the tunneling rates: Fig. 6.7. shows the first three normalized cumulants of a system with asymmetric tunnel coupling to source and drain. It is noticeable that the width of the divergencies is greatly reduced for $a = (\Gamma_L - \Gamma_R)/(\Gamma_L + \Gamma_R) \to +1$, i.e., with the drain lead being the bottleneck. Due to the complexity of the problem an analyic analysis of the generating function is not possible in this regime. However, plotting the cumulants Poissonian behavior is found for sufficiently large values of a.

Apparently the bunching effect has disappeared. In order to understand this, the behavior of the $+$- and $-$-subspaces needs to be investigated. Bunching requires the two states to have different transport properties. It turns out that for $a \to 1$ the properties of the $+$- and $-$-space become the same. Figure 6.8 shows the current I_- (I_+) under the condition that the system is in the $+$-($-$-)space as a function of the the asymmetry. These currents are obtained from the generating functions for each subspace (see previous section Eqn. 6.17). They become equal for $a \to +1$.

In the limit $a \to \pm 1$ the generating functions simplify and a perturbative expansion around $a = 1$ shows that not only the currents, but also the generating functions are equal to leading order:

$$S_+|_{a\to 1} = t_0\, 2\Gamma_R(e^{i\chi} - 1) - \frac{1}{4}\Gamma(a-1)^3 e^{2i\chi}(e^{i\chi} - 1) \tag{6.18}$$

$$S_-|_{a\to 1} = t_0\, 2\Gamma_R(e^{i\chi} - 1) - \frac{1}{3}\Gamma(a-1)^2 e^{i\chi}(e^{i\chi} - 1) \tag{6.19}$$

In the opposite case $a \to -1$ they are also Poissonian, but with different mean

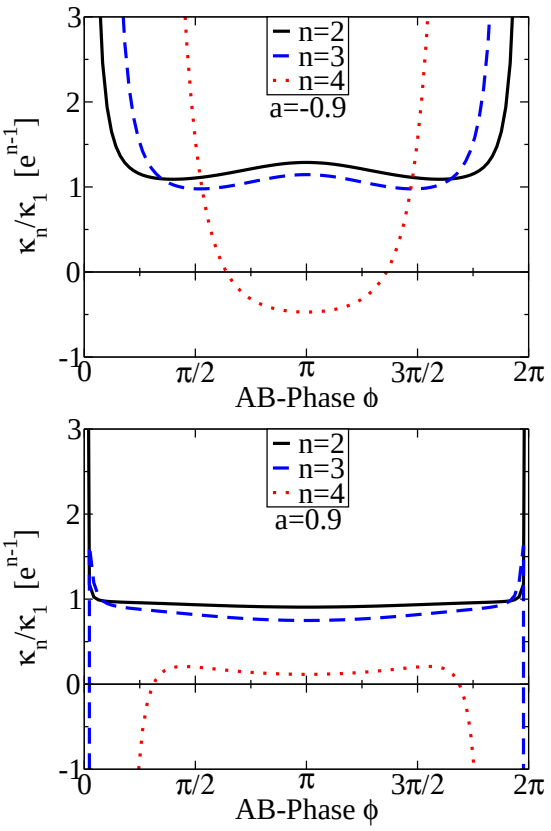

Figure 6.7: The normalized n-th cumulants κ_n/κ_1 of the non-symmetric system also diverge (upper plot: $a = (\Gamma_L - \Gamma_R)/(\Gamma_L + \Gamma_R) = -0.9$, lower plot: $a = +0.9$). It is however visible the width of the divergence is greatly reduced for positive a. In the limit of $a \to +1$ the divergence disappears and transport becomes Poissonian.

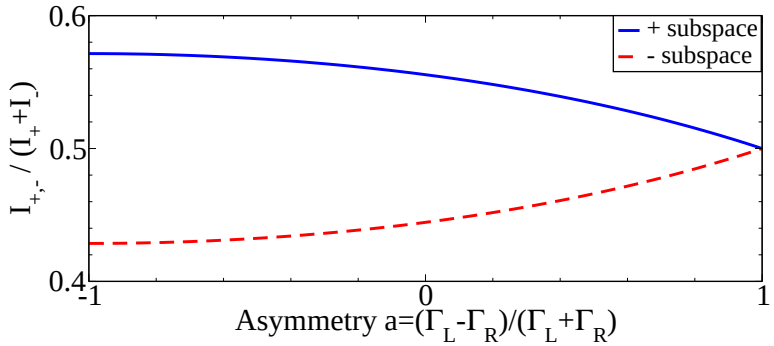

Figure 6.8: For stronger coupling to the drain ($a < 0$) the $+$-occupation is enhanced as compared to that of the $-$-space (upper plot). Additionally, the currents carried by these states differ. This results in super-Poissonian statistics. For $a \to 1$ both currents and occupation are equal. This results in the first 3 cumulants becoming Poissonian (see Fig. 6.7)

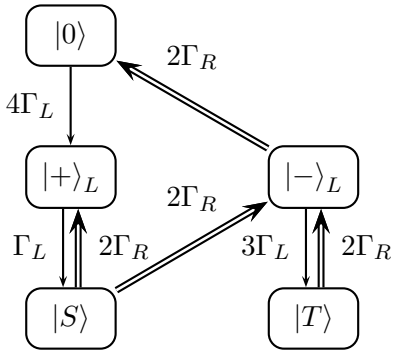

Figure 6.9: Internal system dynamics for flux $\phi = \pi$ and strong coupling to the drain $a \to -1$. The double lines denote transitions much faster (with rate $2\Gamma_R$) than the single lines (with rates $\propto \Gamma_L$).

current

$$S_+|_{a\to -1} = t_0\, 4\Gamma_L(e^{i\chi}-1) - \frac{3}{2}\Gamma(a+1)^2 e^{i\chi}(e^{i\chi}-1) \tag{6.20}$$

$$S_-|_{a\to -1} = t_0\, 3\Gamma_L(e^{i\chi}-1) - \frac{9}{8}\Gamma(a+1)^2 e^{i\chi}(e^{i\chi}-1) \tag{6.21}$$

In addition, in this case the +-space is preferred over the −-space ($P_+ = \frac{4}{5} + \mathcal{O}(a^1)$ and $P_- = \frac{1}{5} + \mathcal{O}(a^1)$). Correspondingly bunching persists.

6.4 Super-Poissonian statistics for flux $\phi = \pi$

Figure 6.7 reveals that the statistics for $\phi = \pi$ are peculiar also for $a \to -1$: The noise and the third normalized cumulant are enhanced beyond the Poissonian value, while the fourth normalized cumulant remains negative. The enhanced noise can be understood by studying the states which predominantly contribute to transport. They can be read off from the master equation Eq. (6.5,6.6) and are summarized in Figure 6.9.

Due to the strongly different coupling strengths, filling the dot is much slower than emptying. Therefore one could expect that the dot is predominantly empty, while single and double occupation are strongly suppressed. However, the isospin of an electron originating from the left lead has no overlap with the isospin polarization of the right lead. The direct transition $|+\rangle_L \to |0\rangle$ is therefore forbidden (like in coherent population trapping [18, 19, 20, 194]) and single occupation turns out to be more likely than an empty dot, as can be seen from the stationary occupation probabilities

for $a \approx -1$:

$$\mathbf{p} \approx \frac{1}{5}\begin{pmatrix} 1-(a+1) \\ 4 \\ a+1 \\ 0 \end{pmatrix} + \mathcal{O}((a+1)^2) \tag{6.22}$$

$$\mathbf{I} \approx \begin{pmatrix} 0 \\ -\frac{2}{5} + \frac{a+1}{5} \\ 0 \end{pmatrix} + \mathcal{O}((a+1)^2) \text{ parallel to } \mathbf{n}_L. \tag{6.23}$$

Due to the fact that filling the dot with a single electron occurs with rate $4\Gamma_L$ and adding a second electron only with rate Γ_L the singly occupied state $|+\rangle_L$ is, in lowest order in $(a+1)$, four times more likely than an empty dot. Occupation of the triplet is even rarer than singlet occupation: it starts in order $(a+1)^2$, because it can only be reached via singlet occupation and subsequent decay to the state $|-\rangle_L$.

It is eminent from the flowchart Fig. 6.9 that there are several distinct cycles through which electrons are transported from left to right: the transitions $|+\rangle_L \leftrightarrow |S\rangle$ and $|0\rangle \rightarrow |+\rangle_L \rightarrow |S\rangle \rightarrow |-\rangle_L$ and then back to $|0\rangle$, or several subcycles via $|T\rangle$. As these cycles transfer electrons at different mean currents and with different statistics, it is clear that a telegraph effect will lead to increased noise. In contrast to the channel exclusion described in the previous sections this effect is not related to separated Hilbert spaces.

6.5 Influence of experimental imperfections

For the $+$- and $-$-subspaces to decouple, a very special set of parameters is needed, so that experimental imperfections are bound to lift the degeneracy. In this section several such mechanisms are discussed and all are found to prevent a divergence of the normalized cumulants for $\phi = 0$. Although the divergence is reduced, the bunching effect can still be seen in the cumulants, since they are (for reasonable parameters) still enhanced above the Poissonian value.

6.5.1 Charge relaxation: decay of the isospin

In experiments interaction with the environment can be expected to induce various relaxation mechanisms. Relaxation of the isospin, mediated by electric interactions, will be of particular importance. It can be modelled by introducing a relaxation rate $\Omega_{\mathbf{I}}$ in the master equation Eq. (6.5,6.6) that reduces the isospin isotropically:

$$\frac{d}{dt}\mathbf{I} \propto -\Omega_{\mathbf{I}}\,\mathbf{I}.$$

The effect of this relaxation is primarily a reduction of the visibility of the AB-signal, due to the electrons loosing their coherence. Furthermore it lifts "isospin-blockade" and leads to an effective coupling of the $+$- and $-$-subspaces. Correspondingly the bunching effect is weakened, resulting in the cumulants assuming finite values also for

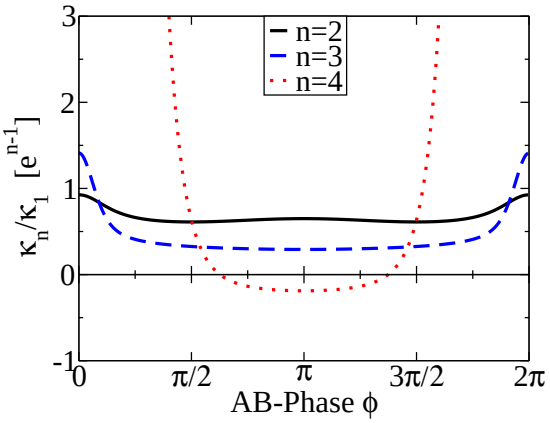

Figure 6.10: Isotropic relaxation of the isospin with a rate $\Omega_{\mathbf{I}} = \Gamma/10$ suppresses the divergence of the normalized cumulants for $\phi = 0$. While the Fano-factor turns sub-Poissonian already for the relaxation rate shown, higher cumulants still show super-Poissonian behaviour.

$\phi = 0$ (see Fig. 6.10). The normalized cumulants are suppressed as $1/\Omega_{\mathbf{I}}$ The figure shows the situation for $\Omega_{\mathbf{I}} = \frac{\Gamma}{10}$. This is the lowest value for which the Fano factor becomes sub-Poissonian, while the third normalized moment still remains greater than one. For sufficiently fast relaxation all cumulants become sub-Poissonian, but as can be seen from the figure, the higher the moment, the faster is the required relaxation rate.

6.5.2 Spin relaxation: conversion of singlet and triplet

Another relaxation mechanism is given by spin-flip processes converting singlets into triplets and vice versa. Since p_T summarizes all three triplets, the following terms have to be added to the master equation:

$$\frac{d}{dt}p_S \quad \propto \quad -\Omega_{ST}\, p_S + 3\Omega_{ST}\, p_T \tag{6.24}$$

$$\frac{d}{dt}p_T \quad \propto \quad +\Omega_{ST}\, p_S - 3\Omega_{ST}\, p_T. \tag{6.25}$$

The factor of three is required to take into account that the triplet probability corresponds to three states, while there is only one singlet.

The +- and −-subspaces are now directly coupled and the divergencies vanish as $1/\Omega_{ST}$, but with a larger factor of proportionality than in the case of isospin relaxation (Fig. 6.11): Already for $\Omega_{ST} = \Gamma/200$ the Fano factor becomes Poissonian. However, since such a relaxation is mediated magnetically, it can be expected to be much slower than isospin relaxation.

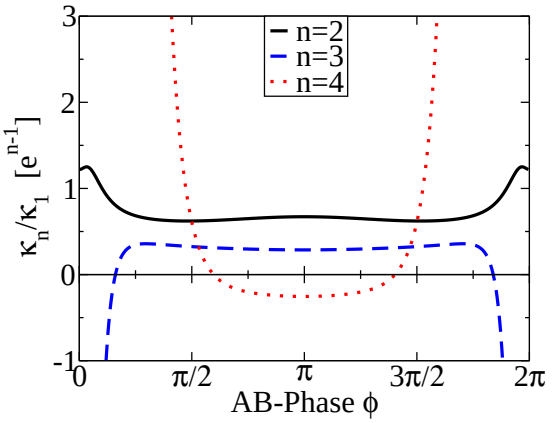

Figure 6.11: Relaxation from singlet to triplet (and vice versa) with a rate $\Omega_{ST} = \Gamma/200$ suppresses the divergence of the normalized cumulants for $\phi = 0$. This suppression occurs already for much lower rates than for Isospin relaxation.

6.5.3 Level detuning: precession of the isospin

A third imperfection which is almost bound to be present in experiments is a detuning of the dot level $\Delta\epsilon = \epsilon_u - \epsilon_d$. As has also been discussed in Ref. [15], if this detuning is of the order of the tunnel coupling $\Delta\epsilon \ll \Gamma$, it causes precession of the isospin. The master equation Eq. (6.6) receives an additional term

$$\frac{d}{dt}\mathbf{I} \propto \Delta\epsilon\,(\mathbf{n} \times \mathbf{I}), \tag{6.26}$$

where $\mathbf{n}$ denotes the quantization axis of the isospin, i.e., $\mathbf{I} \cdot \mathbf{n} = |\sigma, 0\rangle$. For the choice of coordinates made in this chapter ($\mathbf{n}_L = (\cos\phi/2, -\sin\phi/2, 0)$) it is given as $\mathbf{n} = (0, 0, 1)$.

In contrast to the previous effects, this does not directly reduce the value of the isospin, but merely changes its direction. Still, the subspaces are now coupled and cumulants and normalized cumulants decay as $1/\Delta\epsilon$, just as in the other cases. For small values of the detuning and specific values of the flux, the decay need not be monotonic in $|\Delta\epsilon|$. This is owed to the more complex phase dependence that is assumed, as can be seen in Fig. 6.12 for a symmetric system $\Gamma_L = \Gamma_R$. As can be seen from the figure, the phase dependence is not even in flux. This is owed to the fact that the generalization of the Onsager relation to finite bias voltages Eq. (2.11) holds only if both dots have the same properties, which is not the case if their energetic degeneracy is broken. Despite the flux dependence being asymmetric under reversal of the phase, it is symmetric under simultaneous reversal of phase and level splitting ($\phi \to -\phi, \Delta\epsilon \to -\Delta\epsilon$), since then the symmetry argument shown in Fig. 2.9 holds.

It should be noted that the detuning shown in the figure $\Delta\epsilon = \Gamma/3$ is already quite large in comparison to the tunnel coupling (The calculation holds only for $\Delta\epsilon \lesssim \Gamma$). Still, the third and higher moments remain super Poissonian.

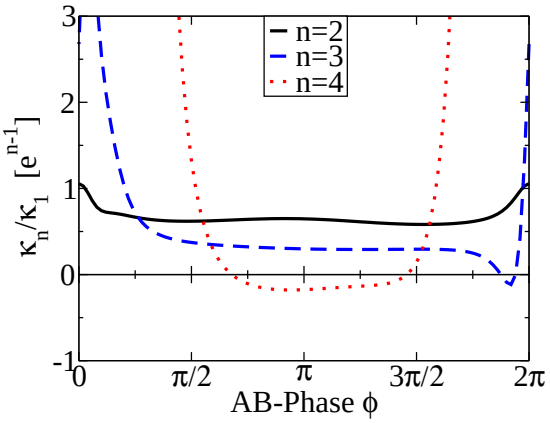

Figure 6.12: A finite detuning of the quantum dot levels lifts the divergence of the normalized cumulants. At a fairly large detuning $\Delta\epsilon = \Gamma/3$ (as shown) the Fano-factor becomes one, but higher cumulants are still clearly super-Poissonian.

6.6 Comparison with a spinless system

We would like to remark that the divergence of the normalized cumulants for $\phi = 2\pi m$ depends crucially on the inclusion of spin in the description of the system. The literature knows a number of examples where finite noise was found in similar, although not equal, double dot systems with spinless electrons [86, 192, 195, 196]. Allowing for different transmission phases of the two dots as well as different dot energies the authors of Ref. [86] find enhanced noise for specific relative transmission phases and small energy splittings $\Delta\epsilon$. In Refs. [192, 195] an interdot coupling results in an energy splitting of the singly occupied symmetric and antisymmetric combinations of the dot levels. This results in dynamical channel blockade. A channel blockade is also the fundanmental origin of enhanced noise in Ref. [196]. Here, diverging cumulants are predicted for zero flux. This is understood in a specific basis for single occupation of the dot: one of the transformed states decouples from the leads, but is coupled to the other state with a rate proportional to the difference in level energies $\Delta\epsilon$. Occupation of the disconnected state enhances noise since it blocks transport through the other state by means of Coulomb repulsion. In our system no Coulomb interaction between the dots is assumed, so that this charge blockade mechanism is not effective.

Neglecting spin in our model reduces the dimensionality of the Hilbert space by one since the distinction between singlet and triplet becomes impossible. Instead there is only one doubly occupied state, which is sufficiently described by its occupation probability p_2. We again arrange the density matrix elements in a vector $\boldsymbol{\pi} = (p_0, p_1, p_2, \mathbf{I})$ so that the master equation can be written in matrix form. Transforming to a new basis $\mathbf{S}\,\boldsymbol{\pi} = (p_0, p_1/2 + \mathbf{I}\cdot\mathbf{n}_L, p_2, p_1/2 - \mathbf{I}\cdot\mathbf{n}_L, \mathbf{I}\cdot(\mathbf{n}_z \times \mathbf{n}_L), I_z)$, the kernel of the spinless

system $\mathbf{W}_{\mathrm{sl}}$ again assumes block-diagonal form for $\phi = 2\pi m$:

$$\mathbf{S}\mathbf{W}_{\mathrm{sl}}\mathbf{S}^{-1} = \left(\begin{array}{cc|cc|cc} -2\Gamma_L & G_R^+ & 0 & G_R^- & e^{i\frac{\chi}{2}}2\Gamma_R\sin\frac{\phi}{2} & 0 \\ G_L^+ & -G_L^- - G_R^+ & G_R^- & 0 & \Gamma\sin\frac{\phi}{2} & 0 \\ \hline 0 & G_L^- & -2\Gamma_R & G_L^+ & e^{i\frac{\chi}{2}}2\Gamma_R\sin\frac{\phi}{2} & 0 \\ G_L^- & 0 & G_R^+ & -G_L^+ - G_R^- & -\Gamma\sin\frac{\phi}{2} & 0 \\ \hline -e^{i\frac{\chi}{2}}\Gamma_L\sin\frac{\phi}{2} & -\frac{1}{2}\Gamma\sin\frac{\phi}{2} & -e^{i\frac{\chi}{2}}\Gamma_R\sin\frac{\phi}{2} & -\frac{1}{2}\Gamma\sin\frac{\phi}{2} & -\Gamma & 0 \\ 0 & 0 & 0 & 0 & 0 & -\Gamma \end{array}\right), \tag{6.27}$$

with the definitions $G_r^{\pm} = e^{i\frac{\chi}{2}}\Gamma_r(1 \pm \cos\frac{\phi}{2})$ and $\Gamma = \Gamma_L + \Gamma_R$. Note that the $G_r^- = 0$ for $\phi = 2\pi m$.

The block structure can be understood by realizing that, for an AB-phase $\phi = 2\pi m$, charging the empty double dot $|0\rangle$ from the source always results in the symmetric state $|+\rangle = (|1,0\rangle + |0,1\rangle)/\sqrt{2}$. From this state the electron may leave to the drain, resulting again in $|0\rangle$. In contrast to the spinful case, the symmetric state $|+\rangle$ cannot be charged with a second electron, so that $|0\rangle$ and $|+\rangle$ constitute a decoupled set of states, whose motion is described by the upper left block of Eq. (6.27). On the other hand, the doubly occupied state $|1,1\rangle$ may loose one electron to the drain, resulting in the antisymmetric combination $|-\rangle = (|1,0\rangle - |0,1\rangle)/\sqrt{2}$, which can also be charged again from the source, but cannot be discharged to the drain. The two states $\{|-\rangle, |1,1\rangle\}$ therefore also form a decoupled set, which is described by the middle block of Eq. (6.27). The remaining components of the isospin are unoccupied.

In contrast to the situation with spinful electrons the statistics of the two subspaces are the same, regardless of the coupling strengths. This is owed to the fact that both subspaces are two-dimensional and describe a single level, the statistics of which is symmetric in source and drain coupling. Correspondingly the statistics of the spinless model becomes that of two independent, non-interacting levels [110, 111] for $\phi = 2\pi m$ (see Fig. 6.13).

The figure also shows that at $\phi = (2m+1)\pi$ the statistics becomes Poissonian. This is due to an isospin-blockade: Adding one electron to the empty system, results in the state $(|1,0\rangle - i\,|0,1\rangle)/\sqrt{2}$. This state cannot decay to the drain. On the other hand, the doubly occupied state may loose one electron, resulting in the combination $(|1,0\rangle + i\,|0,1\rangle)/\sqrt{2}$, which in turn cannot be refilled from the source. As a consequence, the system is trapped in the singly ocupied state and transport events become increasingly rare as the flux approaches $2\pi m$, resulting in Poissonian statistics.

In summary, no super-Poissonian noise is predicted for any value of the magnetic flux when spin is neglected.

The spinless double dot system with degenerate levels discussed here can be regarded as a special case of a non-interacting quantum-dot spin-valve [153], with perfect lead polarization. The statistics of quantum-dot spin-valves have been analyzed in more general contexts, both without and with Coulomb interaction [71].

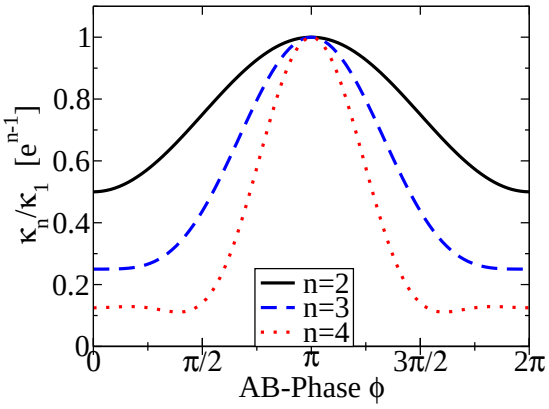

Figure 6.13: The normalized n-th cumulants κ_n/κ_1 show no divergence for $\phi = 2\pi m$ if spin is neglected. Instead they assume the values expected for a non-interacting two-level system. At $\phi = (2m+1)\pi$ the statistics becomes Poissonian due to an isospin blockade effect.

6.7 Chapter summary

The double dot Aharonov-Bohm interferometer exhibits peculiar transport properties, which can be understood by thinking of the leads as being isospin-polarized. The isospin is needed to properly describe the singly occupied subspace. It turns out that the empty state, a specific isospin state and the singlet state for double occupation form a closed subspace of the system. The opposite isospin together with the triplet form a second subspace. A coupling between the subspaces is in the shot noise regime mediated only by the drain lead, which is able to extract electrons with an isospin depending on the AB phase.

This dependence on the AB phase gives rise to a decoupling of the subspaces for $\phi = 0$. Since the subspaces have different transport properties an effect similar to random telegraph noise results in enhanced noise: Both normalized and non-normalized cumulants diverge for $\phi \to 0$. The relation of this enhancement to the different transport properties of the subspaces has been illustrated by considering extremely asymmetric source and drain contacts: If the drain contact is close to pinch off, the statistics of the subspace become the same so that the telegraph mechanism does not apply and the statistics becomes Poissonian.

The decoupling requires a very specific parameter set which would be hard to realize experimentally. However, the effect has been shown to be robust with respect to various relaxation mechanisms.

Also at the special point of $\phi = \pi$ enhanced noise was found. The origin could again be understood in terms of the same two subspaces, although these are not decoupled.

For the calculation of the counting statistics it was necessary to find a formulation that allows the treatment of systems with non-diagonal density matrices. An adaptation of the formalism described in Ref. [173] was found to fulfill this purpose.

The effects of super-Poissonian noise both at $\phi = 0$ and $\phi = \pi$ relies crucially on

the inclusion of spin in the description of the system. If spin is neglected, there is only one doubly occupied state. Although the system's Liouville space decomposes into two subsystems for $\phi = 0$, the dynamics of these subsystems are equal (and equal to the statistics of a two-level system) so that no enhanced noise is predicted.

7 Conclusions

This thesis studies how the transport properties of Aharonov-Bohm interferometers are affected by single charge effects. For this purpose two-path interferometers are examined. In order to introduce charge effects, single level quantum dots are embedded via tunnel contacts in the interferometer arms. The Coulomb interaction strongly affects the transport behavior. In order to characterize the transport processes the counting statistics of the systems were calculated from a generalized master equation approach. It is sufficient to calculate the transition rates in lowest order in the tunnel coupling to capture the essential effects. Charging effects, in contrast, are treated exactly.

The first system, studied in Chapter 5, consists of an interferometer with only a single quantum dot embedded in one arm. In a tunneling approximation transport through the interferometer has three contributions. The first contribution consists of tunneling through the single barrier that connects the leads directly. It has Poissonian statistics and delivers a flux independent background, regardless of interaction on the dot. The second contribution consists of tunneling through the double barrier provided by the quantum dot. This contribution is also flux-independent and obeys the well-known statistics of a quantum dot, [110, 111] including charging effects, which can be appropriately described by rescaled coupling parameters. Finally, the third contribution describes interference between amplitudes going through the direct arm and the quantum dot. One of these amplitudes originates from sequential tunneling, while the other describes coherent co-tunneling, e.g., from one lead to the other, involving a virtual state on the dot. In case of zero charging energy this interfering contribution shows no special behavior: it is off-resonant, an even function of the magnetic flux and obeys Poissonian statistics.

All these three properties change in the case of strong Coulomb interaction. Firstly the processes present in the non-interacting case receive corrections that reduce the amplitude of the AB oscillations depending on the dot occupation [6, 13]. In addition their statistics are no longer Poissonian. Of greater interest is the appearance of additional resonant terms with an odd flux dependence. If either source or drain contact of the dot are tuned close to pinch off, it would be expected that the statistics are determined by the weaker contact. This usually means (e.g., in case of a quantum dot) that the system behaves like a single barrier and exhibits Poissonian statistics. Much in contrast, the resonant interfering contribution to the statistics of the interferometer shows strongly super-Poissonian behavior in this regime. The statistics resemble that for transfer of double charges.

The reason for the appearance of terms with odd flux dependence for large charge interaction lies in the fact that it introduces an asymmetry between filling and emptying of the dot. Such an asymmetry can alternatively be introduced by measuring

the charge of the dot. Both charge detection and strong Coulomb interaction result in the appearance of on-resonant terms with an even flux dependence. However, the two mechanisms are not exactly equivalent: Charge detection also affects the off-resonant processes, so that the giant normalized cumulants are not observable.

As a second system a parallel double quantum dot was studied in Chapter 6. In the case of single occupation of the double dot, the electron reside in a superposition of the two levels, so that the system state is appropriately described by an isospin. Depending on the Aharonov-Bohm flux, the leads can be regarded as isospin polarized. Double occupation is possible if the two electrons enter singlet or triplet combinations. It turns out that these two-particle states couple differently to the leads. Indeed, in absence of a magnetic flux, only the singlet state can be reached when starting from an empty dot. This implies that the Liouville space of the system decomposes into two parts, i.e., the set of master equations splits into to decoupled subsets. One of the subspaces contains singlet, empty state and a specific isospin, while the other consists of a different isospin and the triplet states. A coupling between these subspaces is mediated by tunneling, but disappears if the AB-phase assumes multiples of 2π.

The double dot system is only correctly described when off-diagonal density matrix elements are taken into account. Thus for the calculation of the counting statistics the method described in Ref. [173] had to be extended.

The transport properties of the subspaces differ, in particular they carry different mean currents. Since the system switches continually between these different current states, noise is enhanced in the fashion of random telegraph noise when the switching rate is reduced, as happens for $\phi \to 2\pi$. The complete decoupling of the subspaces at multiples of 2π results in a divergence of the cumulants as the AB phase approaches $n2\pi$. Enhanced moments have often been described in the context of multiple states participating in transport; there are also examples of diverging noise. The novelty value of the present system lies in the fact that the noise diverges although the current remains finite. This is possible since the Liouville space of the system decomposes into two completely decoupled parts, both having internal dynamics that enable transport. Furthermore the effect was explicitly shown to critically depend on the inclusion of spin in the description of the system. While in a spinless treatment also two decoupled subspaces exist, these have equal transport properties, leading to the well known statistics of a two-level system.

With regards to experimental realizations it has been checked that the observed effects are robust with respect to various damping mechanisms. While diverging cumulants cannot be expected in the presence of these imperfections, strongly super-Poissonian statistics are still expected.

A Example diagrams for the single quantum dot interferometer

A.1 Lowest interfering order

In the presence of "cross" vertices at least two tunneling lines must occur, belonging to different leads r, s. This gives rise to two energy integrals and two energy denominators. Still the diagrams are different from conventional second order processes. In order to illustrate the character of the diagrams and the technical steps for their calculation two example diagrams belonging to the kernel component W_{00} are calculated in the following.

The first diagram is

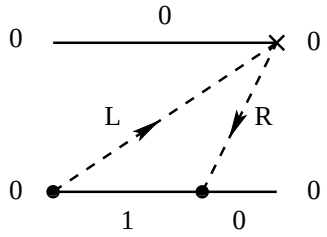

It can be evaluated according to the rules in Section 4.1.3. The appearance of tunnel matrix elements, fermi functions and energy denominators is straightforward. The phase factor $e^{i\phi}$ for the magnetic flux can easily be attributed as well, since a gauge was chosen in which it was fully incorporated in the reference arm $\tilde{t}e^{i\phi}$. Correspondingly the diagram is proportional to $e^{i\phi}$, since the "cross"-vertex appears on the upper arm. The most complicated part of the rules concerns the counting field. Carefully considering all three vertices it becomes apparent that the diagram corresponds to one charge being transferred from left to right lead, i.e. counting factor $e^{i\chi}$. Altogether the diagram is evaluated as:

$$D_1 = \frac{|t^{\mathrm{ref}}|\sqrt{\Gamma_L\Gamma_R}}{4\pi^2} e^{i\chi}e^{i\phi} \int \mathrm{d}\omega_L \int \mathrm{d}\omega_R \frac{f_L^+(\omega_L)}{\epsilon-\omega_L+i\delta}\frac{f_R^-(\omega_R)}{\omega_L-\omega_R+i\delta} \tag{A.1}$$

$$= \frac{|t^{\mathrm{ref}}|\sqrt{\Gamma_L\Gamma_R}}{4\pi^2} e^{i\chi}e^{i\phi} \int \mathrm{d}\omega_L \frac{f_L^+(\omega_L)}{\epsilon-\omega_L+i\delta}\left(-i\pi f_R^-(\omega_L) + \int' \mathrm{d}\omega_R \frac{f_R^-(\omega_R)}{\omega_R-\omega_L}\right) \tag{A.2}$$

$$= \frac{|t^{\mathrm{ref}}|\sqrt{\Gamma_L\Gamma_R}}{4\pi^2} e^{i\chi}e^{i\phi}\Bigg[(-i\pi)^2 f_L^+(\epsilon)f_R^-(\epsilon) + f_L^+(\epsilon)\int' \mathrm{d}\omega_R \frac{f_R^-(\omega_R)}{\omega_R-\epsilon} \tag{A.3}$$

$$+ \int' \mathrm{d}\omega_L \frac{-i\pi f_L^+(\omega_L)f_R^-(\omega_L)}{\epsilon-\omega_L} + \int' \mathrm{d}\omega_L \int' \mathrm{d}\omega_R \frac{f_L^+(\omega_L)}{\epsilon-\omega_L}\frac{f_R^-(\omega_R)}{\omega_R-\omega_L}\Bigg]$$

The integrations are carried out according to Cauchy's formula (p. 50). The first two terms combine with terms from other diagrams in such a way that the single principal values cancel and only Fermi functions remain. The third term contributes to the off-resonant processes $A(\chi)$.

The last term of the result is easier to evaluate when combined with other terms from the kernel element of W_{00}. There are two other diagrams with the same prefactor and one of them turns out to contain a similar term. It should be noted that, in contrast to other calculations regarding this system and in contrast to other application of the diagrammatic technique, here the number of diagrams that can be combined is limited by the comparably large number of prefactors (counting field and flux) and the signs (for electron and hole) at the fermi function. Still, a matching diagram can always be found. The one needed here is

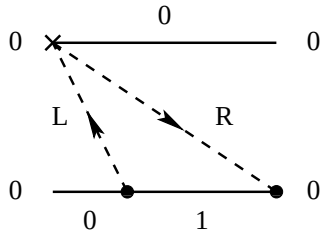

It can be evaluated in the same way, this time integrating first over $\mathrm{d}\omega_L$ and then over $\mathrm{d}\omega_R$:

$$D_2 = \frac{|t^{\mathrm{ref}}|\sqrt{\Gamma_L\Gamma_R}}{4\pi^2} e^{i\chi} e^{i\phi} \int \mathrm{d}\omega_L \int \mathrm{d}\omega_R \frac{f_L^+(\omega_L)}{\omega_L - \omega_R + i\delta} \frac{f_R^-(\omega_R)}{\epsilon - \omega_R + i\delta} \tag{A.4}$$

$$= \frac{|t^{\mathrm{ref}}|\sqrt{\Gamma_L\Gamma_R}}{4\pi^2} e^{i\chi} e^{i\phi} \int \mathrm{d}\omega_R \left(-i\pi f_L^+(\omega_R) + \int' \mathrm{d}\omega_L \frac{f_L^+(\omega_L)}{\omega_L - \omega_R} \right) \frac{f_R^-(\omega_R)}{\epsilon - \omega_R + i\delta} \tag{A.5}$$

$$= \frac{|t^{\mathrm{ref}}|\sqrt{\Gamma_L\Gamma_R}}{4\pi^2} e^{i\chi} e^{i\phi} \Bigg[(-i\pi)^2 f_L^+(\epsilon) f_R^-(\epsilon) + f_R^-(\epsilon) \int' \mathrm{d}\omega_L \frac{f_L^+(\omega_L)}{\omega_L - \epsilon} \tag{A.6}$$

$$\int' \mathrm{d}\omega_R \frac{-i\pi f_L^+(\omega_R) f_R^-(\omega_R)}{\epsilon - \omega_R} + \int' \mathrm{d}\omega_L \int' \mathrm{d}\omega_R \frac{f_L^+(\omega_L)}{\omega_L - \omega_R} \frac{f_R^-(\omega_R)}{\epsilon - \omega_R} \Bigg]$$

Now, the last terms of both diagrams can be combined

$$P = \int' \mathrm{d}\omega_L \int' \mathrm{d}\omega_R \frac{f_L^+(\omega_L)}{\epsilon - \omega_L} \frac{f_R^-(\omega_R)}{\omega_R - \omega_L} + \frac{f_L^+(\omega_L)}{\omega_L - \omega_R} \frac{f_R^-(\omega_R)}{\epsilon - \omega_R} \tag{A.7}$$

$$= \int' \mathrm{d}\omega_L \int' \mathrm{d}\omega_R \frac{f_L^+(\omega_L) f_R^-(\omega_R)}{\omega_L - \omega_R} \left(\frac{1}{\epsilon - \omega_R} - \frac{1}{\epsilon - \omega_L} \right) \tag{A.8}$$

This results in a double principal value integral of the form ($\epsilon - \omega_L = x$, $\epsilon - \omega_R = y$)

$$I = \int' \mathrm{d}x \int' \mathrm{d}y \; f(x) g(y) \; \frac{1}{y - x} \left(\frac{1}{y} - \frac{1}{x} \right) \tag{A.9}$$

For the evaluation of this integral it is helpful to introduce the representation of the

principal value

$$I = \int \mathrm{d}x \int \mathrm{d}y \frac{y-x}{(y-x)^2+\eta^2} \left(\frac{y}{y^2+\delta^2} + \frac{x}{x^2+\delta^2} \right) \tag{A.10}$$

$$= \int \mathrm{d}x \int \mathrm{d}y \frac{(y-x)^2}{(y-x)^2+\eta^2} \left(\frac{\delta}{x^2+\delta^2}\frac{\delta}{y^2+\delta^2} - \frac{x}{x^2+\delta^2}\frac{y}{y^2+\delta^2} \right) \tag{A.11}$$

In this expression the representations of the principal value ($\int' \mathrm{d}x \frac{1}{x} = \frac{x}{x^2+\delta^2}$) and the Dirac-$\delta$-function ($\pi\delta(x) = \frac{\delta}{x^2+\delta^2}$) are recognized, so that the entire integral Eq. (A.9) equals

$$I = \pi^2 f(x=0)g(y=0) - \left(\int' \mathrm{d}x \frac{f(x)}{x} \right) \left(\int' \mathrm{d}y \frac{g(y)}{y} \right) \tag{A.12}$$

For the double principal value integrals appearing in the diagrams discussed above (Eq. (A.8)) this means that they are equal to

$$P = \pi^2 f_L^+(\epsilon) f_R^-(\epsilon) - \left(\int' \mathrm{d}\omega_L \frac{f_L^+(\omega_L)}{\epsilon - \omega_L} \right) \left(\int' \mathrm{d}\omega_R \frac{f_R^-(\omega_R)}{\epsilon - \omega_R} \right) \tag{A.13}$$

In all other diagrams similar steps have to be taken to cancel all double principal value integral. Once this is achieved, all single principal values drop out as well, so that the kernel assumes the form Eq. (5.9).

Usually, diagrams which are related by shifting the rightmost vertex from the upper to the lower contour cancel each other. The reason lies in the fact that the diagrams' values are equal apart from a relative minus sign introduced by the rightmost vertex on the lower contour. In the presence of counting fields, moving the rightmost vertex between the contours in general introduces not only a relative minus sign, but also changes the counting factor. Correspondingly the pair of diagrams does not add to zero. This is of importance in the following section.

A.2 Lowest order for direct tunneling between two leads

It is also possible to calculate within the diagrammatic approach the, trivially Poissonian, transport contributions that originate from direct tunneling between two leads. Since these processes do not change the dot state, they appear only as diagonal components of the kernel $\mathbf{W}$. Furthermore, since they do not depend on the initial state of the dot, all diagonal components are the same, $W_\alpha^\alpha = W_\beta^\beta$. This implies that the contribution to the generating function, which is given as the eigenvalue, it just W_α^α.

For the diagrammatic calculation the counting field is a vital ingredient, since without it the diagrams would exactly cancel, since they are related by shifting the rightmost vertex between upper and lower contour. As mentioned in the previous section, this is not the case in the presence of counting fields, since one of the addends receives a factor $e^{\pm i\chi}$, while the other does not. This means that the pair of diagrams appears with the prefactor $(e^{\pm i\chi} - 1)$ in the kernel. This prefactor is the usual counting factor,

normalized in the sense that it preserves probability normalization by vanishing for $\chi \to 0$.

With this in mind, all four diagrams for W_α^α are drawn:

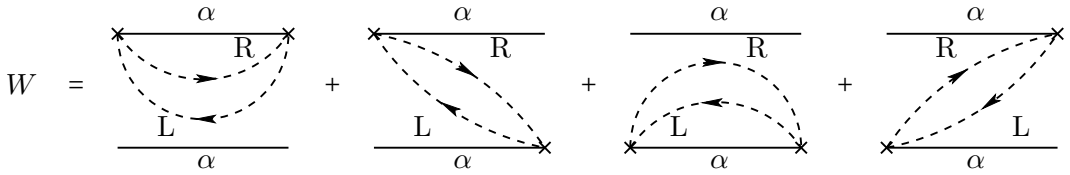

Since each diagram contains one vertex into which a line enters from the left lead and one vertex into which a line enters from the right lead, the Aharonov-Bohm phase drops out and all diagrams are proportional to $|t^{\mathrm{ref}}|^2 = |\tilde{t}|^2 \rho_L \rho_R$. Further application of the rules in Sec. 4.1.3 gives

$$\begin{aligned} W_{\alpha\alpha}^{\alpha\alpha} &= \frac{|t^{\mathrm{ref}}|^2}{4\pi^2} \int \mathrm{d}\omega_L \int \mathrm{d}\omega_R \left(\frac{f_L^+(\omega_L) f_R^-(\omega_R)}{\omega_L - \omega_R + i\delta} - e^{i\chi} \frac{f_L^+(\omega_L) f_R^-(\omega_R)}{\omega_L - \omega_R + i\delta} \right. \\ &\qquad \left. + \frac{f_L^-(\omega_L) f_R^+(\omega_R)}{\omega_R - \omega_L + i\delta} - e^{-i\chi} \frac{f_L^-(\omega_L) f_R^+(\omega_R)}{\omega_R - \omega_L + i\delta} \right) + (L \leftrightarrow R) \qquad \text{(A.14)} \\ &= \frac{|t^{\mathrm{ref}}|^2}{4\pi^2} \int \mathrm{d}\omega_L \int \mathrm{d}\omega_R \left((1 - e^{i\chi}) f_L^+(\omega_L) f_R^-(\omega_R) + (1 - e^{-i\chi}) f_L^-(\omega_L) f_R^+(\omega_R) \right) \\ &\qquad \times \left(\frac{1}{\omega_L - \omega_R + i\delta} + \frac{1}{\omega_R - \omega_L + i\delta} \right) \\ &= i \frac{|t^{\mathrm{ref}}|^2}{4\pi^2} \int \mathrm{d}\omega \left[f_L^+(\omega) f_R^-(\omega)(e^{i\chi} - 1) + f_L^-(\omega) f_R^+(\omega)(e^{-i\chi} - 1) \right] \qquad \text{(A.15)} \end{aligned}$$

where in the last step it was realized that the particular combination of resolvents results in $-2\pi i \delta(\omega_L - \omega_R)$. In the shot noise regime ($f_L = 1$, $f_R = 0$) the energy integral becomes equal to eV.

Bibliography

[1] L. P. Kouwenhoven, G. Schön, L. L. Sohn, *Introduction to Mesoscopic Electron Transport*, in "Mesoscopic Electron Transport", edited by L. L. Sohn, L. P. Kouwenhoven und G. Schön (Kluwer Academic Publishers, Dordrecht, Boston, London, 1997). 5

[2] D. V. Averin and K. K. Likharev, in *Mesoscopic Phenomena in Solids*, edited by B. L. Altshuler, P. A. Lee, R. A. Webb, (Elsevier, Amsterdam, 1991). 8, 43

[3] *Single Charge Tunneling*, NATO ASI Series, Vol. B **294**, edited by H. Grabert and M. H. Devoret (Plenum Press, New York, 1992). 8

[4] Y. Aharonov and D. Bohm, Phys. Rev. **115**, 485 (1959). 10

[5] B. Kubala and K. König, Phys. Rev. B **67**, 205303 (2003). 11

[6] J. König, and Y. Gefen, Phys. Rev. Lett. **86**, 3855 (2001); Phys. Rev. B **65**, 045316 (2002). 12, 14, 18, 57, 65, 67, 68, 99

[7] L. D. Landau, E. M. Lifshitz, *Course of Theoretical Physics, Vol. 3: "Quantum Mechanics: Non-Relativistic Theory",* Butterworth-Heinemann, 3rd edition (1981). 12, 61

[8] A. Yacoby, M. Heiblum, D. Mahalu, and H. Shtrikman, Phys. Rev. Lett. **74**, 4047 (1995). 12, 13

[9] R. Schuster, E. Buks, M. Heiblum, D. Mahalu, V. Umansky, H. Shtrikman, Nature **385**, 417 (1997). 14

[10] G. Hackenbroich and H. A. Weidenmüller, Europhys. Lett. **38**, 129 (1997). 14

[11] G. Hackenbroich, Phys. Rep. **343**, 463 (2001). 14

[12] M. Avinun-Kalish, M. Heiblum, O. Zarchin, D. Mahalu and V. Umansky Nature **436**, 529 (2005). 14

[13] H. Aikawa, K. Kobayashi, A. Sano, S. Katsumoto, and Y. Iye, Phys. Rev. Lett. **92**, 176802 (2004). 15, 16, 57, 99

[14] D. Loss and D. P. DiVincenzo, Phys. Rev. A **57**, 120 (1998). 16

[15] S. Legel, J. König, G. Burkard, G. Schön, Phys. Rev. B **76**, 085335 (2007). 16, 44, 79, 84, 93

[16] S. Legel, J. König, G. Schön, New. J. Phys. **10** 045016 (2008). 16, 44, 79, 84

[17] E. Arimondo, in *Progress in Optics*, edited by E. Wolf, (Elsevier, Amsterdam, 1996), Vol. 35, p. 257. 17, 79

[18] B. Michaelis, C. Emary, and C. W. J. Beenakker, Europhys. Lett. **73** (5), 677 (2006). 18, 90

[19] C. W. Groth, B. Michaelis, and C. W. J. Beenakker, Phys. Rev. B **74**, 125315 (2006). 18, 28, 79, 90

[20] C. Emary, Phys. Rev. B **76**, 245319 (2007). 18, 52, 79, 90

[21] M. J. M. de Jong and C. W. J. Beenakker, *Shot noise in mesoscopic systems*, in "Mesoscopic Electron Transport", edited by L.L. Sohn, L.P. Kouwenhoven, and G. Schoen, NATO ASI Series Vol. **345**, 225 (Kluwer Academic Publishers, Dordrecht, 1997). 21

[22] Ya. M. Blanter, M. Büttiker, Phys. Rep. **336**, 1 (2000). 21

[23] "Quantum Noise in Mesoscopic Systems", ed. by Yu. V. Nazarov and Ya. M. Blanter (Kluwer, Dordrecht, 2003). 21, 30

[24] S. Machlup, J. Appl. Phys. **25**, 341 (1954). 21

[25] A. van der Ziel, *Fluctuation phenomena in semiconductors*, Butterworths Scientific Pub., London (1959). 21

[26] Aldert van der Ziel, Proc. IEEE, **76**, 233 (1988). 21

[27] Y. Imry, *Introduction to mesoscopic physics*, Oxford University Press (2002). 21

[28] R. Landauer, Philos. Mag. **21**, 863 (1970). 22, 35

[29] M. Büttiker, Y. Imry, R. Landauer, and S. Pinhas, Phys. Rev. B **31**, 6207 (1985). 22, 35

[30] M. Büttiker, Phys. Rev. Lett. **65**, 2901 (1990). 22

[31] M. Büttiker, Phys. Rev. B **46**, 12485 (1992). 22, 35

[32] Th. Martin and R. Landauer, Phys. Rev. B **45**, 1742 (1992). 22

[33] M. B. Johnson, Phys. Rev. **29**, 367 (1927). 22

[34] H. Nyquist, Phys. Rev. **32**, 110 (1928). 22

[35] U. Fano, Phys. Rev. **72**, 26 (1947). 22, 24

[36] M. Reznikov, M. Heiblum, Hadas Shtrikman, and D. Mahalu, Phys. Rev. Lett. **75**, 3340 (1995). 24

[37] A. Kumar, L. Saminadayar, D. C. Glattli, Y. Jin, and B. Etienne, Phys. Rev. Lett. **76**, 2778 (1996). 24

[38] R. Cron, M. F. Goffman, D. Esteve, and C. Urbina, Phys. Rev. Lett. **86**, 4104 (2001). 24

[39] A. N. Korotkov and K. K. Likharev, Phys. Rev. B **61**, 15975 (2000). 24

[40] V. A. Svedlov, A. N. Korotkov, and K. K. Likharev, Phys. Rev. B **63**, 081302(R) (2001). 24

[41] S. S. Safonov, A. K. Savchenko, D. A. Bagrets, O. N. Jouravlev, Y. V. Nazarov, E. H. Linfield, and D. A. Ritchie, Phys. Rev. Lett. **91**, 136801 (2003). 24, 26

[42] I. Djuric, B. Dong, and H. L. Cui, Appl. Phys. Lett. **87**, 032105 (2005). 24, 26, 87

[43] Y. Chen and R. A. Webb, Phys. Rev. B **73**, 035424 (2006). 24

[44] H. Birk, M. de Jong, and C. Schönenberger, Phys. Rev. Lett. **75**, 1610 (1995). 24

[45] A. Nauen, I. Hapke-Wurst, F. Hohls, U. Zeitler, R. Haug, and K. Pierz, Phys. Rev. B **66**, 161303 (2002). 24

[46] A. Nauen, F. Hohls, N. Maire, K. Pierz, and R. J. Haug, Phys. Rev. B **70**, 033305 (2004). 24

[47] E. Onac, F. Balestro, B. Trauzettel, and C. Lodewijk, Phys. Rev. Lett. **96**, 026803 (2006). 24

[48] A. Aassime, G. Johansson, G. Wendin, R. Schoelkopf, and P. Delsing, Phys. Rev. Lett. **86**, 3376 (2001). 24

[49] S. Kafanov and P. Delsing, arXiv:0812.0282 (2008). 24

[50] T. Jeltes, J. M. McNamara, W. Hogervorst, W. Vassen, V. Krachmalnicoff, M. Schellekens, A. Perrin, H. Chang, D. Boiron, A. Aspect, and C. I. Westbrook, Nature **445**, 402 (2007). 25

[51] M. Henny, S. Oberholzer, C. Strunk, T. Heinzel, K. Ensslin, M. Holand, and C. Schönenberger, Science **284**, 296 (1999). 25

[52] W. D. Oliver, J. Kim, R. C. Liu, and Y. Yamamoto, Science **284**, 299 (1999). 25

[53] G. Burkard, D. Loss, and E. V. Sukhorukov, Phys. Rev. B **61**, 16303 (2000). 25

[54] G. B. Lesovik, T. Martin, and G. Blatter, Eur. Phys. J. B **24**, 287 (2001). 25

[55] F. Taddei and R. Fazio, Phys. Rev. B **65**, 075317 (2002). 25

[56] F. Hassler, G. B. Lesovik, and G. Blatter, Phys. Rev. Lett. **99**, 076804 (2007). 25

[57] F. Hassler, M. V. Suslov, G. M. Graf, M. V. Lebedev, G. B. Lesovik, and G. Blatter, Phys. Rev. B **78**, 165330 (2008). 25

[58] X. Jehl, M. Sanquer, R. Calemczuk, and D. Mailly, Nature **405**, 50 (2000); A. A. Kozhevnikov, R. J. Schoelkopf, and D. E. Prober, Phys. Rev. Lett. **84**, 3398 (2000); F. Lefloch, C. Hoffmann, M. Sanquer, and D. Quirion, Phys. Rev. Lett. **90**, 067002 (2003). 25

[59] J. C. Cuevas and W. Belzig, Phys. Rev. Lett. **91**, 187001 (2003); Phys. Rev. B **70**, 214512 (2004). 25, 72

[60] G. Johansson, P. Samuelsson, A. Ingerman, Phys. Rev. Lett. **91**, 187002 (2003). 25, 72

[61] Eran Sela, Yuval Oreg, Felix von Oppen, and Jens Koch, Phys. Rev. Lett. **97**, 086601 (2006). 25

[62] A. Golub, Phys. Rev. B **75**, 155313 (2007). 25

[63] O. Zarchin, M. Zaffalon, M. Heiblum, D. Mahalu, and V. Umansky, Phys. Rev. B **77**, 241303(R) (2008). 25

[64] Yu. V. Nazarov and J. J. R. Struben, Phys. Rev. B **53**, 15466 (1996). 26

[65] O. Zarchin, Y. C. Chung, M. Heiblum, D. Rohrlich, and V. Umansky, Phys. Rev. Lett. **98**, 066801 (2007). 26

[66] W. Belzig, Phys. Rev. B **71**, 161301(R) (2005). 26, 29, 52, 72, 87

[67] S. Gustavsson, R. Leturcq, B. Simovic, R. Schleser, P. Studerus, T. Ihn, K. Ensslin, D. C. Driscoll, and A. C. Gossard, Phys. Rev. B **74**, 195305 (2006). 27, 40, 72, 73, 87

[68] G. Kießlich, A. Wacker, and E. Schöll, Phys. Rev. B **68**, 125320 (2003). 27

[69] A. Thielmann, M. H. Hettler, J. König, and G. Schön, Phys. Rev. Lett. **95**, 146806 (2005); Phys. Rev. B **71**, 045341 (2005). 27, 54

[70] J. Aghassi, A. Thielmann, M. H. Hettler, and G. Schön, Phys. Rev. B **73**, 195323 (2006). 27

[71] S. Lindebaum, D. Urban, and J. König, Phys. Rev. B **79**, 245303 (2009). 27, 28, 95

[72] B. R. Bułka, Phys. Rev. B **62**, 1186 (2000). 27

[73] M. Braun, J. König, and J. Martinek, Phys. Rev. B **74**, 075328 (2006). 27, 80

[74] I. Weymann, Phys. Rev. B **78**, 045310 (2008). 27

[75] O. A. Tretiakov and K. A. Matveev, Phys. Rev. B **71**, 165326 (2005). 27

[76] A. N. Jordan and E. V. Sukhorukov, Phys. Rev. Lett. **93**, 260604 (2004). 27

[77] C. Flindt, T. Novotný, and A.-P. Jauho, Europhys. Lett. **69**, 475 (2005). 28

[78] J. Koch and F. von Oppen, Phys. Rev. Lett. **94**, 206804 (2005). 28

[79] F. Elste and C. Timm, Phys. Rev. B **73**, 235305 (2006). 28

[80] W. G. van der Wiel, S. De Franceschi, J. M. Elzerman, T. Fujisawa, S. Tarucha and L. P. Kouwenhoven, Rev. Mod. Phys. **75**, 1 (2002). 28

[81] N. Shaji, C. B. Simmons, M. Thalakulam, L. J. Klein, H. Qin, H. Luo, D. E. Savage, M. G. Lagally, A. J. Rimberg, R. Joynt, M. Friesen, R. H. Blick, S. N. Coppersmith, and M. A. Eriksson, Nature Physics **4**, 540 (2008). 28

[82] M. R. Buitelaar, J. Fransson, A. L. Cantone, C. G. Smith, D. Anderson, G. A. C. Jones, A. Ardavan, A. N. Khlobystov, A. A. R. Watt, K. Porfyrakis, and G. A. D. Briggs, Phys. Rev. B **77**, 245439 (2008). 28

[83] P. Barthold, F. Hohls, N. Maire, K. Pierz, and R.J. Haug, Phys. Rev. Lett. **96**, 246804 (2006). 28

[84] G. Kießlich, E. Schöll, T. Brandes, F. Hohls, and R. J. Haug, Phys. Rev. Lett. **99**, 206602 (2007). 28

[85] R. Sánchez, Sigmund Kohler, Peter Hänggi, and Gloria Platero, Phys. Rev. B **77**, 035409 (2008). 28

[86] S.-K. Wang, H. Jiao, F. Li, and X.-Q. Li, Phys. Rev. B **76**, 125416 (2007). 29, 79, 94

[87] F. Li, H. Jiao, J. Luo, X.-Q. Li, S. A. Gurvitz, arXiv:0812.0846v1 (2008). 29

[88] B. Dong, X. L. Lei, and N. J. M. Horing, J. App. Phys. **104**, 033532 (2008); Phys. Rev. B **77**, 085309 (2008). 29

[89] S. Welack, M. Esposito, U. Harbola, and S. Mukamel, Phys. Rev. B **77**, 195315 (2008). 29

[90] R. Sánchez, G. Platero, and T. Brandes, Phys. Rev. Lett. **98**, 146805 (2007). 29

[91] R. Sánchez, G. Platero, and T. Brandes, Phys. Rev. B **78**, 125308 (2008). 29

[92] F. Bodoky, W. Belzig, and C. Bruder, Phys. Rev. B **77**, 035302 (2008). 29

[93] S. Pilgram, K. E. Nagaev, and M. Büttiker, Phys. Rev. B **70**, 045304 (2004). 29

[94] K. E. Nagaev, S. Pilgram, and M. Büttiker, Phys. Rev. Lett. **92**, 176804 (2004). 29

[95] M. H. Pedersen, S. A. van Langen, and M. Büttiker, Phys. Rev. B **57**, 1838 (1998). 29

[96] D. B. Gutman and Y. Gefen, Phys. Rev. B **68**, 035302 (2003). 29

[97] L. S. Levitov and M. Reznikov, Phys. Rev. B **70**, 115305 (2004). 29, 70

[98] L. Mandel, Optics Lett. **4** 205 (1979). 29

[99] R. J. Cook, Phys. Rev. A, **23**, 1243 (1981). 29, 52

[100] L. S. Levitov and G. B. Lesovik, Pis'ma Zh. Eksp. Teor. Fiz. **58**, 225 (1993) [JETP Lett. **58**, 230 (1993)]; L. S. Levitov, H.-W. Lee, and G. B. Lesovik, J. Math. Phys. **37**, 4845 (1996). 29, 31, 35, 65

[101] W. Schottky, Ann. Phys. (Leipzig) **57**, 541 (1918). 31

[102] C. W. J. Beenakker and C. Schönenberger, *Quantum Shot Noise*, in Physics Today, May 2003, p. 37. 33

[103] R. de Picciotto, M. Reznikov, M. Heiblum, V. Umansky, G. Bunin, and D. Mahalu, Nature **389**, 162 (1997). 33, 70

[104] L. Saminadayar, D. C. Glattli, Y. Jin, and B. Etienne, Phys. Rev. Lett. **79**, 2526 (1997). 33, 70

[105] M. Reznikov, R. de Picciotto, T. G. Griffiths, M. Heiblum, and V. Umansky, Nature **399**, 238 (1999). 33

[106] H. Lee, L. S. Levitov, and A. Yu. Yakovets, Phys. Rev. B **51**, 4079 (1995). 35

[107] M. J. M. de Jong and C. W. J. Benakker, Phys. Rev. B **51**, 18867 (1995). 35

[108] P.-E. Roche, B. Derrida, and B. Douçot, Eur. Phys. J. B **43**, 529 (2005). 35

[109] F. Liefrink, J. I. Dijkhuis, M. J. M. de Jong, L. W. Molenkamp, and H. van Houten, Phys. Rev. B **49**, 14066 (1994). 35

[110] M. J. M. de Jong. Phys. Rev. B **54**, 8144 (1996). 35, 95, 99

[111] D. A. Bagrets and Y. V. Nazarov, Phys. Rev. B **67**, 085316 (2003). 33, 35, 52, 60, 64, 66, 68, 74, 95, 99

[112] I. Klich, in "Quantum Noise in Mesoscopic Systems", ed. by Yu. V. Nazarov and Ya. M. Blanter (Kluwer, Dordrecht, 2003). 35

[113] B. Reulet, J. Senzier, and D. E. Prober, Phys. Rev. Lett. **91**, 196601 (2003); confer also the explanatory notes arXiv:cond-mat/0403437v1 and arXiv:cond-mat/0502077v1 and the first version arXiv:cond-mat/0302084v1. 37

[114] M. Kindermann, Yu. V. Nazarov, and C. W. J. Beenakker, Phys. Rev. Lett. **90**, 246805 (2003). 37

[115] C. W. J. Beenakker, M. Kindermann, and Yu. V. Nazarov, Phys. Rev. Lett. **90**, 176802 (2003). 37

[116] Yu. Bomze, G. Gerschon, D. Shovun, L. S. Levitov, and M. Reznikov, Phys. Rev. Lett. **95**, 176601 (2005). 38

[117] G. B. Lesovik and N. M. Chtchelkatchev, JETP Lett **77**, 393 (2003); arXiv:cond-mat/0303024v2 (2003). 38

[118] J. Tobiska and Yu. V. Nazarov, Phys. Rev. Lett. **93**, 106801 (2004). 38

[119] M. Tinkham, *Introduction to Superconductivity*, (McGraw-Hill, New York, 1996). 38

[120] B. Huard, H. Pothier, N. O. Birge, D. Esteve, X. Waintal, and J. Ankerhold, Ann. Phys. (Leipzig) **16**, 736 (2007); J. Ankerhold, Phys. Rev. Lett. **98**, 036601 (2007). 38

[121] E. B. Sonin, Phys. Rev. B **70**, 140506(R) (2004); R. K. Lindell, J. Delahaye, M. A. Sillanpää, T. T. Heikkilä, E. B. Sonin, and P. J. Hakonen, Phys. Rev. Lett. **93**, 197002 (2004); P-M. Billangeon, F. Pierre, H. Bouchiat, and R. Deblock, Phys. Rev. Lett. **96**, 136804 (2006). 39

[122] J. P. Pekola, Phys. Rev. Lett. **93**, 206601 (2004); J. P. Pekola, T. E. Nieminen, M. Meschke, J. M. Kivioja, A. O. Niskanen, and J. J. Vartiainen, Phys. Rev. Lett. **95**, 197004 (2005); T. T. Heikkilä, P. Virtanen, G. Johansson, and F. K. Wilhelm, Phys. Rev. Lett. **93**, 247005 (2004). 39

[123] J. Ankerhold and H. Grabert, Phys. Rev. Lett. **95**, 186601 (2005). 39

[124] J. T. Peltonen, A. V. Timofeev, M. Meschke, and J. P. Pekola, J. Low Temp. Phys. **146**, 135 (2007). 39

[125] J. Bylander, T. Duty, and P. Delsing, Nature **434**, 361 (2005). 39

[126] M. W. Keller, A. L. Eichenberger, J. M Martinis, and N. M. Zimmermann, Science **285**, 1706 (1999). 39

[127] R. J. Schoelkopf , P Wahlgren, A. A. Kozhevnikov, P. Delsing, and D. E. Prober, Science **280**, 1238 (1998). 39

[128] W. Lu, Z. Ji, L. Pfeiffer, K. W. West, and A. J. Rimberg, Nature **423**, 422 (2003). 40

[129] R. Landauer, J. Phys. Condens. Matter **1**, 8099 (1989). 40

[130] M. Field, C. G. Smith, M. Pepper, D. A. Ritchie, J. E. F. Frost, G. A. C. Jones, and D. G. Hasko, Phys. Rev. Lett. **70**, 1311 (1993). 40

[131] J. M. Elzerman, R. Hanson, J. S. Greidanus, L. H. Willems van Beveren, S. De Franceschi, L. M. K. Vandersypen, S. Tarucha and L. P. Kouwenhoven, Phys. Rev. B **67**, 161308 (2003). 40

[132] J. M. Elzerman, R. Hanson1, L. H. Willems van Beveren, B. Witkamp1, L. M. K. Vandersypen and L. P. Kouwenhoven, Nature **430**, 431 (2004). 40

[133] S. Gustavsson, R. Leturcq, B. Simovic, R. Schleser, T. Ihn, P. Studerus, K. Ensslin, D. C. Driscoll, A. C. Gossard, Phys. Rev. Lett. **96**, 076605 (2006). 40

[134] C. Fricke, F. Hohls, W. Wegscheider, and R. J. Haug, Phys. Rev. B **76**, 155307 (2007). 40, 72, 73

[135] T. Fujisawa, T. Hayashi, R. Tomita, Y. Hirayama, Science **312**, 1634 (2006). 40, 41, 72, 73

[136] S. Gustavsson, M. Studer, R. Leturcq, T. Ihn, K. Ensslin, D. C. Driscoll, and A. C. Gossard, Phys. Rev. B **78**, 155309 (2008). 41

[137] S. Gustavsson, R. Leturcq, M. Studer, T. Ihn, K. Ensslin, D. C. Driscoll, and A. C. Gossard, Nano Lett. **8**, 2547 (2008), arXiv: cond-mat/0807.1881v1 (2008). 41

[138] S. Gustavsson, M. Studer, R. Leturcq, T. Ihn, K. Ensslin, D. C. Driscoll, and A. C. Gossard, Phys. Rev. Lett. **99**, 206804 (2007). 41

[139] R. Aguado and L. P. Kouwenhoven, Phys. Rev. Lett. **84**, 1986 (2000). 41

[140] B. Küng, O. Pfäffi, S. Gustavsson, T. Ihn, K. Ensslin, M. Reinwald, and W. Wegscheider, Phys. Rev. B **79**, 035314 (2009). 41

[141] J. Güttinger, C. Stampfer, S. Hellmüller, F. Molitor, T. Ihn, and K. Ensslin, Appl. Phys. Lett. **93**, 212102 (2008). 41

[142] O. Naaman and J. Aumentado, Phys. Rev. Lett. **96**, 100201 (2006). 41, 73

[143] C. Flindt, A. Braggio, and T. Novotný, in *Noise and Fluctuations: 19th International Conference on Noise and Fluctuations.* AIP Conf. Proc. No. 922, p. 531 (AIP, New York, 2007). 41, 42, 73, 74, 75

[144] S. Gustavsson, R. Leturcq, T. Ihn, K. Ensslin, M. Reinwald, and W. Wegscheider, Phys. Rev. B **75**, 075314 (2007). 42

[145] C. Hermite, *"Sulla risoluzione delle equazioni del quinto grado"*, Annali di math. pura ed appl. **1**, 256 (1858). 43

[146] J. Rammer and H. Smith, Rev. Mod. Phys. **58**, 323 (1986). 43

[147] U. Meirav and E. B. Foxman, Semicond. Sci. Technol. **11**, 255 (1996). 43

[148] G. Mahan, *Many Particle Physics*, Plenum Publishing Corporation, (2000). 43

[149] D. V. Averin, A. N. Korotkov, and K. K. Likharev, Phys. Rev. B **44**, 6199 (1991). 43

[150] C. W. J. Beenakker, Phys. Rev. B **44**, 1646 (1991). 43

[151] Y. Meir, N. S. Wingreen, and P. A. Lee, Phys. Rev. Lett. **66**, 3048 (1991). 43

[152] C. Bruder and H. Schoeller, Phys. Rev. Lett. **72**, 1076 (1994). 43

[153] M. Braun, J. König, and J. Martinek, Phys. Rev. B **70**, 195345 (2004). 43, 44, 50, 82, 95

[154] J. König, J. Martinek, J. Barnas, and G. Schön, in "CFN Lectures on Functional Nanostructures", Eds. K. Busch, A. Powell, C. Röthig, G. Schön, and J. Weissmüller Lecture Notes in Physics **658**, Springer, 145 (2005). 44

[155] I. Weymann, J. Barnaś, J. König, J. Martinek, and G. Schön, Phys. Rev. B **72**, 113301 (2005); I. Weymann, J. König, J. Martinek, J. Barnaś, and G. Schön, Phys. Rev. B **72**, 115334 (2005). 44

[156] I. Weymann, Phys. Rev. B **75**, 195339 (2007). 44

[157] B. Kubala, G. Johansson, and J. König, Phys. Rev. B **73**, 165316 (2006). 44

[158] J. König, J. Schmid, H. Schoeller, and G. Schön, Phys. Rev. B **54**, 16820 (1996); H. Schoeller and G. Schön, Phys. Rev. B **50**, 18436 (1994); J. König, H. Schoeller, and G. Schön, Europhys. Lett. **31**, 31 (1995). 44

[159] J. Könemann, B. Kubala, J. König, R. J. Haug, Phys. Rev. B **73**, 033313 (2006); H. Schoeller and G. Schön, Physica B **203**, 423 (1994). 44

[160] M. Governale, M. G. Pala, and J. König, Phys. Rev. B **77**, 134513 (2008); Phys. Rev. B **78**, 069902(E) (2008). 44

[161] D. Urban, M. Braun, and J. König, Phys. Rev. B **76**, 125306 (2007). 44

[162] J. König, *Quantum Fluctuations in the Single-Electron Transistor*, Shaker, Aachen, (1999). 44, 50

[163] J. König, H. Schoeller, and G. Schön, Phys. Rev. Lett. **76**, 1715 (1996); J. König, J. Schmid, H. Schoeller, and G. Schön, Phys. Rev. B **54** 16820 (1996). 44

[164] H. Schoeller, in *Mesoscopic Electron Transport*, edited by L. L. Sohn, L. P. Kouwenhoven, and G. Schön (Kluwer, Dordrecht, 1997). 44

[165] D. Futterer, M. Governale, M. G. Pala, and J. König, Phys. Rev. B **79**, 054505 (2009). 44

[166] J. Splettstoesser, M. Governale, J. König, and R. Fazio, Phys. Rev. Lett. **95**, 246803 (2005); J. Splettstoesser, M. Governale, J. König, and R. Fazio, Phys. Rev. B **74**, 085305 (2006). 44

[167] J. Splettstoesser, M. Governale, J. König, F. Taddei, and R. Fazio, Phys. Rev. B **75**, 235302 (2007). 44

[168] J. Splettstoesser, M. Governale, and J. König, Phys. Rev B. **77**, 195320 (2008). 44

[169] N. Winkler, M. Governale, and J. König, in preparation. 44

[170] S. Legel, *Coherence and Correlation Effects in Coupled Quantum Dot Systems*, Ph.D. thesis, urn:nbn:de:swb:90-75231, Karlsruhe (2008). 50

[171] C. Flindt, T. Novotný, A. Braggio, M. Sassetti, and A.-P. Jauho, Phys. Rev. Lett. **100**, 150601 (2008). 52, 54

[172] C. Flindt, *Electrons in Nanostructures: coherent manipulation and counting statistics*, Ph.D. thesis, Technical University of Denmark, Copenhagen (2007). 54

[173] A. Braggio, J. König and R. Fazio, Phys. Rev. Lett. **96**, 026805 (2006). 52, 59, 60, 68, 85, 96, 100

[174] U. Harbola, M. Esposito, and S. Mukamel, Phys. Rev. B **74**, 235309 (2006). 52

[175] G. Kießlich, P. Samuelsson, A. Wacker, and E. Schöll, Phys. Rev. B **73**, 033312 (2006); G. Kießlich, E. Schöll, T. Brandes, F. Hohls, and R. J. Haug, Phys. Rev. Lett. **99**, 206602 (2007). 52

[176] F. Pistolesi, Phys. Rev. B **69**, 245409 (2004). 52

[177] M.-S. Choi, F. Plastina, and R. Fazio, Phys. Rev. Lett. **87**, 116601 (2001). 52

[178] Y. Makhlin, G. Schön, and A. Shnirman, Phys. Rev. Lett. **85**, 4578 (2000). 52

[179] R. A. Pucel, Proc. IRE, **49**, 1080 (1961); G. Lecoy and L. Gouskov, Physica Status Solidi (b) **30**, 9 (1968); S. T. Liu and A. Van Der Ziel, Physica **37**, 241 (1967). 59

[180] M. Büttiker, Phys. Rev. Lett. **57**, 1761 (1986); L. J. van der Pauw, Philips Res. Rep. **13**, 1 (1958). 67

[181] C. Bruder, R. Fazio, and H. Schoeller, Phys. Rev. Lett. **76**, 114 (1996). 67

[182] L. Onsager, Phys. Rev. **38**, 2265 (1931); H. B. G. Casimir, Rev. Mod. Phys. **17**, 343 (1945). 65

[183] B. Kubala and J. König, Phys. Rev. B **67**, 205303 (2003). 66

[184] W. Hofstetter, J. König, and H. Schoeller, Phys. Rev. Lett. **87**, 156803 (2001). 66

[185] R. Kubo, Rep. Prog. Phys. **29**, 255 (1966). 69

[186] H. B. Callen and T. A. Welton, Phys. Rev. **83**, 34 (1951). 69

[187] Ya. M. Blanter, "Recent Advances in Studies of Current Noise", to be published in: *Springer Lecture Notes*, edited by Ch. Röthig, G. Schön and M. Vojta, preprint: arXiv:cond-mat/0511478v2 (2005). 70

[188] F. Lefloch, C. Hoffmann, M. Sanquer, and D. Quirion, Phys. Rev. Lett. **90**, 067002 (2003); D. Averin and H. T. Imam, Phys. Rev. Lett. **76**, 3814 (1996); P. Dieleman, H. G. Bukkems, T. M. Klapwijk, M. Schicke, and K. H. Gundlach, Phys. Rev. Lett. **79**, 3486 (1997). 70

[189] E. Buks, R. Schuster, M. Heiblum, D. Mahalu and V. Umansky, Nature **391**, 871 (1998). 73

[190] G. L. Khym and K. Kang, Phys. Rev. B **74**, 153309 (2006). 73

[191] D.-I. Chang, G. L. Khym, K. Kang, Y. Chung, H.-J. Lee, M. Seo, M. Heiblum, D. Mahalu, and V. Umansky, Nat. Phys., **4**, 205 (2008). 73

[192] B. Dong, X.-L. Lei and N.J.M. Horing, J. Appl. Phys. **104**, 033532 (2008) Phys. Rev. B **77**, 085309 (2008); B. Dong, X.-L. Lei and H.-L. Cui, Commun. Theor. Phys. **49** 1045 (2008). 79, 94

[193] J. Siewert and T. Brandes, Adv. in Solid State Phys. **44**, 181 (2004). 79

[194] X. Xu, B. Sun, P. R. Berman, D. G. Steel, A. S. Bracker, D. Gammon, L. J. Sham, Nature Physics **4**, 692 (2008). 79, 90

[195] L. Qin and Y. Guo, J. Phys.: Condens. Matter **20**, 365206 (2008). 94

[196] F. Li, H. Jiao, J. Luo, X.-Q. Li, S.A. Gurvitz, arXiv:0812.0846v1 (2008); Feng Li, Xin-Qi Li, Wei-Min Zhang, S.A. Gurvitz, arXiv:0803.1618v1 (2008). 94

Publications

[1] Daniel Urban, Matthias Braun, and Jürgen König,
"Theory of a magnetically controlled quantum-dot spin transistor".
Phys. Rev. B **76**, 125306 (2007).

[2] Daniel Urban, Rosario Fazio, and Jürgen König,
"Coulomb-interaction effects in full counting statistics of a quantum-dot Aharonov-Bohm interferometer",
Phys. Rev. B **78**, 075318 (2008).

[3] Daniel Urban, and Jürgen König,
"Tunable dynamical channel blockade in double-dot Aharonov-Bohm interferometers",
Phys. Rev. B **79**, 165319 (2009).

[4] Stephan Lindebaum, Daniel Urban, and Jürgen König,
"Full counting statistics of interacting quantum dots with ferromagnetic leads",
Phys. Rev. B **79**, 245303 (2009).

Parts of this thesis has already been published. Chapters 5 and 6 contain the results of the publications 2 and 3, respectively.

Acknowledgements

It is a great pleasure to thank all people I have met during my studies and who contributed to this work or just made work on it more delightful. First of all I would like to thank my advisor Prof. Dr. Jürgen König for giving me the opportunity to work in his group, always being available for discussion and teaching me how to communicate scientific results in talks, posters, articles and discussions. I am also very grateful for his and Prof. Dr. Rosario Fazio's help in arranging a research stay in Pisa. With regards to this time I would like to thank Prof. Fazio for the friendly reception in his group and his constant willingness to discuss both during my stay and also after I had left.

My thanks furthermore go my former office mates Dr. Björn Kubala and Dr. Matthias Braun who in many discussions furthered my knowledge and understanding of (not only) physics. Both gave me a good example of the skills needed in science. For the same reason I would like to thank my later office mate Björn Sothmann, who additionally contributed by proofreading the manuscript. Along the same lines I thank Stephan Lindebaum who deepened the understanding of my work. With regards to my stay in Pisa I have to thank in particular Dr. Janine Splettstößer for her help in organisational matters.

Furthermore I acknowledge fruitful discussions with W. Belzig, A. Braggio, C. Emary, C. Flindt, H. Förster, M. Governale, F. Haupt, G. Kiesslich, S. Legel, R. Leturcq, S. Lindebaum, D. Marcos, and N. Winkler.

Both the teams of the "Institut für theoretische Physik III" at the Ruhr-Universität Bochum, the group "Quantum Transport and Information" at the Scuola Normale Superiore in Pisa and "Theoretische Tieftemperaturphysik" at the Universität Duisburg-Essen deserve gratitude for creating a very friendly working environment. Here, special thanks go to Dr. A. Hucht who was always prepared to help with minor and major technological problems. I would also like to thank everyone else who is not mentioned here explicitly but whom I met over the years in Bochum, Pisa, Duisburg and the many other places to which my work lead me.

Finally very special thanks go to my parents who supported me during my entire education and in this way prepared the grounds for the possibility of this thesis. I am also deeply indebted to Mirja Richter for her unconditional love and support during the years and across the miles.

Curriculum Vitæ

Daniel Urban, born July 31, 1979, in Oberhausen

1999–2004	Studies of physics at the *Ruhr-Universität Bochum*, Germany
2001–2002	ERASMUS student at the *University of Sussex*, UK
Dec. 2004	Diploma in physics from the *Ruhr-Universität Bochum*, Germany Title: "Spin-dependent transport through quantum dots with three ferromagnetic leads", supervised by Prof. Dr. J. König
Sept. 2005–Apr. 2008	Doctoral studies under supervision of Prof. Dr. J. König at the *Ruhr-Universität Bochum*
Jan. 2006–June 2006	Research stay in the group of Prof. Dr. R. Fazio at *Scuola Normale Superiore*, Pisa, Italy
May 2008–Apr. 2009	Continuation of the doctoral studies under supervision of Prof. Dr. J. König at the *Universität Duisburg-Essen*